TIP-OVER STABILITY ANALYSIS FOR MOBILE BOOM CRANES WITH SINGLE- AND DOUBLE-PENDULUM PAYLOADS

A Thesis
Presented to
The Academic Faculty

by

Daichi D. Fujioka

In Partial Fulfillment
of the Requirements for the Degree
Master of Science in Mechanical Engineering in the
George W. Woodruff School of Mechanical Engineering

Georgia Institute of Technology
December 2010

TIP-OVER STABILITY ANALYSIS FOR MOBILE BOOM CRANES WITH SINGLE- AND DOUBLE-PENDULUM PAYLOADS

Approved by:

Professor William Singhose, Advisor
George W. Woodruff School of Mechanical Engineering
Georgia Institute of Technology

Professor Wayne Whiteman
George W. Woodruff School of Mechanical Engineering
Georgia Institute of Technology

Professor Nader Sadegh
George W. Woodruff School of Mechanical Engineering
Georgia Institute of Technology

Date Approved: July 6, 2010

To my loving family,

who always had supported me,

during my most difficult times.

ACKNOWLEDGEMENTS

First, I want to thank my family for their continuous support and love.

My special thanks goes to Andreas Rauch and Taft Jones for providing assistance and incentives for this research, and conducting experimental work with me.

I also want to thank Dr. Whiteman and Dr. Sadegh for being on my committee and offering knowledge and insights.

Lastly, I thank Dr. Singhose for being my advisor. This work would not have been possible without his directions and academic advice.

TABLE OF CONTENTS

LIST OF TABLES

LIST OF FIGURES

SUMMARY

Mobile boom cranes are widely used to perform important tasks in various applications. Their mobility, unlike other types of the conventional cranes, provides an advantage of faster positioning. During use, the crane base is normally fixed to the ground before lifting heavy payloads to stabilize the base and prevent tip-over. However, this compromises the mobility advantage of the mobile boom cranes. Realizing both maneuverability and stability of the base, while the crane is operated for lifting and transferring materials, can greatly enhance the utility of mobile boom cranes. Combining the base motion with regular crane operations (lifting, luffing and slewing) can expand the crane's workspace to everywhere on the working plane field. Base and crane motion, however, also presents a problem of stability reduction. A payload attached to the crane and its swing due to motion decreases the stability margin of the base and increases the chance of tip-over. Attaching complex payloads, such as a double-pendulum, further complicates the problem.

This thesis investigates a tip-over stability of mobile boom cranes with swinging payloads. The study begins with a point mass single-pendulum to analyze tip-over stability of a mobile boom crane under different conditions. To study the tip-over stability, a tip-over prediction model is developed. The mobile boom crane model consists of four main body parts (base, boom, cable, payload). The boom can be configured at any luffing/slewing angles, and the suspension cable can deflect in tangential and radial directions with respect to the base to simulate payload swings. The model is developed with the goal of limiting the computational cost to a minimum.

First, a static stability analysis of a boom crane is performed using a prediction

model. In this analysis, the boom crane is assumed to be stationary, thus inducing no swing in the payload. This study provides a basic understanding of the relationship between the tip-over stability and the moment contribution from the payload mass and the boom configuration. Tip-over stability is characterized by using tip-over stability margin method. The method utilizes the net force and couple applied to the system's center of mass. Then, it characterizes their contributions to the tip-over moment by measuring the angle between the net force vector and each of the tip-over axis normals. The tip-over axes are determined by projecting the crane base onto the ground and connecting the ground contact points. A crane is stable while the margin angle measure remains positive, which indicates that the net force vector intersects the ground inside the projected surface. The margin is calculated for various payload values and boom luffing/slewing configurations, and their effects on the tip-over stability are compared. The crane's tip-over stability is also represented by the maximum possible payload it can carry throughout the workspace without tipping over.

Next, a pseudo-dynamic stability analysis is conducted. A pseudo-dynamic method incorporates the payload swing into the tip-over stability analysis by adding estimated maximum payload swing due to base/boom motion as a fixed constant rather than a variable. To estimate the angles, the differential equations of motion of payload swings from each type of motion input are derived. Again, the tip-over stability margin is calculated for various payload masses and boom configurations, and is used to determine the maximum payload values. The maximum payload is found to be highly dependent on the magnitude of the acceleration and velocity input command. Experiments verify that the pseudo-dynamic stability analysis is a good method to predict tip-over.

The thesis then extends the study to more complex, double-pendulum cases. The similar studies from the single-pendulum case are performed. The maximum swing

angles estimated from the single-pendulum case are directly applied to the double-pendulum case to simplify the model/analysis and minimize the computational cost. The results from the experiments validate the analysis method. The results from the double-pendulum case are also compared to those of the single-pendulum case to observe the effect of having different payload types.

A full dynamic multi-body simulation model of a mobile boom crane is developed. The results are compared to validate the prediction model and the tip-over stability analysis methods introduced. A crane is considered as stable when two or more wheel contact forces are positive, or making good ground contact enough to experience ground reaction forces. The prediction calculation from the prediction model are then verified by simulation results. The outcomes are analyzed to make final conclusions about the tip-over stability of mobile boom cranes.

The prediction model and the results in the thesis provide a significant tool for practical application of tip-over stability analysis to mobile boom cranes. The experimental results increase the confidence of the study's accuracy and accountability.

CHAPTER I

INTRODUCTION

1.1 Heavy Machineries and Tip-Over

There are many types of heavy machinery used in various applications worldwide. Heavy machinery, such as loaders, dozers, excavators, scrapers, trucks, cranes, and material handlers are widely used for agriculture, demolition, forestry, general construction, industry, mining and more. However, they pose a great danger to users and the surroundings when they tip-over. One such type of heavy machinery that is particulary susceptible to tip-over accidents is mobile boom cranes, an example of which is shown in Figure 1.

1.1.1 Mobile Boom Cranes

Cranes with a fixed-base are commonly used for heavy lifting. The drawback of these cranes is that they have a limited workspace. Allowing the base of a crane to move can greatly expand the workspace and increase productivity. Mobile cranes have wheel or track drives to translate their base. Their mobility, unlike other types of conventional cranes, provides an advantage of fast positioning. Generally, mobile cranes are equipped with boom arms because of the structural advantages [2]. Boom cranes are moved using slewing, luffing, and hoisting motions. These degrees of freedom are illustrated in Figure 2. Achieving both maneuverability and stability of the base, while the crane is operated for lifting and transferring, can greatly enhance the utility of the mobile boom cranes. Combining base motion with regular crane operations (lifting, luffing and slewing) can also significantly expand the crane's workspace.

Figure 1: Example of a Mobile Boom Crane in Operation [50]

1.1.2 Tip-Over Stability

Mobile boom cranes carrying loads pose a stability hazard of tipping over. During use, the crane base is normally secured to the ground before lifting heavy payloads to stabilize the base and prevent tip-over. Fixed configuration compromises the mobility advantage of the mobile boom cranes. Base motion, however, also reduces the base stability. Payloads attached to the crane and their oscillatory motion decrease the stability margin of the base and increase the chance of tip-over. Payload swing extends the mass outward, which increases the moment arm of the payload and the resultant moment that de-stabilizes the base [38]. Attaching complex payloads, such as double-pendulums, further complicates the problem [47][11]. The inertia forces of the entire body from the base acceleration and the centripetal force from the rotating boom and swinging payload also degrade the tip-over stability. In the worst case, the crane

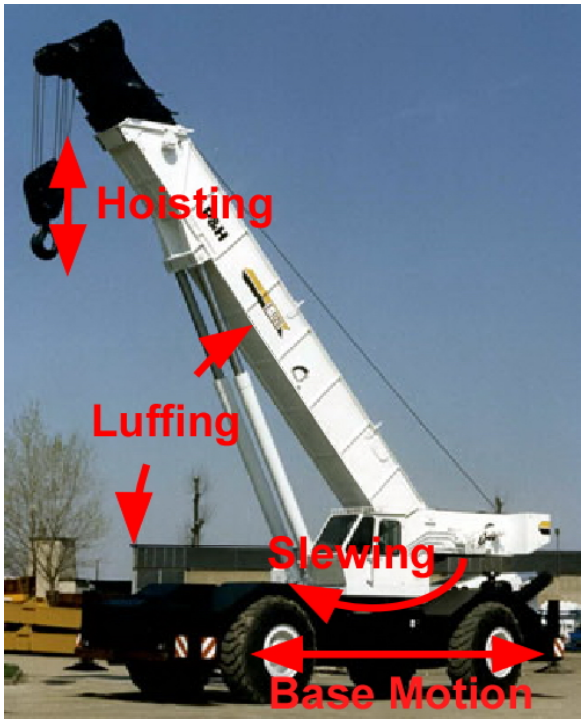

Figure 2: Mobile Boom Crane and Common Crane Motions [36]

tips-over and causes extensive damage to itself and to the surroundings, as well as injures humans operators and workers nearby. Figure 3 shows a tip-over accident site of a mobile boom crawler.

Another issue that must be addressed for mobile crane instability is bucking. Bucking occurs when some tires or portions of the tracks of the crane are lifted off the ground. In this case, a portion of the base temporary loses contact with the ground. The crane tires or tracks return to the ground and the base recovers stability because bucking does not involve a tipping torque large enough to bring the entire crane to the ground. Figure 4 shows a simulated bucking motion. The weight of the boom and the payload temporary lifts up the tires on back of the base. The crane base rises up to a certain pitch angle, and then returns back to the stable position.

When a crane experiences a bucking motion, it induces a significant amount of unpredictable payload swing, which can collide with nearby objects. Bucking also significantly reduces slewing performance because the base and the tires can no longer

Figure 3: Tip-over Accident of a Mobile Boom Crane [10]

provide frictional resistance to the slewing rotation. This makes the boom crane vulnerable to disturbance forces, such as a strong gust and a large payload oscillation, and can lead to a loss of control. Even a slight bucking potentially leads to an uncontrollable crane behavior and, therefore, results in a loss of tip-over stability margin. Although it does not result in a complete tip-over, bucking can cause damage and should be avoided for safety reasons. For this reason, this thesis will consider a crane to be unstable when it undergoes bucking.

1.1.3 Current Solutions to Tip-Over

The tip-over stability problem occurs with all kinds of similar applications, such as aerial platforms, scissor lifts, cherrypickers, and lifting trucks. One common solution to prevent a tip-over is to utilize a counter-weight to balance the base. Some types of heavy machinery, such as excavators, attach a counter-weight on the opposite side to balance the moment created by the end-effecter load. Another solution that is frequently utilized are stabilizing arms. Many machines, such as cherrypickers, are

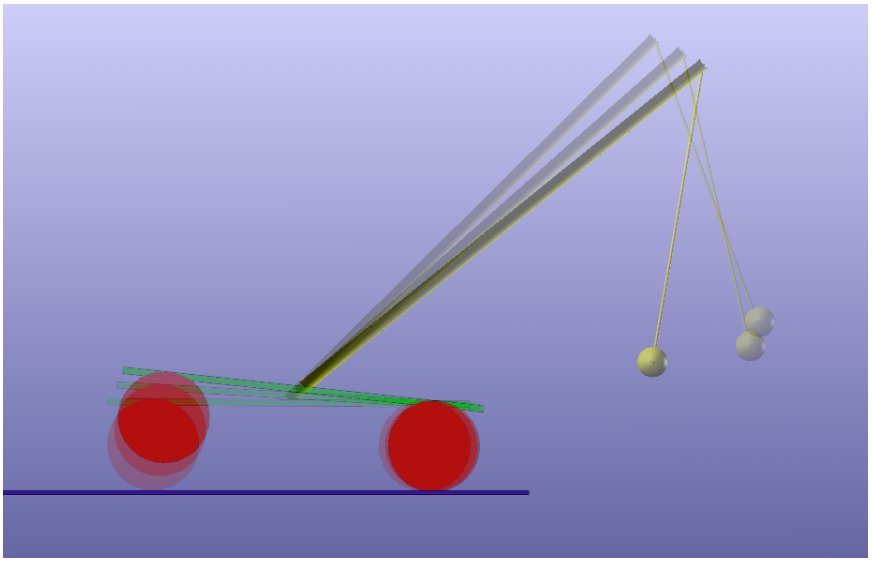

Figure 4: Illustration of a Bucking Motion [38]

equipped with extending arms, as shown in Figure 5 and Figure 6. The arms are extended out and locked in place before the workers in the basket are lifted up. These solutions, however, are all preventive measures. They are always put into use to avoid the worst case scenario, whether it happens or not. Users also sometimes forget to properly utilize the safety features. For example, the cherrypicker in Figure 5 tipped-over at the Miami airport and killed a worker in the basket when he forgot to extend the stabilizing arms.

Some machines may not even require, or be equipped with, such features. For example, the scissor lift shown in Figure 7 is equipped with no tip-over prevention features to limit the maximum load. To cut down on the extra cost and decrease accidents while maintaining high working efficiency, there is a need for a system that predicts tip-over and alerts the users with proper warning signals. The current warning systems completely rely on the operator's ability and skill to prevent accidents. Such warning systems, however, can not guarantee the safety of the machine from entering a dangerous configuration. Simply adding a large number of warning labels is ineffective, as demonstrated by the excessive warnings in the cab of a mobile boom

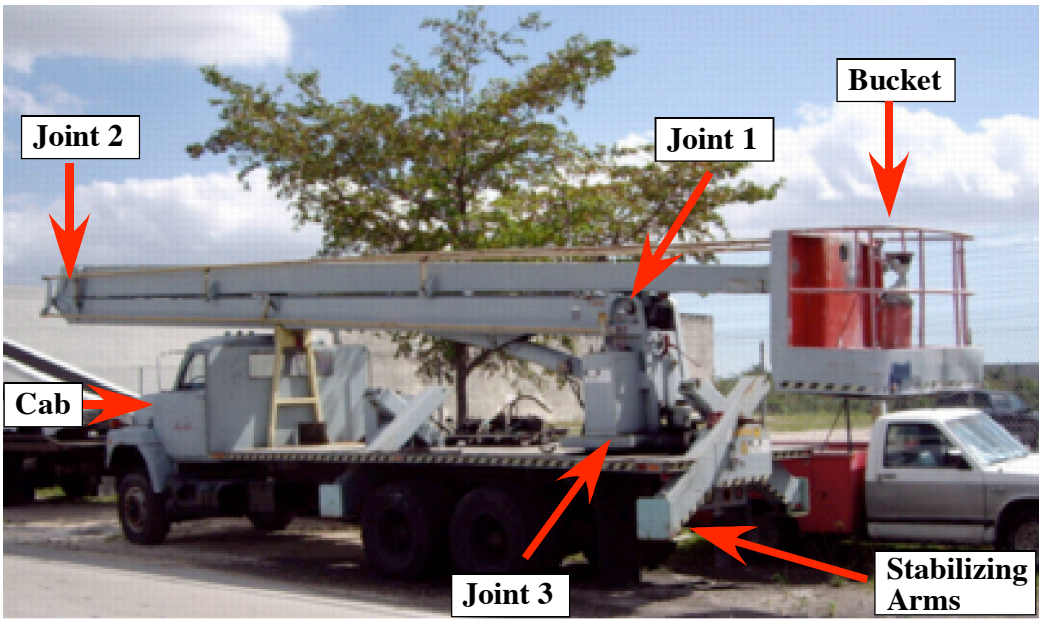

Figure 5: Cherrypicker Vehicle

crane shown in Figure 8.

1.1.4 Related Fields and Past Research

There have been several studies conducted to understand and control the tip-over and roll-over issue. One previous investigation suggested an algorithm that limits the lifting truck's maximum speed to stabilize its base [8]. The roll-over initiation speed in the longitudinal direction was determined as a function of the loading condition and cornering maneuver. To avoid roll-overs, an anti-roll controller was developed to limit the speed command entered by the driver. In [27], the tip-over stability of an hydraulic excavator lifting heavy payloads was analyzed.

A tip-over/roll-over prevention system for heavy trucks was introduced in [4]. A sliding mode controller was implemented to stabilize the truck in the presence of slosh dynamics of a liquid cargo. Tip-over prevention is a critical factor also in the development of All Terrain Vehicles (ATVs). To predict potential tip-over and roll-over conditions, highly complex dynamic models that integrate tire stiffness, wheel slip condition, and lateral load transfer was developed in [9]. Similar investigations were

Figure 6: Stabilizing Arm

conducted for problems occurring with Sport Utility Vehicles (SUVs) [25]. Malcher, Eskandarian and Delaigue presented more general dynamic models for tip-over/roll-over motions that is applicable to a wide variety of vehicle types and sizes [32]. Previous investigations in the area also suggested methods to prevent roll-over, such as by limiting the maximum lifting speed [8]. Also, several different investigations were performed to develop the methods to determine the tip-over stability of the systems with different kinds of manipulators and task constraints [15][18][37][53].

There are also many investigations to study the tip-over stability of cranes. Kogan studied the tip-over stability of cranes under different loading situations, including wind disturbances [23]. Towarek investigated the dynamic stability of a boom crane on flexible soil foundation [49]. In [3], a complex dynamic simulation model of a hydraulic crane with a fixed base was developed. The model analyzed the crane's tip-over responses during the load lifting, load swivel, ground failure and several other conditions. Kiliçaslan, Balkan and Ider determined the maximum allowable payload a mobile crane can carry when its base is kept fixed and supported by stabilizing arms, while moving around the arm and the payload [20].

Figure 7: Scissor Lift Vehicle

Most of previous work in this area, however, has been limited to investigations of the crane's stability in a fixed location during its operation. They usually omitted some other critical factors, such as inertia effects and payload swing, which can greatly contribute to the tip-over.

Payload oscillations are known to have a significant influence on a crane's tip-over stability. In [6], the anti-sway problem was formulated as a nonlinear, constrained optimal control problem. In [1], payload swing caused by base excitation was investigated. An oscillation limiting technique using the reeling and unreeling of the hoisting cable was then presented. Lewis, Parker, Driessen and Robinett presented a method to reduce payload oscillation with adaptive command filters [26]. Certain types of payloads and riggings can induce double-pendulum effects that increase the complexity of the problem [28, 16, 45, 47, 22].

Figure 8: Excessive Warning Labels in the Cab

In this thesis, the tip-over stability of mobile boom cranes is investigated. Mobile boom cranes utilizing their moving base and boom to transport heavy loads is investigated in detail. As mentioned, the mobile cranes are designed as boom cranes because of their structural advantages [2]. However, the methodologies and results presented in this research can easily be extended to other types of cranes.

1.2 Thesis Contributions

This thesis investigates the tip-over stability of mobile boom cranes with swinging payloads. This thesis work contributes to the knowledge of the tip-over stability of mobile boom cranes by providing:

- Development of a simple tip-over prediction model with very low computational cost for a mobile boom crane
- Development of a practical analysis method to predict the tip-over stability of mobile boom cranes in various motions, which can also easily be extended to

other types of machinery such as cherrypickers

- Analysis of tip-over stability of mobile boom cranes equipped with different types of payloads
- Development of a full dynamic simulation model of a mobile boom crane

1.3 Thesis Overview

In this thesis, the tip-over stability of a mobile boom crane is analyzed under various conditions. In Chapter 2, a simple prediction model of a mobile boom crane equipped with a single-pendulum point mass payload is presented. A method to determine the tip-over stability margin is also explained. A static stability analysis is then performed to provide the initial insights into the relationship between the crane configuration and the tip-over stability of the mobile boom crane. Chapter 3 introduces a pseudo-dynamic stability analysis which is used to study the tip-over stability of a mobile boom crane when it performs simple motions. The analysis incorporates the payload swing and the dynamic effects due to the motions into the consideration. Chapter 4 extends the analysis to the double-pendulum payload setup by making minor modifications to the pseudo-dynamic method. The tip-over stability analysis is performed for the same cases investigated in the single-pendulum setup. Experiments are performed to verify the analysis results. In Chapter 5, a dynamic multi-body simulation model of the crane is developed to more accurately analyze the crane's tip-over behavior. The simulation is run for the cases investigated above, and the results are used to validate the analytical methods. Chapter 6 summarizes the conclusions obtained from the analysis performed, and suggests some possible future works in the area of the tip-over stability.

CHAPTER II

SINGLE-PENDULUM STATIC STABILITY ANALYSIS

To develop a fundamental understanding of the tip-over stability of mobile boom cranes, a static stability analysis is first conducted. In this case, the entire system remains stationary and thus exhibits no dynamic nor inertial effects. The boom is attached with only a single-pendulum payload so it does not induce any non-linear complex oscillatory behavior. This is the simplest system setup, and the analysis is used to identify the basic characteristics of the tip-over stability of mobile boom cranes and to investigate the effects of varying basic boom crane configuration parameters.

2.1 Tip-Over Prediction Model of Mobile Boom Crane

To investigate mobile boom crane stability, a representative model of a crane is developed. The tip-over of the actual crane system is predicted by observing the tip-over behavior of the model. The model is utilized in all tip-over stability analysis that will be discussed in this thesis.

2.1.1 Model Schematics

Figure 9 illustrates a representative model of a mobile boom crane with a single-pendulum payload. The model is composed of a cart platform with tires, a rotational boom arm, and a suspension cable with an end point mass. The cart is modeled as a thin plate with a mass of m_c and has a center of gravity at l_{com} and b_{com} away from its the geometric center. The boom can be rotated through an angle β about a point located at a distance of l_a from the geometric center. The boom is mounted on top of the rotational platform, at a distance of l_{a2} from the platform's rotational center. It has a length of l_b, a mass of m_b, and a center of mass at a distance l_{bcom} from the

attachment. The boom can be luffed through an angle α.

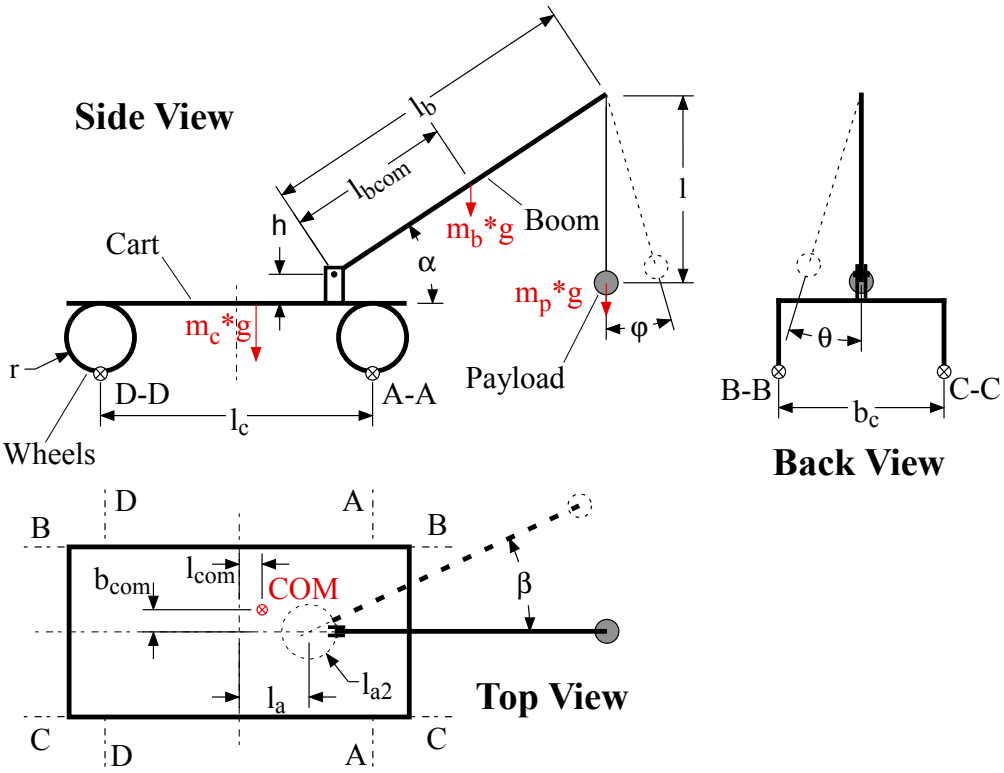

Figure 9: Schematic Diagram of a Mobile Boom Crane with Single-Pendulum [38]

There are four wheels attached to the bottom of the cart platform. The wheels are separated by l_c in the longitudinal direction, and b_c in the lateral direction. These are also assumed to be the same as the cart's platform dimension. The contact forces exerted on the wheels are limited to be compressive forces only. The suspension cable has a length l and a negligible mass compared to the payload m_p attached at the end of the cable. For use in the subsequent pseudo-dynamic stability analysis in Chapter 3, the model also defines swing angles of the payload. The payload oscillations of the single-pendulum crane are defined in the longitudinal and the lateral directions with respect to the cart. The angle φ describes the payload oscillation in the longitudinal direction. Similarly, the angle θ describes the payload oscillation in the lateral direction with respect to the cart. In this static analysis, the entire mobile boom crane is assumed to be stationary; there are no payload swings. Therefore, the

swing angles φ and θ are set equal to 0°.

In summary, following assumptions on the prediction model were made to simplify the analysis.

- Crane only moves on the horizontal flat surface
- Each body is rigid
- Unspecified dimensions of the bodies have negligible length
- Suspension cable is massless and incompressible
- Payload is a point mass

2.1.2 Tip-Over Stability Margin

In order to evaluate the system's tip-over stability properties and to determine whether the entire mobile boom crane tips-over, a stability index based on the tip-over stability margin method (Force-Angle Stability Measure) [35] is introduced. This analysis method utilizes the net force and couple applied to the system's center of mass, and characterizes its contribution to the tip-over moment by measuring the angle between the net force vector and the normal of each of the tip-over axes. It has a simple graphical interpretation and is easily computed yet remains sensitive to loads and applicable to general case of uneven terrain and external disturbances. The method is advantageous because it does not require any integration in its computation, thus provides very simple measure of tip-over stability with minimum computation cost.

In this method, it is assumed that the vehicle is normally in contact with the ground, and its mobility is provided via wheels, tracks, alternating (statically stable) legged support, or a combination of such devices. A tip-over instability is defined when there is a reduction in the number of ground contact points (bucking), and the ground contact forces vanish.

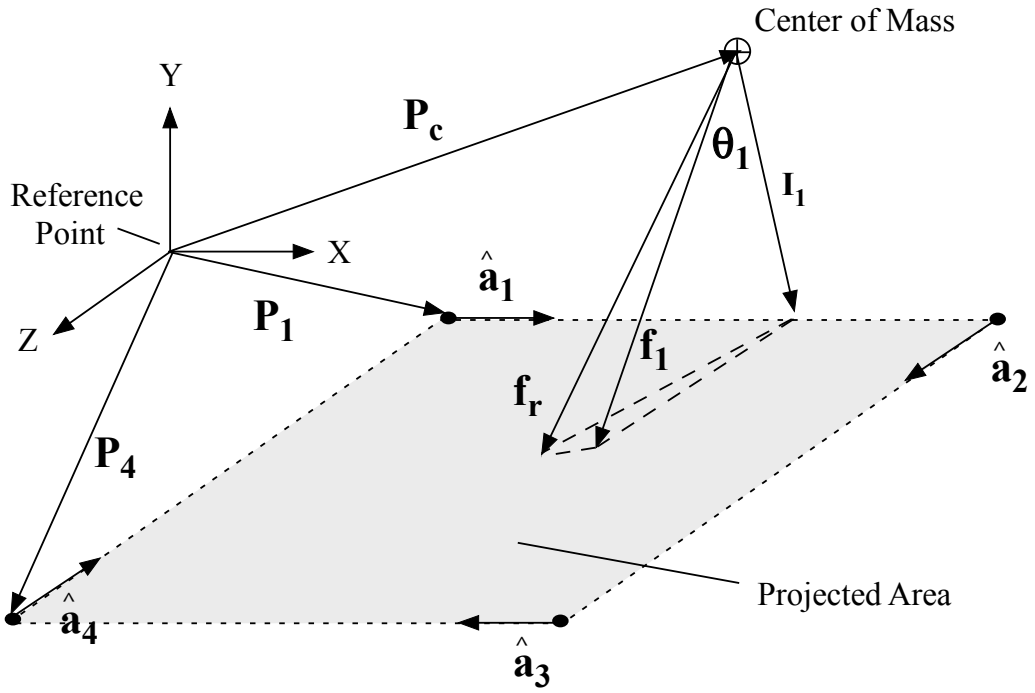

Figure 10: General 3D Tip-Over Stability Margin Geometry

Figure 10 shows the general geometry of a vehicle system setup for the tip-over stability margin method. To apply the method, it is only necessary to consider those outermost ground contact points which form a convex support polygon when projected onto the horizontal plane. Let P_i be the location of the i^{th} ground contact point expressed in Newtonian frame.

$$P_i = [p_x p_y p_z]_i^T \quad \text{for i=1,...,n} \tag{2.1}$$

Also, P_c denotes the location of the vehicle's center of mass. The P_i are numbered in clockwise order when viewed from above. The possible tip-over axes a_i, which constitutes the perimeter of the support polygon, are then defined by:

$$a_i = P_{i+1} - P_i \quad \text{for i=1,...,n-1} \tag{2.2}$$

$$a_n = P_1 - P_n \tag{2.3}$$

Vehicle tip-over of mobile boom crane will always occur about one of these axes. Therefore, the tip-over condition for the mobile boom crane is split into distinct cases: The crane will tip-over either to the front (tip-over axis indicated as A-A in Figure 9), to the back (tip-over axis indicated as D-D in Figure 9), or to the side (tip-over axes indicated as B-B and C-C in Figure 9). Defining $\hat{a} = a/\|a\|$, from vector subtraction the tip-over axis normals l which intersect the center of mass are given by subtracting from $P_{i+1} - P_c$ that portion which lies along $\hat{a}_i$.

$$l_i = (I - \hat{a}_i \hat{a}_i{}^T)(P_{i+1} - P_c) \tag{2.4}$$

where, I is the 3x3 identity matrix.

The net force, f_r, applied to the center of mass is a sum of all forces acting on the mobile boom crane body. These forces include the inertial forces, gravitational loads (*i.e.* weight contributions from the cart and the boom), loads transmitted by the manipulator (*i.e.* end-effector/crane payload masses and reaction forces), and other external disturbance forces acting on the body. Similarly, the net moment acting about the center of mass is denoted by n_r.

For a given tip-over axis $\hat{a}_i$, the components of f_r and n_r which contribute to the tip-over moment are given by:

$$f_i = (I - \hat{a}_i \hat{a}_i{}^T) f_r \tag{2.5}$$

$$n_i = (\hat{a}_i \hat{a}_i{}^T) n_r \tag{2.6}$$

Next, it is necessary to replace each moment n_i with an equivalent force couple $f_{n,i}$. The equivalent force couple needs to lie on the plane normal to the moment n_i. Figure 11 illustrates the equivalent force couple acting on the center of mass about the tip-over axis.

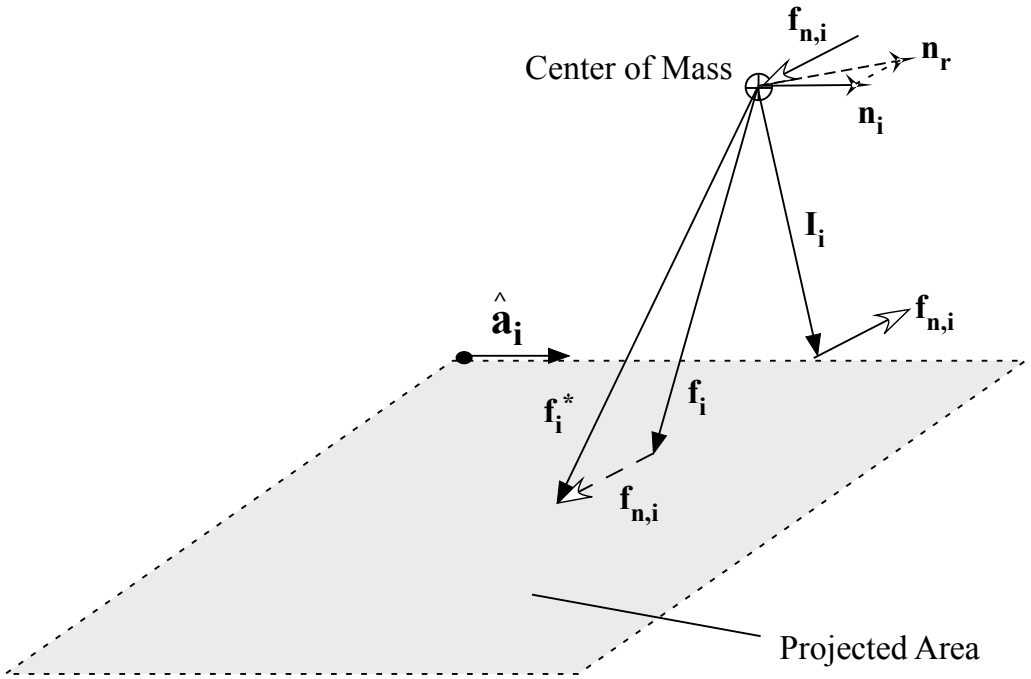

Figure 11: Equivalent Force Couple at Center of Mass

The member of the force couple acting on the center of mass is then given by:

$$f_{n,i} = \frac{\hat{I}_i \times n_i}{||I_i||} \tag{2.7}$$

where $\hat{I} = I/\|I\|$ by normalizing. The new net fore vector, f_i^*, for the i^{th} tip-over axis is:

$$f_i^* = f_i + f_{n,i} = f_i + \frac{\hat{I}_i \times n_i}{||I_i||} \tag{2.8}$$

Normalizing f_i^* by $\hat{f}_i^* = f^*/\|f^*\|$, the angles measured between the net force vector and each of the tip-over axis normals are determined by:

$$\theta_i = \sigma_i cos^{-1}(f_i^* \cdot \hat{I}_i); \quad \text{for i=1,...,n} \tag{2.9}$$

where $-\pi \leq \theta_i \leq \pi$. The σ_i determines the sign of θ_i *by* :

$$\sigma_i = \begin{cases} +1 & (\hat{I}_i \times f_i^*) \cdot \hat{a}_i < 0 \\ -1 & otherwise \end{cases} \tag{2.10}$$

The overall tip-over stability margin of the system, θ^*, is then determined by the minimum value of θ_i. The magnitude of a positive θ^* defines the magnitude of the tip-over stability margin of a stable system. Note that the appropriate sign of the angle measure associated with each tip-over axis is determined by establishing whether or not the net force vector lies inside the support polygon. That is, the tip-over instability occurs when θ^*=0. Negative θ^* indicates that there is a tip-over instability happening to the system.

The method's algorithm indicates that a low center of gravity that is close to the geometric center is always desirable from a stability point of view. Also, heavier system components contribute to stability in lower velocity motions, but they are destabilizing at high velocities because of their larger inertia effects.

In an application to mobile boom cranes, it is assumed that there are four ground contacts points, one for each tire. In addition, to apply the prediction model directly to the calculation the ground contact points, or tires, are assumed to be separated by the same length as the cart's dimension, l_c and b_c. The location of the center of mass and the knowledge of all external forces and moments acting on the mobile boom crane, as well as the system's linear and angular accelerations are all assumed to be known. Note that all of this necessary information is either measurable or can be determined from given parameters on a real system equipped with appropriate sensory devices.

2.2 Static Stability Analysis

The prediction model is used to perform a tip-over stability analysis by calculating the stability angle margin when the crane remains stable, *i.e.* it does not tip-over. Utilizing the prediction model, the static stability analysis is conducted for every

possible boom angle configuration. For every boom position, the tip-over stability margin angles are computed for the configuration.

2.2.1 Experimental Verification Apparatus

To verify the accuracy of the prediction model, experimental data are taken and compared to predicted values. Figure 12 shows the crane apparatus which is used to experimentally verify the analysis. The apparatus consists of a base platform, a boom ,and a suspension cable where payload masses can be attached at its end. It has a capability to configure the boom in various setups by setting slewing and luffing angles β and α. The geometric parameters and constants for the experimental setup are listed in Table 1.

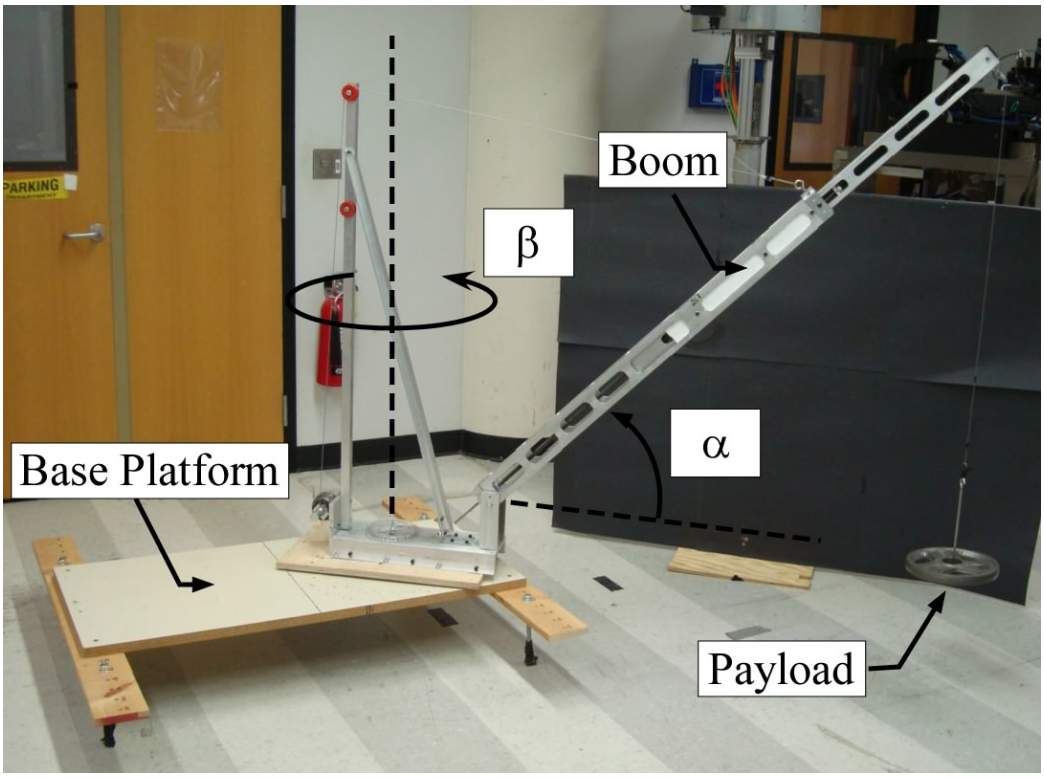

Figure 12: Experimental Setup

In order to obtain the experimental data, the boom was fixed in the desired position by adjusting luffing angle α and slewing angle β. Note that the tip-over stability

Table 1: Test Configuration for the Mobile Boom Crane

m_c	$24.9kg$	l_b	$1.70m$
m_b	$8.0kg$	l_{bcom}	$0.80m$
l_c	$1.10m$	l_{com}	$0.12m$
b_c	$0.70m$	b_{com}	$0.0m$
l_a	$0.30m$	r	$0.14m$
l_{a2}	$0.28m$	h	$0.14m$

margin angle measure is a conceptual index which cannot be measured/observed directly from the experiment. Therefore, the payload masses attached to the apparatus were recorded instead. For each individual configuration of the boom crane, the mass of the attached payload was increased incrementally until the entire setup starts to tip-over. The last payload value when the system remained stable was recorded as the maximum possible payload of the respective boom configurations. Because of the symmetry in the setup, the experiments were performed only for the slew angle β between 0° and 180°.

2.2.2 General Tip-Over Stability Analysis

Figure 13 shows an example result of the static stability analysis. The parameters from Table 1 are used for calculation. The polar plot shows tip-over stability margins for all slewing angle configuration (β=0°-360°) when the luffing angle α is 0°, *i.e.* the boom is extended straight out horizontally. The β=0° case corresponds to the configuration when the boom is pointed toward the front of the cart (boom pointing to the right of the polar plot), and the β=180° case corresponds to the configuration when the boom is pointed toward the back of the cart (boom pointing to the left of the polar plot). The polar plot, therefore, is oriented in a similar manner as the top view of the mobile boom crane schematics shown in Figure 9.

The figure indicates that the crane has considerably less stability margin when the boom is extended to the front of the crane. It also has less marginal stability when the boom is pointed to either side. Toward the back, however, the crane shows very high

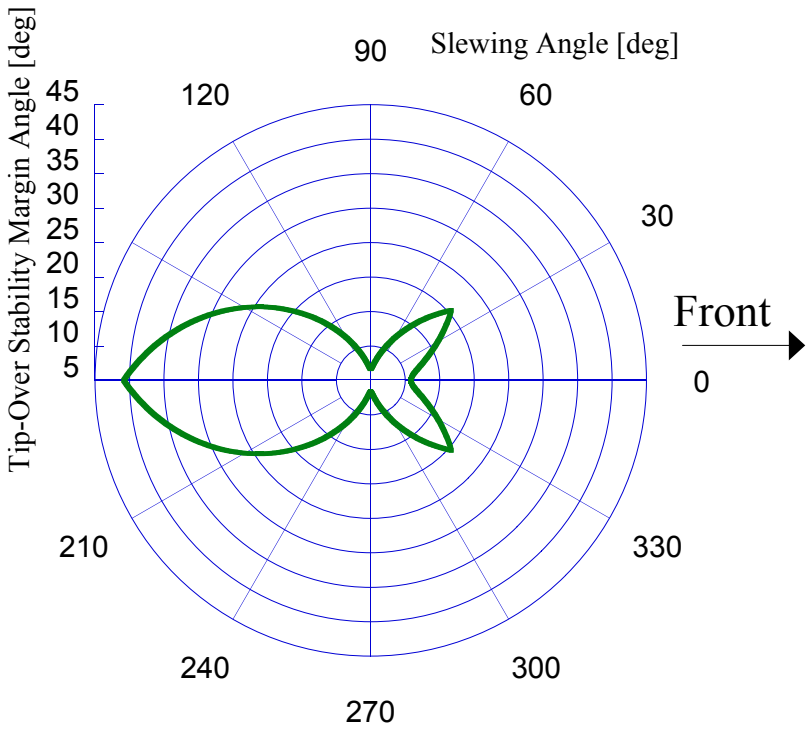

Figure 13: Tip-Over Stability Margin of Static Stability Analysis - [α=0°]

stability margin. This is because of the geometric location of the boom connection point to the platform. As seen in Figure 9, the boom is located toward the front of the cart, which makes the cart more vulnerable to the tip-over. In addition, since the cart platform is longer in the longitudinal direction than in the lateral direction (l_c larger than b_c) the mobile boom crane is more vulnerable to the tip-over to the sides, or in the lateral direction. Near the front, there are also two local maximums observed around β=±40°. These are the cases when the boom is pointing where the front wheels are. Since the wheels provide supporting forces to the mobile boom crane, the platform has extra tip-over stability margin when the boom is positioned toward the wheels. This behavior in the tip-over stability margin, however, is only observable when its magnitude is small. Small stability margin angles are more sensitive to the crane's configuration changes because the change has more significant weight relative to them than to large stability margin angles. Toward the back, the local maximums are not observed because the stability margin is too large to react on the change.

This insensitivity could lead to an error in the tip-over stability prediction because the model may fail to reflect on mobile boom crane's condition accurately.

To verify the accuracy of the tip-over prediction by experiment, the tip-over stability margins calculated in Figure 13 were converted into maximum possible payload values by finding the mass that makes the angle measures 0°. Figure 14 shows the maximum payload for the crane apparatus. In the figure, the polar plot shows the maximum possible payload against the slew angle β at the luffing angle α=0°. The solid line represents the predicted values, and the diamond marks indicate the experimental results. The experimental results show high agreement with the prediction line. Similar to the tip-over stability margins, the maximum possible payload values have local minimums at $\beta = 0°$, 90°, and 270°. There is also a local minimum at $\beta = 180°$, but the system shows high stability at the configuration due to how the apparatus is setup. The local minimum at $\beta = 90°$ and 270° are also the global minimum. Because at $\beta = 90°$ (and $\beta = 270°$), and $\alpha = 0°$, the boom points horizontally to the side and extends out the arm the farthest, which is intuitively the most unstable configuration that causes tip-over. Therefore, by limiting the payload mass to the maximum value at $\beta = 90°$, a tip-over stability of the mobile boom crane can be guaranteed over the whole workspace.

The prediction model was also tested at different configurations to check its robustness. Figure 15 shows the maximum payload values for the crane apparatus on Table 1 against the slew angle β at the different luffing angle of α=30°. The polar plot shows very similar tip-over stability trends from Figure 14. The maximum payload line presents the same shape for the stability-safe boundary, but on a different scale. The experimental results, again, shows a high agreement with the prediction line.

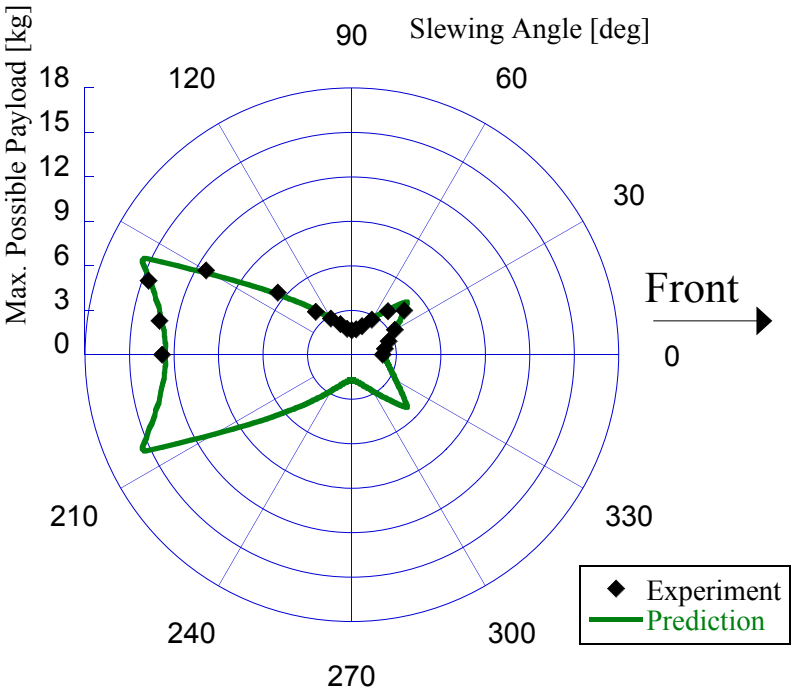

Figure 14: Maximum Possible Payload of Static Stability Analysis - [α=0°]

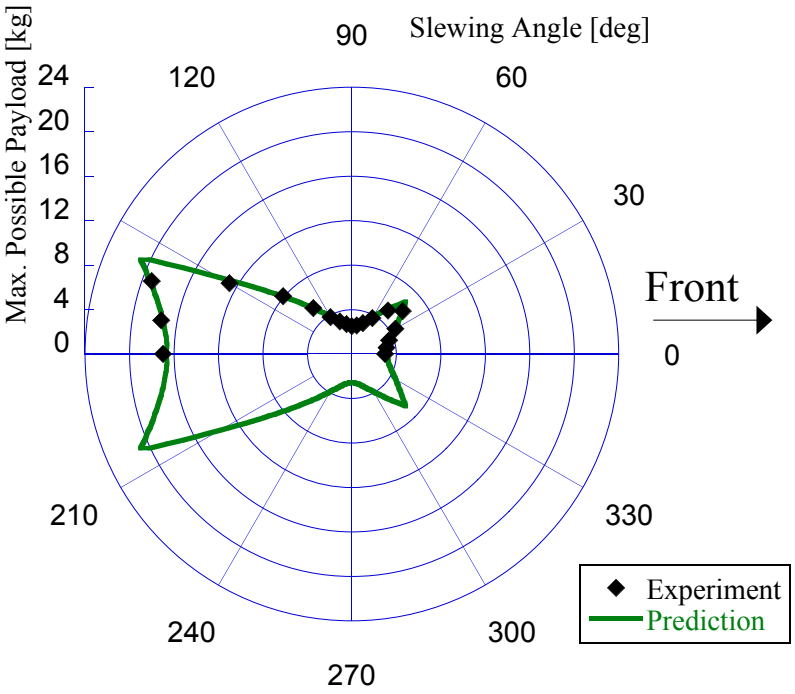

Figure 15: Maximum Possible Payload of Static Stability Analysis - [α=30°]

2.3 Effects of Variable Parameters

The behavior of the tip-over stability margin of the mobile boom crane can be altered by adjusting key geometric parameters. Some of the critical parameters that have the effects on the tip-over stability margin in the static stability analysis are the suspension cable length l, and the boom's center of rotation (adjusted by l_a) and the boom mass m_b [38]. In case if the crane is moving, longer cable allows the payload mass to swing wider, thus displaces the mass further away from the tip-over axis which leads to an increase of the tip-over torque. Changing the boom mass, m_b, influences the tip-over stability margin because the boom is often massive and long compared to the cart platform. It composes a significant portion of the mobile boom crane structure. Having a heavier boom decreases the tip-over stability of the crane and limits the maximum payload weight it can lift. Changing the rotational center position in the longitudinal direction (l_a) also changes the boom's position with respect to the cart. Because the boom is massive compared to the cart, this alters the behavior of the tip-over stability of the mobile boom crane. Depending on its position with respect to the system's center of mass, the boom can affect the tip-over stability of the crane either positively or negatively.

2.3.1 Effects of Varying the Luffing Angle

Another important parameter that also influences the tip-over stability margin is the luffing angle α. Through luffing motion, the location of the boom's center of mass can be displaced, similar to changing l_{bcom}. The plot in Figure 16 shows the tip-over stability margins of the system for a whole range of slewing angle β, at different luffing values; $\alpha = 0°, 30°, 45°$.

In all cases the stability margin exhibits a very similar shape, but with a different magnitude scale. For the front half of the boom crane, prediction lines with higher luffing angle shows higher stability margin than with lower values of α. This is because

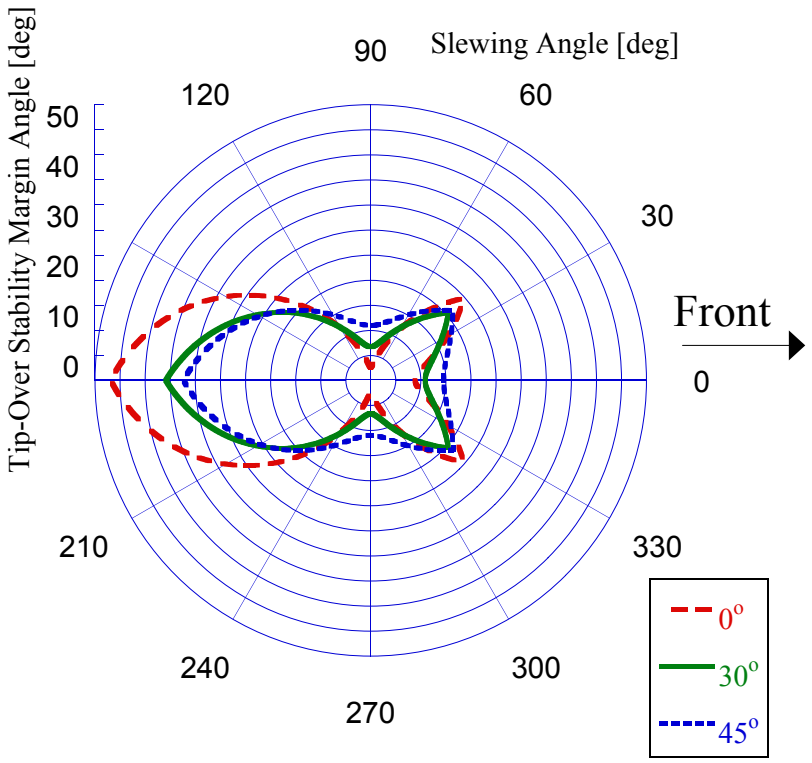

Figure 16: Tip-Over Stability Margin of Static Stability Analysis - Different Luffing Angles

when the boom is pointing toward the front the boom mass tends to contribute as a stabilizing force as the luffing angle increases, or the boom points up. Luffing up the boom brings the boom's center of mass closer to the geometric center and away from the tip-over axis of the cart at the front. Thus provides more stability. Luffing downward moves the boom mass closer to the cart's front tip-over axis, thus leads to a reduction in the tip-over stability. Therefore, in theory, the mobile boom crane system exhibits the highest tip-over stability at $\alpha = 90°$, and the lowest tip-over stability at $\alpha = 0°$. Therefore, by maintaining the luffing angle α to a high angle can contribute greatly to tip-over safety.

For the rear half of the cart, however, the tip-over stability behavior is reversed. The tip-over stability margin angle shows a decrease in its magnitude as the luffing

angle increases. This is because when the boom is pointed toward the rear, luffing the boom up brings the center of mass closer to the tip-over axis at the cart's front. Therefore, it is more desirable to keep the luffing angle low when the boom is pointed to the back of the cart. This helps to bring the center of mass closer to the cart's geometric center and away from the front tip-over axis, thus leading to greater stability.

2.3.2 Effects of Varying the Payload Mass

The payload mass m_p also significantly impacts the tip-over stability margin characteristics of mobile boom crane system. Because the payload is attached to the suspension cable at the boom tip, it can be positioned at a long distance away from the crane. This leads to a longer arm length in the tip-over torque calculation about the tip-over axis, thus creating greater tipping torque and lessening the tip-over stability. Adding more payload can further decrease the tip-over stability margin of the boom crane. Because the weight of the payload is a key parameter in the crane's operation, it is important to know how much weight the crane can handle without causing a tip-over accident. Some cranes come with configuration charts that show the maximum payloads throughout the configuration space. Such charts are shown in Figure 17.

Figure 18 shows the tip-over stability margin angle calculated for the mobile boom crane when carrying a payload mass of $2.0kg$ and $3.0kg$ at a luffing angle of $30°$ in the static case.

As shown on the plot, the $3.0kg$ case is clearly showing a lesser value of stability margin than the $2.0kg$ case, indicating that carrying a heavier payload does reduce the stability of the crane. In fact, when the boom slewing angle $\beta = 90°$ and $270°$, the tip-over margin for the $3.0kg$ case goes to $0°$, showing that the crane tips-over at that boom configuration. The effect is more apparent toward the front of the cart because

Figure 17: Maximum Payloads Charts

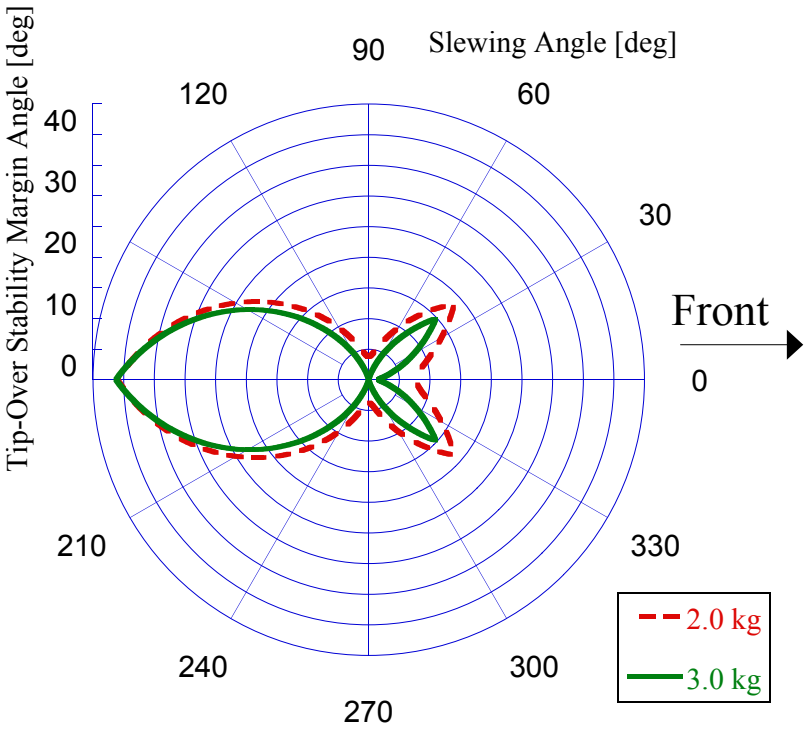

Figure 18: Tip-Over Stability Margin of Static Stability Analysis - Different Payload Mass

again the center of mass is located closer to the front due to the crane structural setup assumed.

Toward the back of the cart, the difference in the tip-over margin between the $2.0kg$ case and the $3.0kg$ case disappears. At $\beta = 180°$, the difference completely disappears and both payload mass cases show the same tip-over stability margin angle value. As mentioned before, the stability margin angle calculation becomes insensitive to the parameter changes as the boom points toward the back of the cart. The results from Figure 18 proves this point. This behavior, however, raises a concern as the tip-over stability margin angle may fail to accurately predict the actual tip-over in the real system. Since the margin angle is insensitive to the changes near the back, this may result in a prediction error at the rear of the cart.

By changing critical geometric parameters and boom crane configuration, the tip-over stability of mobile boom crane can vary significantly. Therefore, the conditions under which the crane is used need to be considered to obtain a full understanding of its tip-over stability behavior. In addition, the fact that the crane configuration is time-varying during operation needs to be highlighted. When the crane is used lift payloads in the area where the target objects are easy to reach, the crane has more freedom to configure its boom orientation. Thus, the boom can be positioned in a tip-over stable configuration and is able to lift heavy payload mass. However, during its operation, there is always a chance that the operator might accidently bring the boom to a less stable configuration after hoisted the heavy payload. This may cause the crane to tip-over. To avoid such dangers, the crane configuration and the tip-over stability margin must be continuously checked throughout the operation. Therefore, a tip-over checking tool that can be easily updated and has fast computation speed is highly important.

2.4 Summary

In this chapter, the most simple case of tip-over stability analysis was introduced to gain a basic understanding of the nature of the problem. The simple prediction model of the mobile boom crane and the stability margin method to determine the stability of the system were described. The prediction model is composed of only the most fundamental structures and was developed to incur the minimal computational cost. The tip-over stability margin provides a useful index which characterizes the system's tendency to tip-over for the given system configuration. The system is considered tip-over stable as long as the index remains positive.

Using these tools, the static stability analysis was performed for the case where the crane is stationary. The maximum possible payload values were calculated for the boom crane setup over the whole range of slewing angles β at different luffing angles α. The analysis reveals the general nature of the mobile boom crane's tip-over stability. The crane is found to be the least stable when the boom is directly pointed to the front or to the sides. The stability margin calculation toward the rear of the cart raises a concern about the accuracy of the tip-over prediction, due to its insensitivity to the parameter changes.

The effects of changing key crane parameters on the tip-over stability was also analyzed. The crane's stability is reduced when the boom is luffed down lower and is attached to a heavier payload. Adjusting the crane configurations by varying some critical geometric parameters brings advantages and disadvantages to the tip-over stability. An experimental apparatus was presented and used to verify the analytical results.

CHAPTER III

SINGLE-PENDULUM PSEUDO-DYNAMIC STABILITY ANALYSIS

3.1 Description of Approach

To develop a practical tool to investigate the tip-over stability of mobile boom cranes, the prediction model developed in the previous section to perform a static stability analysis needs to be extended to incorporate dynamic effects. The two main dynamic effects that need to be considered are payload swing and the inertia forces acting on the cart and the boom. Because one of the goals of this thesis is to develop a simple tip-over prediction tool that requires minimal computational cost, the swing angles φ and θ (in the longitudinal and the lateral direction with respect to the cart) from Figure 9 are still regarded as constants in this Pseudo-Dynamic Stability Analysis, *i.e.* the suspension cable with payload is deflected, but remains fixed in a deflected position as if the cable was a rigid body. The time-dependency of the centripetal and gravitational force derived from the pendulum swing is also simplified as a time-invariant constant force. To make the prediction conservative, the magnitude of the maximum swing angle is computed and applied to the prediction model. This corresponds to the worst case scenario when the payload swing most aggressively compromises the crane's tip-over stability.

The swing deflection reduces the mobile boom crane's tip-over stability because it displaces the payload mass outward, as shown in Figure 19. The deflection increases the moment arms of the payload about the tip-over axes by the lengths d_1 and d_2. As the result, the crane cannot support as much payload as it can in the static case. The maximum possible payload value decreases with increasing payload deflection.

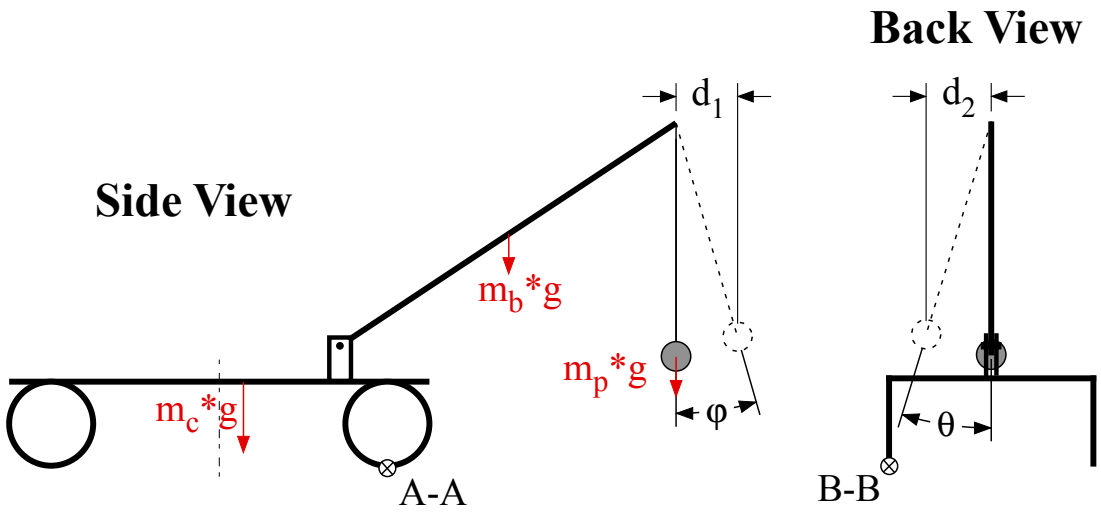

Figure 19: Payload Deflection in Pseudo-Dynamic Stability Analysis [38]

3.1.1 Verification of the Approach

To establish the validity of the method, the tip-over moment contributions calculated from a non-linear simulation, including full dynamic effects such as centripetal forces of swing, are compared with those of the estimations obtained from the fixed swing angle approach described above. Figure 20 illustrates the boom crane model used for the comparison for the longitudinal payload swing case. The boom has a length of l_b. The cable attached at the end of the boom has a length l. To simplify the comparison and observe the moment contribution from the payload clearly, the boom and the cable are assumed to be massless. In addition, by summing the moments at the boom attachment point, the reaction forces acting at the attachment point make zero contribution to the tip-over torque. Thus, they can be omitted from this analysis.

For the full dynamic payload swing case, the torque, T_{long}, caused by the weight and the swing of the payload about the boom attachment point is time dependent and can be expressed as:

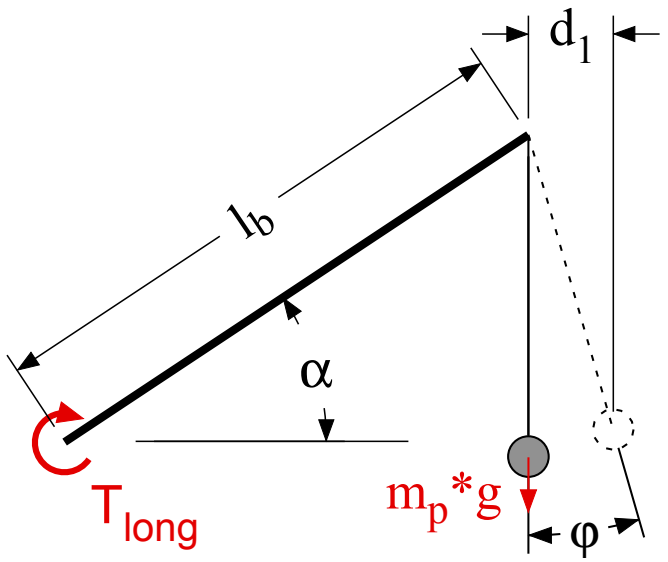

Figure 20: Boom Crane Model for Longitudinal Payload Swing [38]

$$T_{long,dyn} = (m_p g \cos\varphi(t) + m_p l \dot{\varphi}^2(t)) l_b \cos(\alpha - \varphi) \tag{3.1}$$

The pseudo-dynamic estimation method, on the other hand, returns a constant magnitude of T_{long}:

$$T_{long,semi} = m_p g (l_b \cos\alpha + l \sin\varphi_{max}) \tag{3.2}$$

Defining the relative error in T_{long} between the simulation and simple estimation as:

$$\frac{T_{long,semi} - T_{long,dyn}}{T_{long,dyn}} \tag{3.3}$$

the error in tip-over moment calculation using the pseudo-dynamic estimation method is obtained. Note that the payload mass m_p term appears in both the full dynamic and pseudo-dynamic equations. Therefore, the magnitude of the payload weight does not affect the relative error calculation.

Figure 21 shows the relative error of the pseudo-dynamic estimation for the case when $l_b = 1.7m$ and $l = 1.0m$. The error surface plot is given as a function of the

luffing angle α in degree and the maximum swing angle φ_{max}.

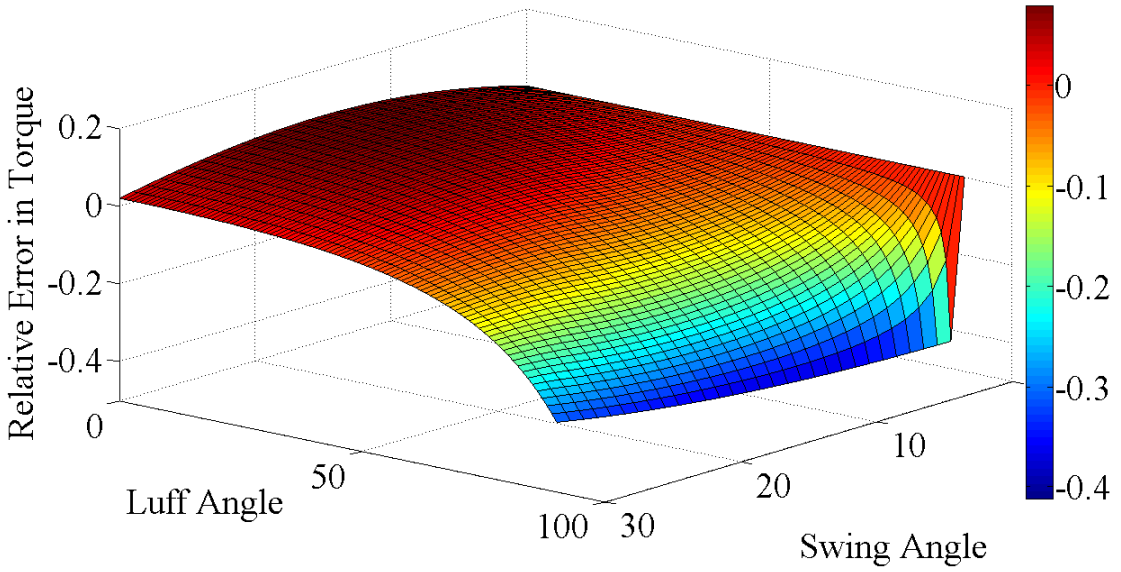

Figure 21: Relative Error of Pseudo-Dynamic Estimation for Longitudinal Payload Swing [38]

From Figure 21, the relative errors in the estimation turn out to be positive for small luffing angles. This indicates that the torque T_{long} is over-estimated by the pseudo-dynamic method. This means that the pseudo-dynamic method produces a conservative estimate of tip-over stability. For large luffing angles, on the other hand, the torque T_{long} is under-estimated by the pseudo-dynamic method. This may become a concern because the pseudo-dynamic estimation is predicting maximum possible payload values that are larger than what a real system can handle. However, as mentioned in previous section, large values of luffing angle are favorable in terms of the tip-over stability. Therefore, it is more critical to accurately predict the tip-over conditions when the boom is extended at small luffing angles. For that reason, the torque estimation error at large luffing angles is investigated no further in this thesis. It was also found that the maximum swing angle contributes much less to the T_{long} estimation error than the luffing angles.

A comparison between the pseudo-dynamic estimation method and the full dynamic payload swing in the lateral direction was also conducted. Figure 22 shows the boom crane model and the payload swing angle in the lateral direction with respect to the cart platform. The torques applied about the boom attachment point are indicated as $T_{lat,1}$ and $T_{lat,2}$. Since the payload swing is now out of plane, there are two torques about two possible tip-over axes that need to be compared.

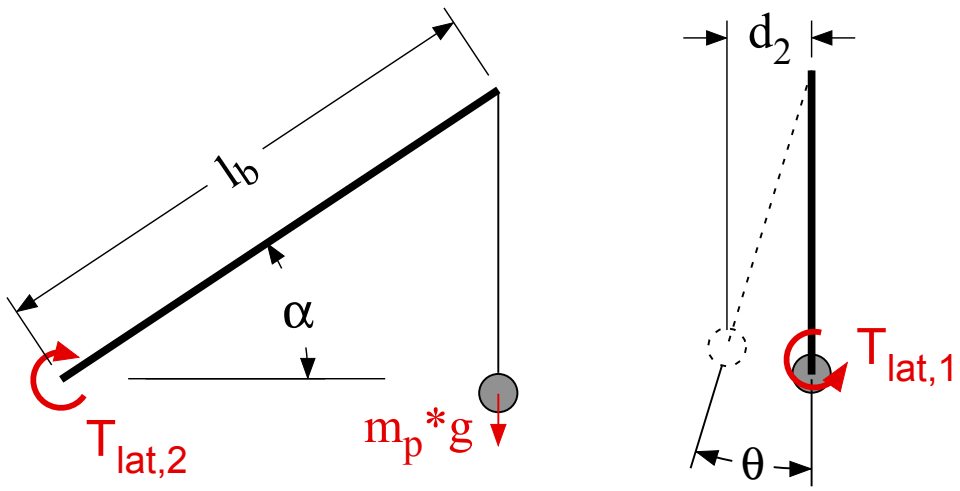

Figure 22: Boom Crane Model for Lateral Payload Swing [38]

The full payload swing dynamics produce time-dependent equations for the torques:

$$T_{lat,1,dyn} = (m_p g \cos\theta(t) + m_p l\dot{\theta}^2(t))l_b \sin\alpha \sin\theta(t) \tag{3.4}$$

$$T_{lat,2,dyn} = (m_p g \cos\theta(t) + m_p l\dot{\theta}^2(t))l_b \cos\alpha \cos\theta(t) \tag{3.5}$$

Using the pseudo-dynamic estimation method, the above equations are simplified to:

$$T_{lat,1,semi} = m_p g l \sin\theta_{max} \tag{3.6}$$

$$T_{lat,2,semi} = m_p g l_b \cos\alpha \tag{3.7}$$

Again, because m_p can be factored out in all the equations, the relative error between the T_{long} and the T_{lat} calculated in the two methods is independent of the payload weight.

Figure 23 shows the relative error plot for $T_{lat,1}$ for the same luffing and swing angles as Figure 21. Again, the relative error is computed for different combinations of the luffing angle α and the maximum swing angle φ_{max}. The plot shows very small error at almost the whole range of luff and swing angles. The error, however, increases and approaches infinity as α approaches to 0°. This is due to the fact that the torque calculated by the full dynamic equation approaches zero in this configuration, which also causes the denominator of the relative error equation to go to zero. The pseudo-dynamic estimation, however, returns a nonzero torque at α=0°. This over-estimation is negligible when there is only a small magnitude of payload swing. It does, however, helps to make the tip-over prediction more conservative.

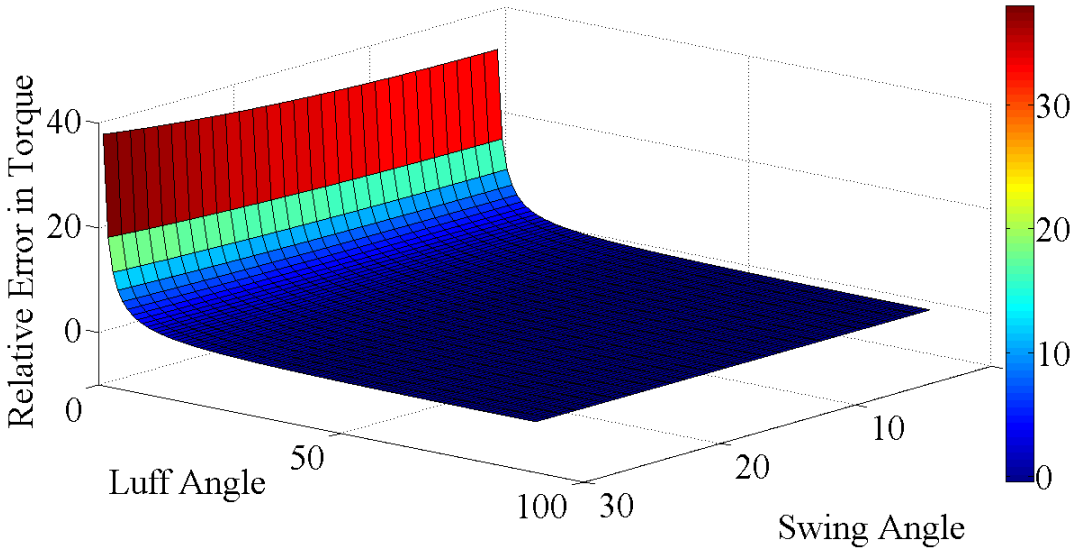

Figure 23: Relative Error of Semi-Dynamic Estimation for Lateral Swing I [38]

Figure 24 presents the relative error for $T_{lat,2}$. The plot shows a steady increase

in the error calculation with increasing payload swing angle. This problem originates from the limitation of the pseudo-dynamic estimation method. In the full pendulum dynamics the payload swing induces a centripetal force pointing down, and thus induces the torque which pulls the boom tip downward. The pseudo-dynamic method, however, omits this torque contribution. The method only considers the maximum payload swing in the lateral direction to simplify the computation. This deficiency is compensated by taking a conservative measure of including the maximum lateral swing angle not only in the lateral direction but also in the longitudinal direction as well. This, however, does not guarantee to eliminate the deficiency. Since a part of the tipping torque is neglected in the pseudo-dynamic stability analysis, this could lead to an over-estimation of the tip-over stability of the mobile boom crane.

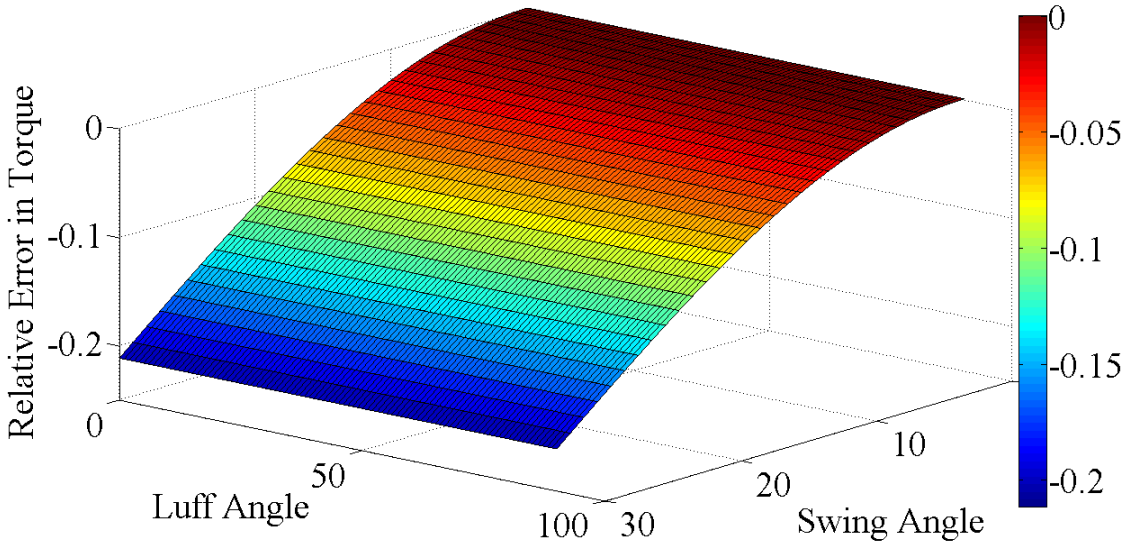

Figure 24: Relative Error of Semi-Dynamic Estimation for Lateral Swing II [38]

In general, the pseudo-dynamic estimation method predicts the tip-over torques due to the payload swinging well when the luffing and the swing angles are limited to small magnitudes. Under this restricted circumstance, there is a high confidence that the pseudo-dynamic estimation method can lead to a reliable tip-over stability prediction. Luckily, these conditions correspond to the configurations that have the

worst tip-over stability. Therefore, the approach works well for finding the worst-case scenario.

In summary, following factors on the mobile boom crane were ignored in the pseudo-dynamic stability analysis.

- Full payload swing dynamics
- Time-dependency of the centripetal and gravitational force derived from the pendulum swing
- Time-dependency of inertia forces acting on the crane at its center of mass
- Payload damping (has a frictionless pivot and no air drag)

3.1.2 Experimental Verification

To obtain the experimental data for the tip-over stability of the mobile boom crane in motion, the setup shown in Figure 12 was used. The boom was fixed to a testing configuration. To re-create the dynamic effects, the payload was given an initial swing angle deflection equal to the maximum expected magnitude it would experience during the motion. The payload mass was increased incrementally until the apparatus exhibited bucking after releasing the payload from the initial position. The largest payload value that did not cause any bucking in the crane apparatus was recorded as the maximum possible payload for that boom configuration.

The experimental setup, however, had one limitation. Because the apparatus was not equipped with any actuators, the crane had to remain fixed during the experiments. Therefore, the inertial forces acting on the system could not be re-created. This may result in some discrepancies between the experimental data and the actual tip-over stability of the mobile boom crane.

3.2 Straight Base Motion

The simplest motion input a mobile boom crane can make is a straightline base acceleration. The straightline base motion considered here as a benchmark is a point-to-point motion.

3.2.1 Crane System and Payload Swing Dynamics

To estimate the maximum swing angle resulting from a base-acceleration input command, a closed-form solution of the pendulum swing is derived. The equation of motion for an undamped, single-pendulum with an accelerating suspension point is given by:

$$\ddot{\varphi}(t) + \omega^2 \sin\varphi(t) = -\frac{d^2x(t)/l}{dt^2}\cos\varphi(t) \tag{3.8}$$

where φ is the swing angle, ω is the natural frequency of the pendulum, and x is the position of the suspension point. Assuming a small angle approximation for φ ($\varphi \ll 1 \Rightarrow \sin\varphi \approx \varphi, \cos\varphi \approx 1$), the equation is linearized as:

$$\ddot{\varphi}(t) + \omega^2\varphi(t) = -\frac{d^2x(t)/l}{dt^2} \tag{3.9}$$

Defining $\frac{d^2x(t)}{dt^2} = a(t)$, (3.9) can be re-written as:

$$\ddot{\varphi}(t) + \omega^2\varphi(t) = -\frac{a(t)}{l} \tag{3.10}$$

Taking the Laplace transformation of (3.10) gives:

$$s^2\Phi(s) + \omega^2\Phi(s) = -\frac{A(s)}{l} \tag{3.11}$$

Re-arranging the equation, the transfer function of the system is then:

$$G(s) = \frac{\Phi(s)}{A(s)} = -\frac{1}{l(s^2+\omega^2)} \tag{3.12}$$

The time-optimal command with an acceleration limit is a bang-coast-bang command, as shown in Figure 25, is used as a representative input to move the base in a point-to-point motion. The bang-coast-bang command can be described as an acceleration step command with magnitude M that consists of four steps; two positive and two negative.

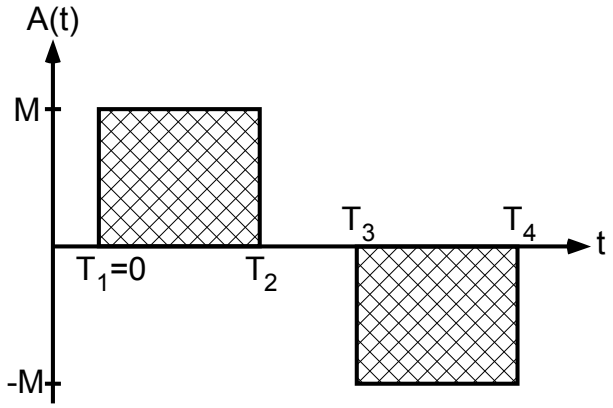

Figure 25: Bang-Coast-Bang Acceleration Command

The bang-coast-bang command creates a trapezoidal velocity profile. In the Laplacian domain, the command can be expressed as:

$$A(s) = \frac{M}{s}(1 - e^{-T_2 s} - e^{-T_3 s} + e^{-T_4 s}) \tag{3.13}$$

where M is the magnitude of the acceleration input and the T_i is the corresponding timings of the i^{th} step in the command. The pendulum swing is going to cause the most significant contribution to the tip-over instability when the swing angle is maximized. This happens when the impulse timings are in phase with each other so that the payload swing caused by each acceleration step adds constructively and produces the highest payload swing amplitude.

The maximum payload swing amplitude can be determined from the dynamic equation of motion of a single-pendulum in time-domain. To obtain this worst case swing angle, the bang-coast-bang acceleration input command in Laplacian domain

shown in (3.13) is substituted into the system transfer function in (3.12). The resulting expression for $\Phi(s)$ is then transformed back into the time domain by taking inverse Laplace transformation.

$$\begin{aligned}\varphi(t) = -\frac{M}{l\omega^2}\Big(\Big(1-\cos\big(\omega t\big)\Big) - \Big(1-\cos\big(\omega(t-T_2)\big)\Big)\sigma(t-T_2) - \\ - \Big(1-\cos\big(\omega(t-T_3)\big)\Big)\sigma(t-T_3) + \\ + \Big(1-\cos\big(\omega(t-T_4)\big)\Big)\sigma(t-T_4)\Big)\end{aligned} \tag{3.14}$$

Equation (3.14) shows that the maximum swing angle occurs when each of the cosine terms are all in phase, and the multiplying step functions σ are all equal to 1 (which means that the running time is long enough, $t \geq T_4$, to supply an entire set of the bang-coast-bang command). The cosine terms are in phase when the four steps of the bang-coast-bang command are supplied in a perfect timing to add constructively. Thus, in the worst case, the payload swing angle reaches as large as four times that of the swing caused by a single step input. The maximum swing angle magnitude then can be expressed as:

$$|\varphi_{max}(t)| = \frac{4M}{g} \tag{3.15}$$

The steps are perfectly in phase to produce the maximum pendulum swing only when the following conditions are satisfied. First, the time interval between the first and the second steps, as well as the third and the fourth steps, must be half of the oscillation period T; $T_2 - T_1 = T_2 = T_4 - T_3 = (0.5+n)T$ where n = 1,2,3 ... . The time delay is necessary because the steps in the sets have opposite signs. Thus, this time delay is equivalent of inducing a phase delay of π to opposite sign functions, which ultimately cancels the phase shift and brings two functions in phase. Secondly, the time interval between the second and the third impulses must contain the time delay of a multiple of the period T; $T_3 - T_2 = nT$ where n = 1,2,3... . Similarly, this

is because the second and the third steps have the same sign, so a phase shift of 2π is required to have them in phase.

To verify the accuracy of this result, a nonlinear single-pendulum simulation is used to obtain the swing angle response and the maximum swing amplitude at various conditions. Note that because the swing angles φ and θ are measured with respect to the cart, the boom configuration is arbitrary. In the test cases examined here, the crane's base is accelerated at a constant rate of $1.0m/s^2$ up to a maximum speed. The base decelerates at the same rate, but negative in value. The suspension cable length l is set to $1m$, which induces the swinging natural frequency of $\omega_n = \sqrt{\frac{g}{l}} \approx 3.13rad/s$. At this natural frequency and the base acceleration, the command steps are in phase when the time interval between the first and the second steps, as well as the third and the fourth steps, is roughly equals to $1sec$. The maximum velocity of $1m/s$ is reached ($T_2\omega = (T_4 - T_3)\omega = 1s \times 3.13rad/s \approx \pi$).

Figure 26 shows the maximum swing angles for different maximum speeds at an acceleration of $1m/s^2$. The humps in the curves indicate when the first and the second pair of cosine terms in (3.14) are in phase. According to the linear approximation in (3.15), the maximum swing angle for this maneuver is $0.41rad$. That value agrees well with the plot of these nonlinear results.

The plot also shows that the maximum swing angle occurs at the maximum velocity of $1m/s$, as predicted. The other maximum velocity cases produce lower swing angles because neither the first and the second nor the third and the fourth cosine terms in (3.14) are in phase.

Another interesting behavior that can be observed is that the maximum swing angle cannot be reduced below $0.2rad$ for v greater than or equal to $1m/s$. This lower boundary limit is the amplitude of deflection caused by the first positive acceleration to speed up the base. The only way to reduce the maximum swing angle lower than this value is to limit the positive acceleration pulse very short and lower the

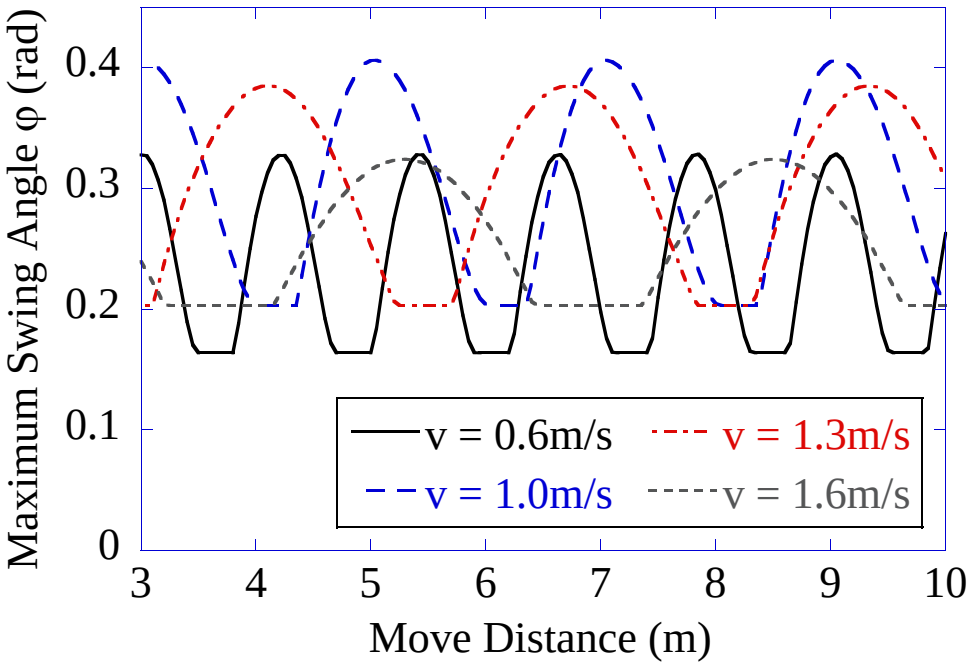

Figure 26: Maximum Swing Angles as a Function of Move Distance [38]

maximum velocity v below $1m/s$. This option is shown in Figure 26 for the case of $v = 0.6m/s$. Another way to reduce the maximum swing angle is to introduce a jerk limitation in acceleration, which leads to a trapezoidal acceleration profile and realizes the smoother crane motion. However, this thesis only investigates the time optimal bang-coast-bang command because it is very common and aggressive, so it often induces noticeable swing deflections. Furthermore, many cranes are operated with on/off accelerations due to ease of implementation.

With a high-magnitude acceleration and deceleration commands, the mobile boom crane experiences the inertia forces acting on the cart and boom mass. These significantly influence the tip-over stability of the crane. The effect is more apparent when the crane's center of mass is located high above the ground because it makes the crane system more susceptible to tip-over, as mentioned in Section 2.1. The location of the center of mass can be raised by luffing the boom upward. This effect increases with increasing boom mass and distance from the boom attachment point to the boom

center of mass. Therefore, the inertia effects must be included to obtain a reliable estimation of the tip-over stability margin of the crane.

The inertial force effect can be incorporated in the prediction model shown in Figure 9 by using the concept presented in Section 2.1. At the shown configuration (when the boom points toward the front), the inertia force acts toward the center of mass during the acceleration phase, thus, it contributes positively to the tip-over stableness. On the other hand, the tip-over stability is compromised when the crane base is decelerating. Thus, the prediction model takes into account the inertial effects during the deceleration of the crane. The effects are estimated by applying D'Alembert's Principle. D'Alembert's Principle states that if the dynamic behavior of a mass is analyzed in an accelerated, body-fixed reference frame, then the inertia forces, which are fictitious forces in general, have to be regarded as real forces acting on the mass. Applying this concept, Figure 27 shows the free body diagram with the inertia forces acting horizontally on the crane system during deceleration.

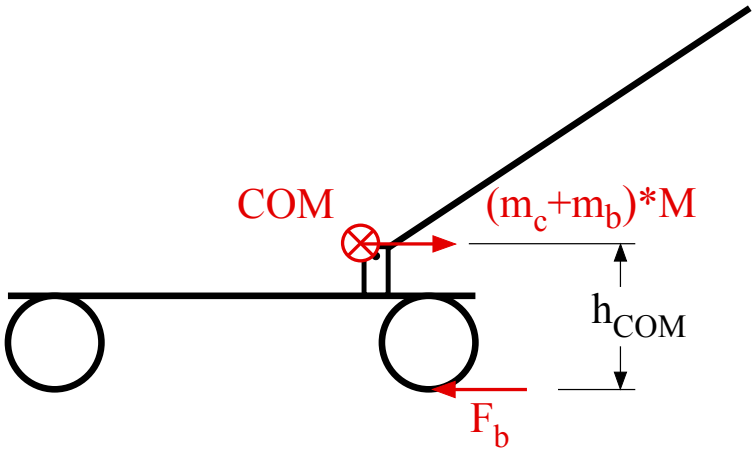

Figure 27: Free Body Diagram of Mobile Boom Crane with Inertia Forces During Deceleration [38]

The center of mass of the crane system itself lies somewhere on the line connecting the centers of mass of the cart and the boom. The inertia force acting on the crane center of mass and the braking force F_b acting on the wheels cancel in the horizontal

direction. However, they create a couple that contributes to the tip-over instability. This couple is determined by multiplying the inertia force by the height of the center of mass above the ground, h_{COM}. Since it is assumed that the cart decelerates at a constant rate, M, the couple is also assumed to be constant.

3.2.2 Tip-Over Stability Analysis

Figure 28 shows the maximum possible payload values predicted by the pseudo-dynamic stability analysis for the straightline base motion. The dashed line and the solid line indicate the cases when the base is given an acceleration of $0m/s^2$ (the static case) and $1.0m/s^2$ respectively. The luffing angle is fixed at $\alpha = 30^\circ$ for the comparison. The plot clearly illustrates the effect of driving the base forward. Compared to the static case, the maximum payload values of the $1.0m/s^2$ case are reduced over a wide range of boom slew angles. This is because the payload swing and the inertia force caused by the driving acceleration are making the crane less stable. Toward the back of the cart, however, the pseudo-dynamic method is predicting an increase in the tip-over stability. In Chapter 5, the full dynamic simulation results reveal that this is an over-estimation and does not accurately reflect on the actual tip-over stability of the mobile boom crane. As mentioned in Section 2.2, the tip-over stability margin calculation tends to cause prediction error toward the back of the cart. In addition, the pseudo-dynamic stability analysis treats the payload swing as a constant deflection to the front of the base. As discussed, this simplifying assumption amplifies the estimation error as the magnitude of the input increases and causes more payload swing.

Experiments were conducted to verify the above results. In Figure 29 and Figure 30, the experimental results of the straightline base motion with acceleration magnitude of a=$1.0m/s^2$ at luffing angles of α=30° and 45° respectively are plotted along with the pseudo-dynamic stability analysis predictions. The prediction is shown by

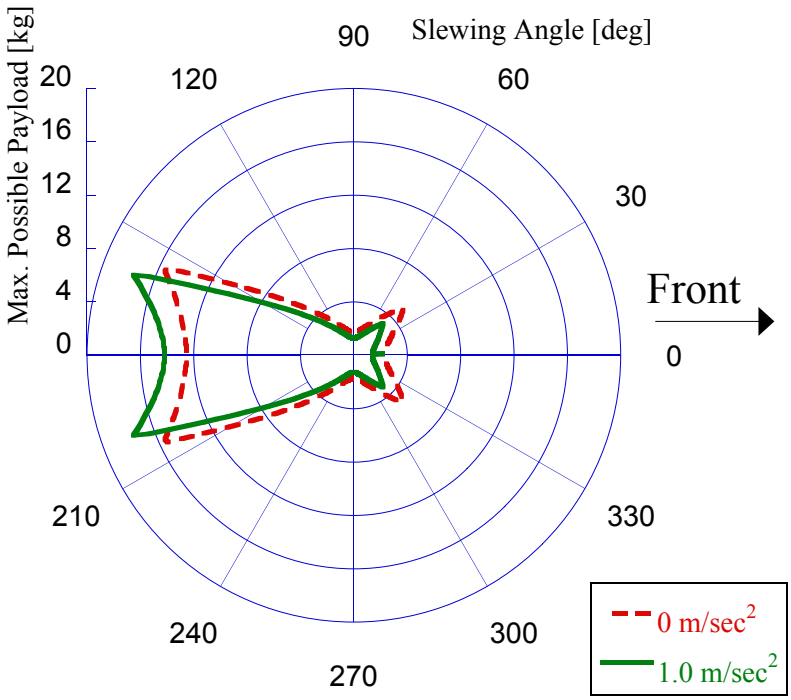

Figure 28: Maximum Possible Payload of Pseudo-Dynamic Stability Analysis for Straight Base Motion

the solid line, and the experiment results are shown in the diamonds. In both figures, the plots show a high agreement between the data and the prediction over most of the critical areas. The predictions return the values that are close to and yet conservative compared with the experimental data. The slight difference may be due to the effect of the inertia forces which are unable to be reproduced with the experimental apparatus. The results verify that the pseudo-dynamic stability analysis successfully includes the dynamics effects and the payload swing into the tip-over prediction. The method is also robust enough to be applicable at the different luffing angles. The method, however, shows a mismatch near the rear of the cart. For the slewing angle range of $\beta = 160°$-$180°$, the prediction is returning excessive over-estimation of the maximum payload values. This again is due to the limitation in the pseudo-dynamic stability analysis and the tip-over stability margin calculation. This region, however, is the most stable; the method functions well in more critical operational

configurations.

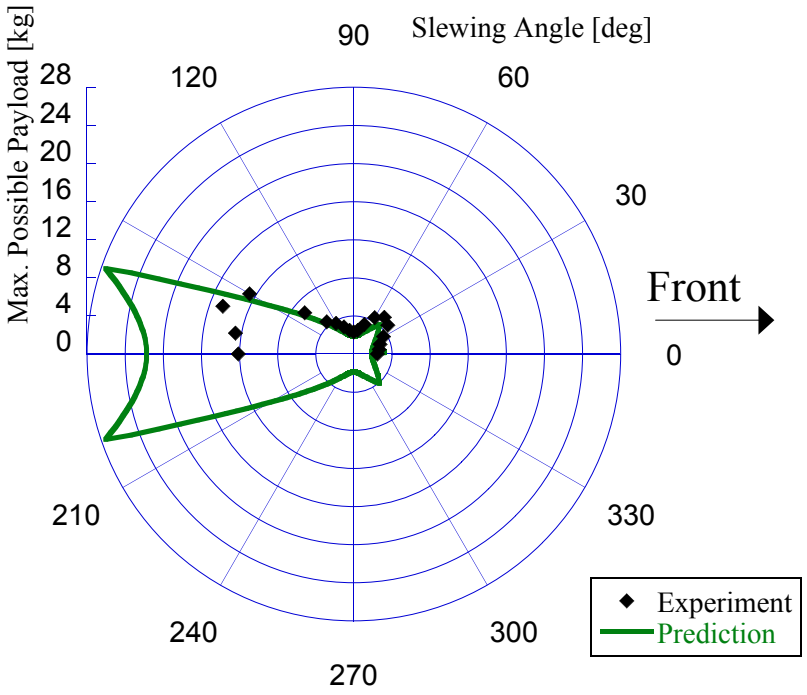

Figure 29: Experimental Data of Pseudo-Dynamic Stability Analysis for Straight Base Motion - [a=1.0m/s^2, α=30°]

3.3 Circular Path Motion

To extend the pseudo-dynamic stability analysis to a more general planar driving motion, the dynamic effects of the mobile boom crane undergoing a curvature path, thus moving in the 2D plane, was studied. In the past research, a study was conducted to investigate the mobile boom crane's behavior moving through a 90° corner [38]. Although the study suggested the applicability of the pseudo-dynamic stability analysis method to the 2D planar motion case, it did not conclude with a clear proof of the method's applicability on the concept. For that reason, this thesis investigates the simpler planar motion of a mobile boom crane moving in a circular path with a constant velocity.

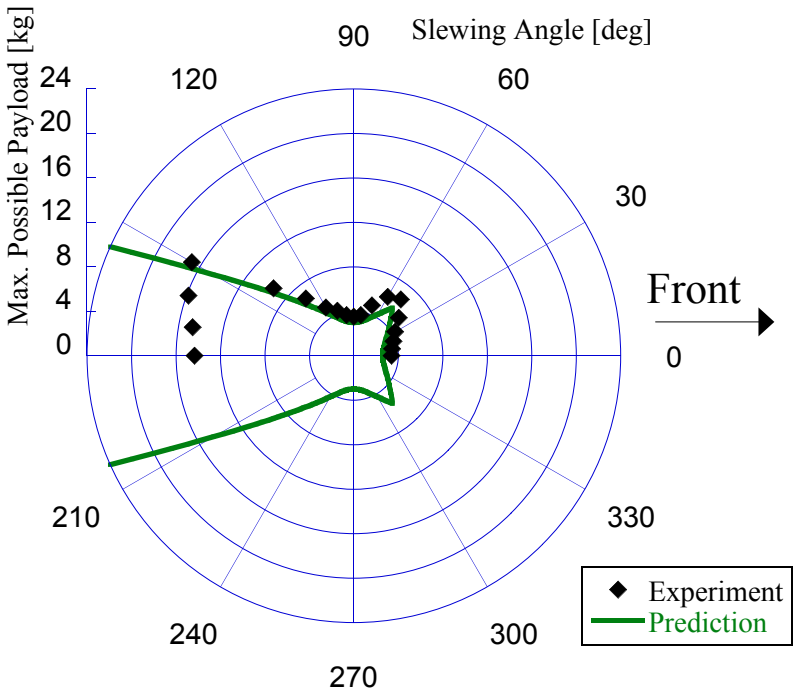

Figure 30: Experimental Data of Pseudo-Dynamic Stability Analysis for Straight Base Motion - [a=1.0m/s^2, α=45°]

3.3.1 Crane System and Payload Swing Dynamics

Figure 31 illustrates the circular path setup considered for the thesis. In the figure, the mobile boom crane cart drives in the counter-clockwise direction at a constant velocity, v. The cart has its center of mass and the steering center at its front wheel axis, consistent with the locations indicated in Figure 9. The circular path has a radius of curvature, r_{curv}, between the path center and the steering center. The radius of curvature is defined as:

$$r_{curv} = \frac{l_c}{tan(\gamma_{max})} \tag{3.16}$$

where l_c is the wheel base and γ_{max} is the maximum steering angle. For this study, the values of 1.1m and 0.35rad are used for lc and γ_{max} respectively. These values correspond to r_{curv} of about 3.0m.

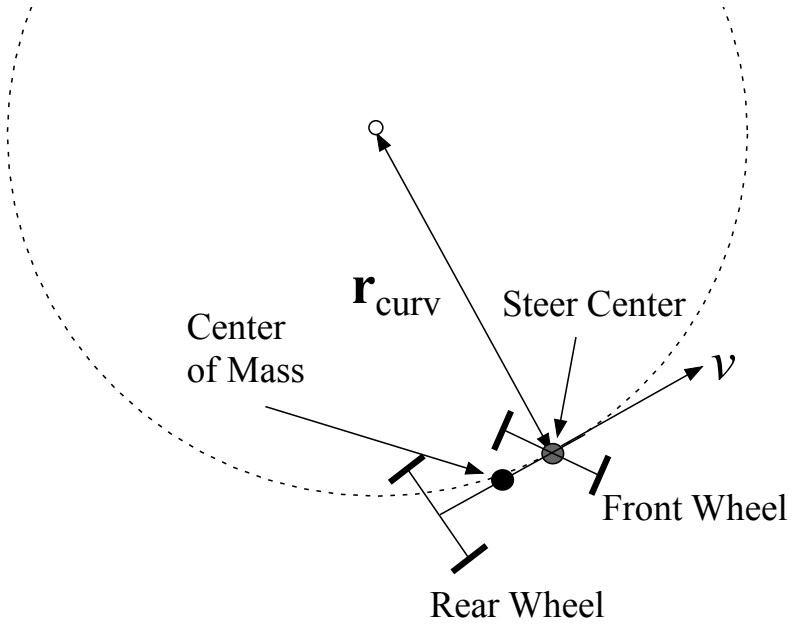

Figure 31: Geometrical Sketch of Circular Path Motion

When the mobile boom crane drives in a circular motion, it experiences an acceleration perpendicular to the direction it is driving (the centripetal force). This causes the crane to experience the inertial forces and payload swing, as shown in Figure 32. Since the cart velocity is constant, there is no acceleration tangential to the circular path.

The mobile boom crane's main body, the cart with mass m_c plus the boom of mass m_b, experiences the inertia force F_{cm} at its center of mass. By assuming that all of the cart's mass is concentrated at a point, and the inertia force acts only in a 2D plane, the F_{cm} can be computed as:

$$F_{cm} = \frac{(m_c + m_b)v^2}{r_{cm}} \tag{3.17}$$

where r_{cm} is the distance between the curvature center and the mobile boom crane's center of mass. This distance can be computed from r_{curv} and the cart's geometric parameters. The centripetal force acts on the center of mass in the same direction as r_{cm}.

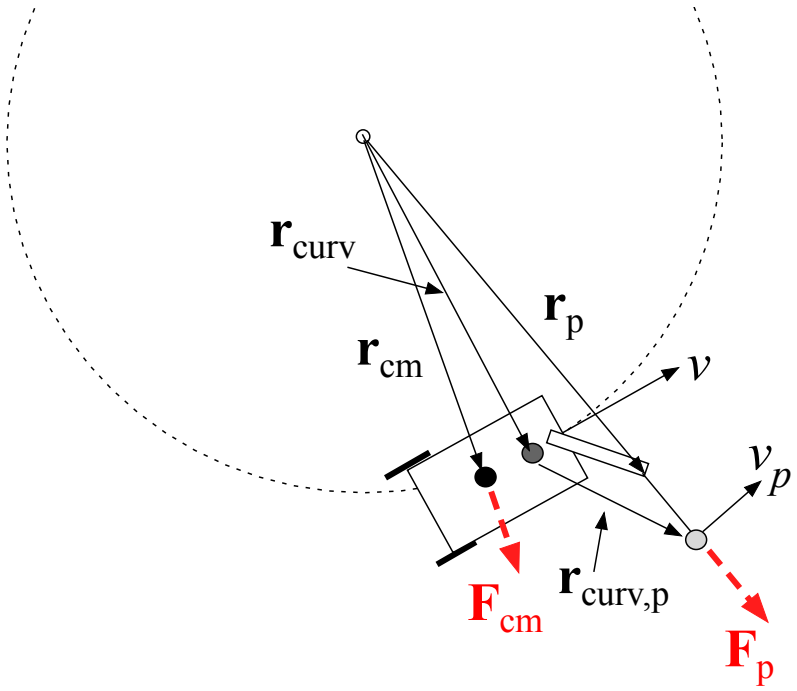

Figure 32: Inertia Forces in Circular Path Motion

The pendulum payload mass, m_p, is also subjected to the centripetal force F_p. The position of the payload from the curvature center is defined by r_p, which is computed from the sum of the position vectors $\vec{r}_{curv}$ and $\vec{r}_{curv,p}$. If the cart is traveling at the constant rotational speed ω, then the speed of the payload, v_p, is given by:

$$v_p = \omega r_p = \frac{v}{r_{curv}} r_p \tag{3.18}$$

Similar to the inertia force calculation at the center of mass, the centripetal force acting on the payload is then calculated by:

$$F_p = \frac{m_p v_p^2}{r_p} \tag{3.19}$$

Again, it is assumed that F_p acts in the same direction as r_p in 2D. Since the cart is traveling at the constant speed, the inertia forces F_{cm} and F_p also have constant magnitudes, but with varying directions. The payload swing angle traveling is calculated from the forces applied to the payload.

Figure 33 shows the forces applied to the payload. The payload is subjected to the gravitational force vertically and the centripetal force F_p horizontally. This produces a swing angle of φ which is calculated by:

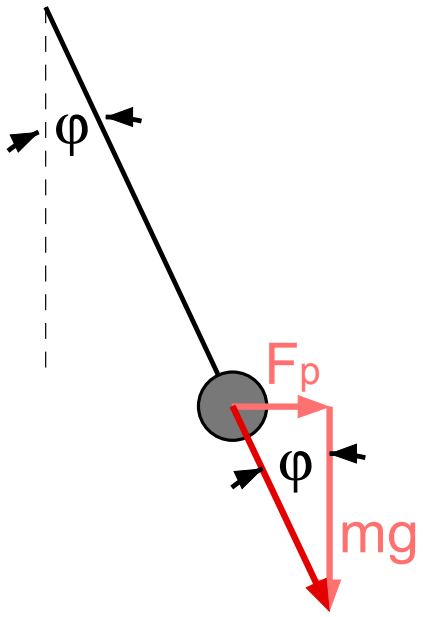

Figure 33: Forces Acting on the Payload in Circular Path Motion

$$\varphi = tan^{-1}\frac{F_p}{mg} \tag{3.20}$$

The horizontal deflection of the payload is then obtained by $l\sin(\varphi)$, where l is the suspension cable length. Because the deflection is in the same direction as F_p, it needs to be decomposed into the longitudinal and the lateral direction with respect to the cart to be included into the tip-over prediction model.

3.3.2 Tip-Over Stability Analysis

The inertia force F_{cm} and the payload swing angle were included to the simple prediction model shown in Figure 9. Figure 34 shows the maximum possible payload values predicted by the pseudo-dynamic stability analysis at the different cart velocities of: $1.0m/s$, $2.0m/s$, and $3.0m/s$. Unlike the static and the straightline base motion case,

the polar plots are not in a mirror image about the 0°-180° axis. It can be observed that the plots are slightly shifted to upward (toward the 90° direction). This indicates that the mobile boom crane is more stable when the boom is pointed to the left and less stable when it is pointed to the right from the driving direction. The behavior is more apparent at the higher cart velocities. This shift occurs because the cart is driving a circular path in the counter-clockwise direction. Having the boom pointed toward the center of the curvature (to the left) reduces the curvature distance, thus decreases the centripetal force applied and makes the cart platform more stable than pointing the boom away from the curvature center (to the right). If the cart drove in the clockwise direction, then the shift would to occur in the opposite direction (toward the 270° direction). The pseudo-dynamic stability analysis successfully reflects this behavior into the tip-over prediction.

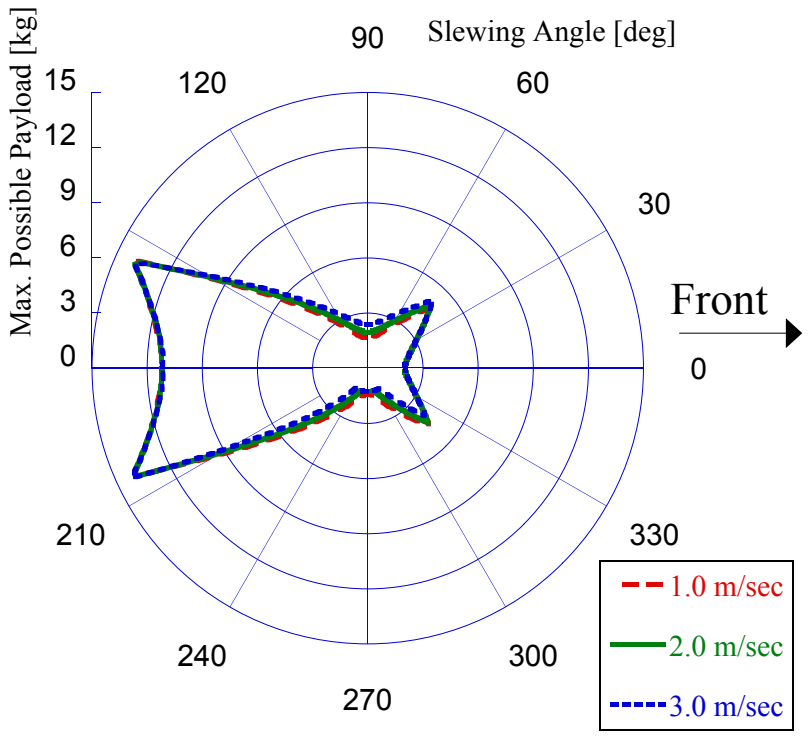

Figure 34: Maximum Possible Payload of Pseudo-Dynamic Stability Analysis for Circular Path Motion

Experiments were performed on the v=1.0m/s case when the boom is at $\alpha = 45°$ to

verify the pseudo-dynamic stability analysis prediction accuracy. Figure 35 compares the maximum possible payload mass predicted by the pseudo-dynamic method against the experimental data over a whole range of β. The prediction is plotted in the solid line, and the data is shown by the diamonds. The figure shows a very close match between the data and the predicted values. This indicates that the pseudo-dynamic stability analysis correctly calculates the effect of circular motion on the tip-over stability of the mobile boom crane. The high congruence in data may stem from the fact that the cart is driving at a relatively slow speed, thus it does not induce much payload swing and centripetal force. The experimental data near the back of the cart were not obtained due to the restriction on the amount of payload weight that can be added during an experiment. However, in terms of verifying the method's applicability and performance in the tip-over prediction, validating with the data at the least stable configuration of the boom crane is sufficient.

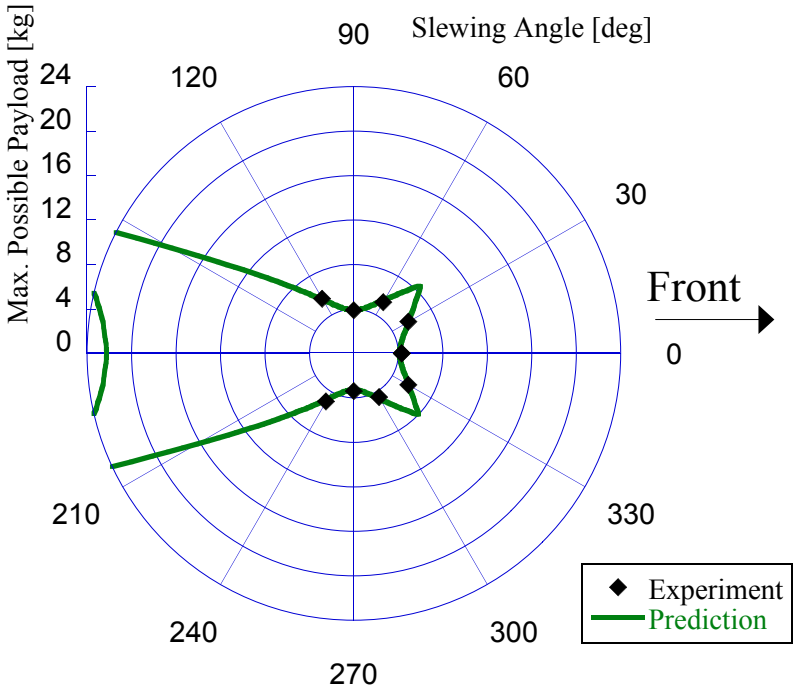

Figure 35: Experimental Data of Pseudo-Dynamic Stability Analysis for Circular Path Motion - [v=1.0m/s, α=45°]

3.4 Boom Slewing Motion

Slewing is one of the most essential motions for a boom crane operation. The motion, however, induces the inertia forces and the payload swings that reduce the tip-over stability margin of the mobile boom crane. To analyze their influences, a stationary mobile boom crane base with a slewing boom motion is considered. Similar to the circular path motion discussed in the previous section, the boom is set to a constant rotation rate to simplify the dynamic calculation. In past research, a pure rotational motion of a tower crane was investigated [24]. Since the boom slewing motion in the condition described above exhibits an analogous dynamics to that of the tower crane, a similar analysis approach is taken to study the dynamics of the mobile boom crane.

3.4.1 Crane System and Payload Swing Dynamics

Figure 36 shows the top view of the constant slewing motion. The boom rotates at a constant rate of ω, which causes the boom center of mass to move at the steady speed of $v_{b,ss}$ when it is located at a distance of $r_{b,cm}$ from the boom attachment point. The slewing motion also causes the payload of mass m to rotate at the speed of v_{ss} at the distance of r away from the slewing axis. The speed of the boom and the payload can be obtained by the linear speed relationship $v_{b,ss}$=$\omega r_{b,cm}$ and v_{ss}=ωr.

The motion also induces the centripetal forces $F_{b,ss}$ to the boom and F_{ss} to the payload. Similar to the circular path motion case, the forces act on the boom's center of mass and on the payload on the horizontal 2D plane as shown in Figure 37.

The forces also points to the direction perpendicular to the velocities $v_{b,ss}$ and v_{ss}, and away from the slewing axis of rotation. Since the slewing rate is assumed to be constant, the resultant forces are also assumed to be constant values at the steady state. The direction of the forces, however, changes continuously as the boom rotates. To establish the most conservative tip-over prediction, the tip-over stability margin of the mobile boom crane when the boom is at the most tip-over unstable

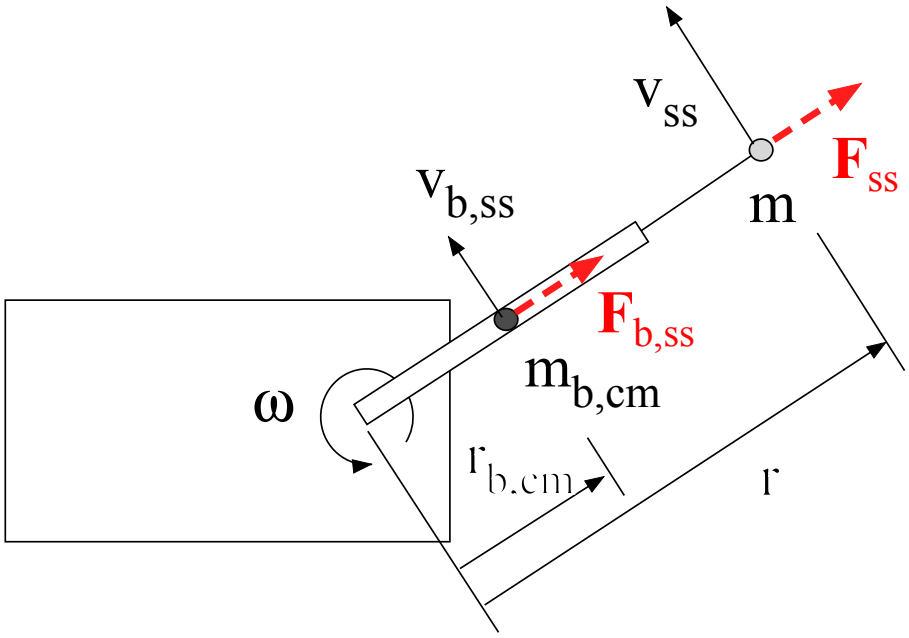

Figure 36: Dynamics in Constant Slewing Motion - Top View

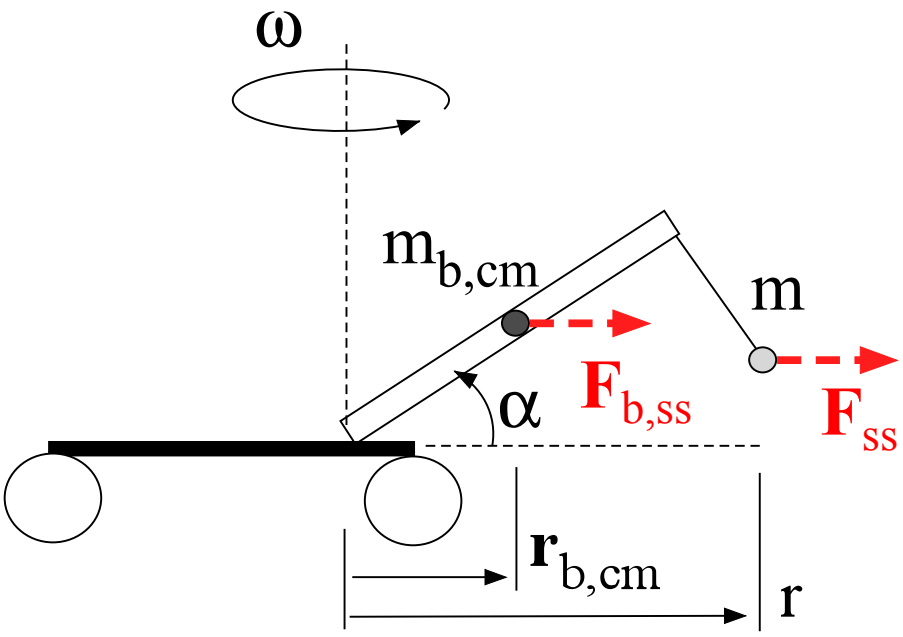

Figure 37: Dynamics in Constant Slewing Motion - Side View

configuration (β=0°, 90°, and 270° as discussed in Section 2.2) is calculated and used for the analysis.

The pendulum swing angle is computed using the single-pendulum boom crane equations of motion [24]. The full dynamic differential equations of motion for the boom crane with a point mass payload, ignoring the payload twisting about the suspension cable, are given by:

$$\begin{aligned} l\ddot{\theta}cos\varphi - 2l\dot{\theta}\dot{\varphi}sin\varphi + gsin\theta = R\dot{\omega}cos\theta + 2\omega\dot{R}cos\varphi + 2l\omega\dot{\varphi}cos\varphi cos\theta + \\ + l\dot{\omega}sin\varphi cos\theta + l\omega^2 sin\theta cos\varphi cos\theta \end{aligned} \tag{3.21}$$

and,

$$\begin{aligned} l\ddot{\varphi} + l\dot{\theta}^2 cos\varphi sin\varphi + gsin\varphi cos\theta = -\ddot{R}cos\varphi + R\omega^2 cos\varphi - R\dot{\omega}sin\varphi sin\theta - \\ - 2\dot{R}\omega sin\varphi sin\theta - 2l\omega\dot{\theta}cos^2\varphi cos\theta - \\ - l\dot{\omega}sin\theta + l\omega^2 sin\varphi cos^2\theta cos\varphi \end{aligned} \tag{3.22}$$

where l is the suspension cable length, ω is the slewing rotation rate, and R is the horizontal distance between the boom tip and the slewing axis. The angles φ and θ describes the payload swing in the longitudinal and lateral direction with respect to the cart's orientation respectively.

In a pure slewing rotation motion, the boom configuration remains fixed, which implies $\dot{R} = \ddot{R} = 0$. Also, it is assumed that the boom slews at the constant rate ω, thus implies $\dot{\omega} = 0$. This steady-state angular velocity leads to a steady-state angle deflections of φ_{ss} and θ_{ss}. At the steady state, the payload has zero velocity and acceleration with respect to the boom: $\dot{\varphi} = \dot{\theta} = \ddot{\varphi} = \ddot{\theta} = 0$. Substituting these assumptions into the equations of motion in (3.21) and (3.22) yields:

$$gsin\theta_{ss} = l\omega^2 sin\theta_{ss} cos\varphi_{ss} cos\theta_{ss} \tag{3.23}$$

$$gsin\varphi_{ss}cos\theta_{ss} = R\omega^2 cos\varphi_{ss} + l\omega^2 sin\varphi_{ss}cos^2\theta_{ss}cos\varphi_{ss} \tag{3.24}$$

At the steady-state deflection, zero lateral swing angle (θ_{ss}=0rad) is also assumed. This assumption satisfies the equality in (3.23) by making both sides zero. Applying this assumption to (3.24) yields:

$$gsin\varphi_{ss} = R\omega^2 cos\varphi_{ss} + l\omega^2 sin\varphi_{ss}cos\varphi_{ss} \tag{3.25}$$

By assuming small angles, φ_{ss} less than $0.3rad$, the solution to the equation can be approximated as:

$$\varphi_{ss} = \frac{R\omega^2}{g - l\omega^2} \tag{3.26}$$

For constant slewing motion, the steady-state pendulum swing angles are given by θ_{ss}=0rad and φ_{ss} in (3.26). In a real boom crane system, this corresponds to the case where the payload swings radially outward. According to (3.26), the steady-state angle φ_{ss} increases as the slewing speed ω, the cable length l, or the horizontal boom tip position from the slewing axis R increases. This angle estimation is then included in the tip-over prediction model to analyze the mobile boom crane's tip-over stability during the slewing motion.

3.4.2 Tip-Over Stability Analysis

Figure 38 shows the maximum possible payload values predicted by the pseudo-dynamic stability analysis. The dashed line is the case where the boom is accelerated at $0.5rad/s^2$ to a constant slew rate of $\omega = 0.73rad/s$, and the solid line is the case where the boom is accelerated at $0.75rad/s^2$ to a constant slew rate of $\omega = 1.09rad/s$. In both cases, the maximum payload value increases as the luffing angle of the boom increases. This is consistent with what was found in Section 2.3. At the faster slewing rate, the tip-over stability of the crane decreases due to the wider payload swing, as

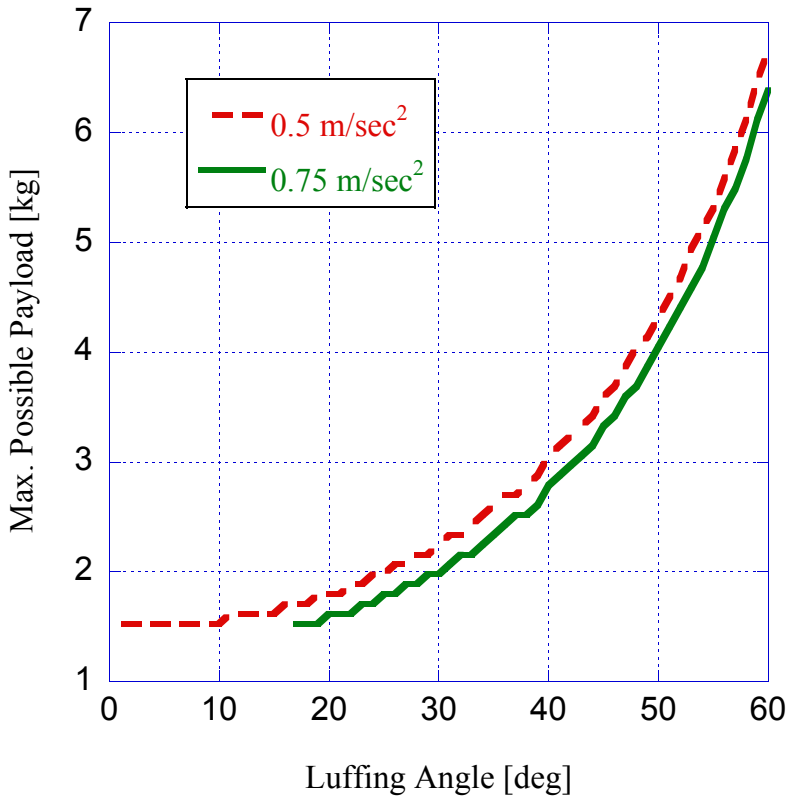

Figure 38: Maximum Possible Payload of Pseudo-Dynamic Stability Analysis for Boom Slewing Motion

seen by the expression in (3.26), and the greater magnitude of the centripetal force acting on the boom. Therefore, in the $0.75 rad/s^2$ case, the crane cannot carry as much payload weight as in the $0.5 rad/s^2$ case. In addition, the crane cannot hold any payload mass when the boom is luffed down any lower than 27° because that results in an immediate tip-over. This is indicated by the sudden cutoff in the prediction line on the plot.

When the boom is luffed up to a high α, the boom's center of mass is also raised up. This increases its distance from the ground, which leads to a greater magnitude of the tip-over torque contribution from the centripetal force acting on the boom, as shown in Figure 37. However, this effect was trivial because the stabilizing effect of raising the boom was more dominant.

To verify the accuracy of the pseudo-dynamic prediction, an experiment was performed for the $\dot{\omega} = 0.5 rad/s^2$ case. Figure 39 shows the maximum payload prediction line and the experiment data collected at the different luffing angles. Data at the luffing angles lower than 30° are not collected due to the geometric restriction of the experimental apparatus. The plot shows that the pseudo-dynamic method predicts very closely at $\alpha = 30°$. However, the prediction line starts deviating from the experiment results as the luffing angle increases. The over-estimation error tends to magnify as the boom raises, which is expected due to the limitation of the pseudo-dynamic stability analysis as discussed in Section 3.1. The centripetal force not recreated in the apparatus, which plays a huge role in determining the tip-over torque, also contributed to the prediction error. Although the pseudo-dynamic method over-estimates, the difference remains relatively small. The method captures the general trend in tip-over stability of the mobile boom crane as it slews. However, to produce a close and meaningful prediction, the slewing speed and the luffing angle must remain relatively low.

3.5 Boom Luffing Motion

Another essential motion for boom crane operation is luffing. Past research on the mobile boom crane system investigated the pendulum dynamics due to luffing motion [12]. Just like other types of crane motions, luffing causes the payload to swing and this leads to a reduction of the tip-over stability. Therefore, its influence needs to be taken into an account to produce a more reliable and applicable tip-over prediction analysis tool.

3.5.1 Crane System and Payload Swing Dynamics

To isolate the effects of luffing motion on the tip-over stability, a stationary crane base with only luffing input, as shown in Figure 40, is considered. A boom configuration of $\beta = 0°$, fixed at the position pointing to the front of the mobile boom crane, is

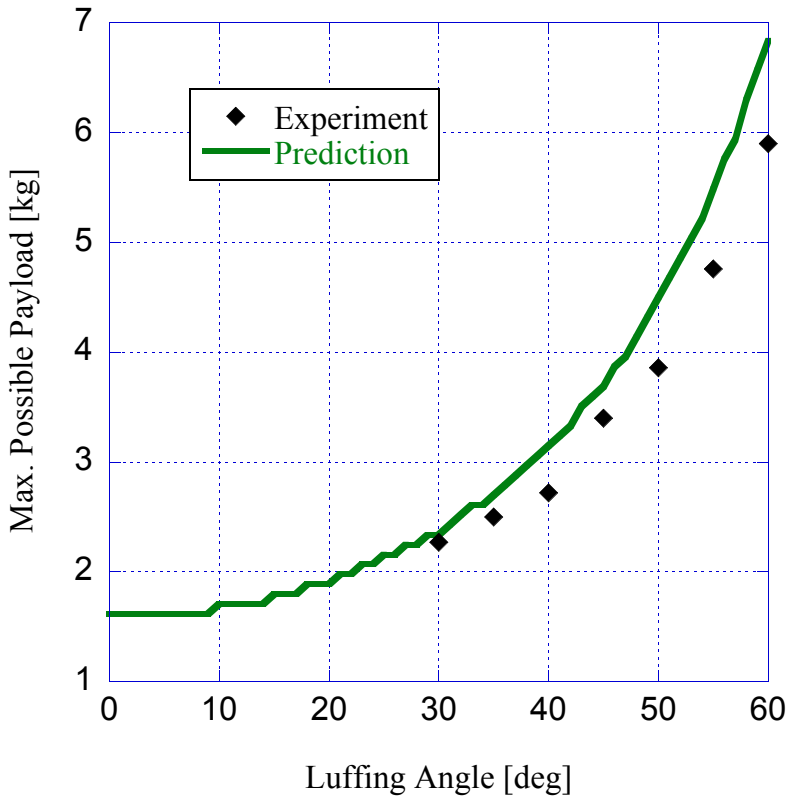

Figure 39: Experimental Data of Pseudo-Dynamic Stability Analysis for Boom Slewing Motion - [$\dot{\omega}$=0.5rad/s^2]

chosen for the analysis. Also, only the luffing downward motion is considered for this analysis because luffing the boom downward significantly reduces the tip-over stability, while luffing the boom upward makes the crane more stable.

Assuming there are no other inputs and there is no out-of-plane pendulum deflection (no swing in the lateral direction, $\theta = 0°$), the equation of motion for the payload swing in the radial or the longitudinal direction φ is:

$$\ddot{\varphi} + \frac{g}{l} sin\varphi = \frac{l_b}{l} \left(\ddot{\alpha} sin(\alpha - \varphi) + \dot{\alpha}^2 cos(\alpha - \varphi) \right) \tag{3.27}$$

where l is the suspension cable length, l_b is the boom length, and α is the boom luffing angle.

For this investigation, the luffing input is set to a constant rotational rate, or

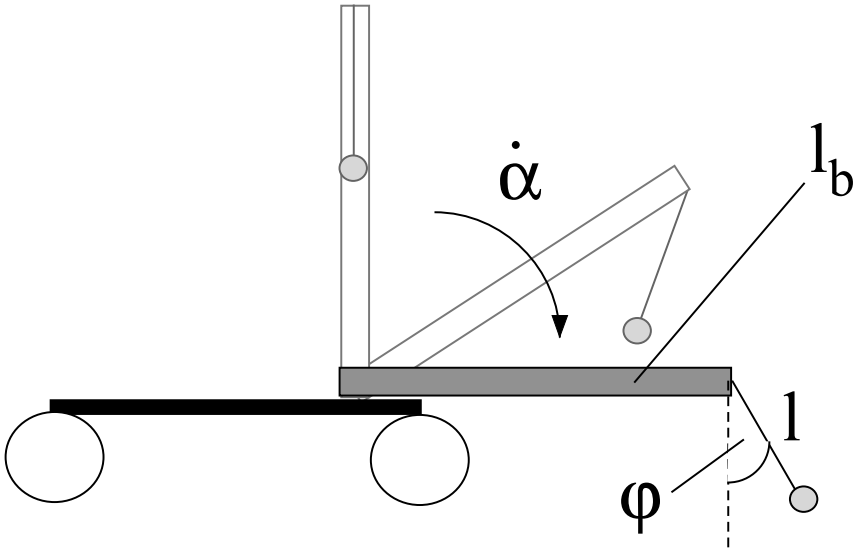

Figure 40: Dynamics in Constant Luffing Down Motion - Side View

$\ddot{\alpha} = 0 rad/s^2$. Although this assumption is not strictly true for the real applications, it still can provide an adequate pendulum dynamics model [12]. The swing angle φ is also assumed to be small. With these assumptions, the equation of motion in (3.27) can be expressed as:

$$\ddot{\varphi} + \frac{g - l_b\dot{\alpha}^2 sin\alpha}{l}\varphi = \frac{l_b}{l}\dot{\alpha}^2 cos\alpha \tag{3.28}$$

This is a linear, homogenous differential equation with time-varying crane configuration in α. Because is assumed to be constant, α can be expressed as $\alpha = (\dot{\alpha}t + \alpha_0)$. In addition, assuming that $g \gg l_b\dot{\alpha}^2 sin\alpha$ the equation can be further simplified to harmonic oscillator with natural frequency $\omega_n = \sqrt{g/l}$. The solution to the differential equation in (3.28) with zero initial conditions ($\varphi(0) = (0) = 0$) is then:

$$\varphi = \frac{l_b\dot{\alpha}^2}{g - l\dot{\alpha}^2}\left(\frac{\dot{\alpha} sin\alpha_0}{\omega_n} sin\omega_n t - cos\alpha_0 cos\omega_n t + cos(\dot{\alpha}t + \alpha_0)\right) \tag{3.29}$$

As seen in (3.29), the magnitude of the swing angle φ has its maximum magnitude when the initial luffing angle $\alpha_0 = 90°$. This is because when the boom is pointing vertically at $\alpha = 90°$), the input command to start the initial luffing downward motion

causes a linear acceleration at the boom tip in the horizontal direction. Because this is the case, all the acceleration applied at the boom tip contributes to the payload swing. It thus produces the maximum possible magnitude of the swing deflection. In addition, the theoretical maximum payload swing occurs when the sine and the cosine terms in (3.29) add up constructively. The maximum payload swing φ_{max} is then given by:

$$\varphi_{max} = \frac{l_b \dot{\alpha}^2}{g - l\dot{\alpha}^2} \left(\frac{\dot{\alpha}}{\omega_n} + 1 \right) \tag{3.30}$$

This maximum swing angle estimation φ_{max} is included in the tip-over prediction model as a constant deflection, as shown in Figure 41. During the luffing motion, there is an inertia force acting on the boom's center of mass. The force changes its direction continuously throughout the motion. However, its magnitude, compared to that of the slewing and base motion, remains very small because it only travels a limited amount of distance at a relatively slow rate. Its effect is negligible in terms of the tip-over stability, and therefore the inertial force is omitted from the analysis. With these factors included, the prediction model is then used to analyze the mobile boom crane's tip-over stability in the luffing down motion.

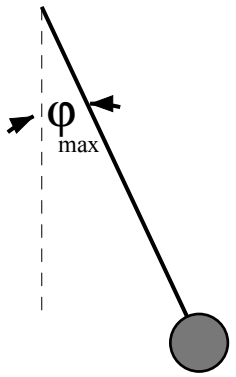

Figure 41: Maximum Payload Swing Sketch in Boom Luffing Motion

3.5.2 Tip-Over Stability Analysis

Figure 42 illustrates the maximum possible payload values estimated by the pseudo-dynamic stability analysis when the boom is luffed down at $\ddot{\alpha}$=$-0.05rad/s^2$, $-0.25rad/s^2$, and $-0.5rad/s^2$ by a bang-coast-bang command with the same maximum luffing speed of $-0.59rad/s$. In each case, the prediction line follows a similar shape produced in other crane motion cases. Interestingly, the plot reveals that the mobile boom crane exhibits identical tip-over stability characteristics in all cases. This is because in all cases the maximum swing angle φ_{max} calculated from (3.30) has the same value because they share the same maximum luffing speed. This may raise a concern because the magnitude of the acceleration input can have a strong influence to the swinging dynamics of the payload. Due to the limitation of the experimental apparatus, no experimental data was collected to verify the accuracy of the pseudo-dynamic stability analysis prediction for the luffing motion. The verification for this motion will be performed by using the full dynamic simulation model in section 5.2.5.

3.6 Summary

In this chapter, a pseudo-dynamic stability analysis was introduced to determine the tip-over stability of the mobile boom crane when it is in motion. The tip-over torque computation about the boom attachment point shows that the approach can return appropriate estimations when the payload swing and the luffing angle α is kept low. The most fundamental and common crane maneuver of straightline base motion, circular path motion, and boom's slewing and luffing motions were investigated. In each case, the maximum payload swing angle was calculated from the pendulum dynamics or the applied forces. The inertia forces and/or the centripetal forces acting on the cart and the boom during the crane motion were also computed and included in the prediction model. Then, the tip-over stability margin was used to determine the maximum possible payload values the crane can carry without causing tip-over

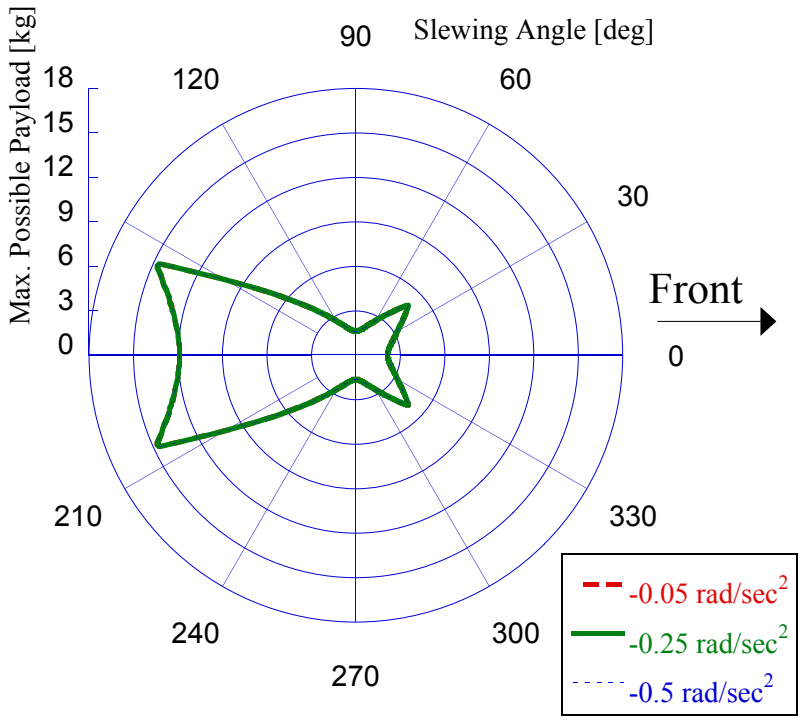

Figure 42: Maximum Possible Payload of Pseudo-Dynamic Stability Analysis for Boom Luffing Motion

for various crane configurations. Different values of the input magnitude were supplied to analyze their effect on the tip-over stability of the crane. The experimental data verified that the pseudo-dynamic stability analysis successfully incorporates the dynamic effects and predicts the tip-over behavior of the mobile boom crane under common maneuvers.

The analysis also revealed some limitations on its performance. In the straightline base motion, the pseudo-dynamic method tends to return an over-estimation toward the back of the cart. The circular path motion also showed some error near the back. In the boom slewing motion, limiting the input magnitude and the luffing angle are found to be critical in maintaining the prediction accuracy. In the boom luffing motion, the assumption made in simplifying the pendulum dynamics leaves a concern in the predicted values. The method does not capture differences due to the acceleration rate. The accuracy of the pseudo-dynamic method will be further

investigated in the following chapter by comparing its predictions with simulation results from a full dynamic multi-body simulation model of the mobile boom crane.

CHAPTER IV

DOUBLE-PENDULUM STABILITY ANALYSIS

The previous chapters investigated the tip-over stability analysis of mobile boom cranes with a single-pendulum. However, in real crane applications, the crane often behaves closer to the dynamics described by a double-pendulum payload because of the presence of a hook. In order to develop a practical tip-over prediction tool, it is critical that the prediction model incudes this factor into an account. In this chapter, the tip-over stability analysis is extended to the mobile boom cranes equipped with a double-pendulum payload mass.

4.1 Description of the Approach

To analyze tip-over stability of the mobile boom crane with a double-pendulum payload, a similar approach to the single-pendulum case is taken. The prediction model and the pseudo-dynamic analysis method used in the single-pendulum case are applied to the double-pendulum case with minor modifications. This is possible because the same mobile boom crane apparatus, except for the suspension cable and the payload, is shared in both cases. Since the analysis approach taken in the single-pendulum case was shown to be valid in the previous chapter, this also provides confidence in the accuracy of the analysis results for the double-pendulum case. The method is also expected to show some similar traits observed in the single-pendulum case.

4.1.1 Modifications to the Tip-Over Prediction Model

To extend the tip-over stability analysis to the double-pendulum case, the prediction model from Figure 9 needs to be modified. The same machine structure can be used, so it remained unchanged. The single-pendulum payload, however, is replaced with a

double-pendulum payload setup by adding new pendulum set, l_2 and m_2. Figure 43 illustrates the modified tip-over prediction model used for the double-pendulum case. The double-pendulum masses m_1 and m_2 are attached to the boom by suspension cable segments l_1 and l_2. Similar to the single-pendulum case, the payloads swing are defined by angles φ_1 and φ_2 in the longitudinal direction, and by angles θ_1 and θ_2 in the lateral direction with respect to the cart.

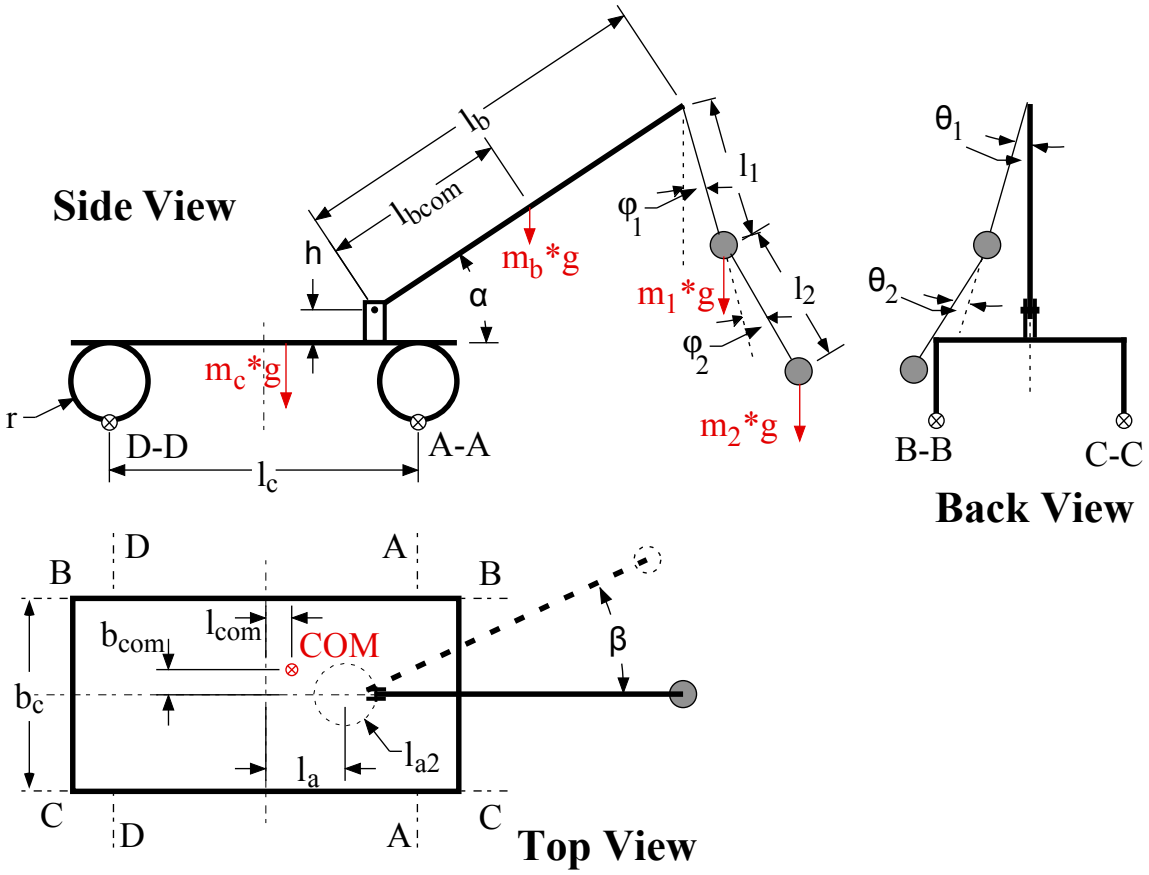

Figure 43: Schematic Diagram of a Mobile Boom Crane with Double-Pendulum Payload

To allow a reasonable comparison between the single-pendulum setup and the double-pendulum mobile boom crane model, the cable lengths l_1 and l_2 were adjusted so that the total length was equal to the cable length used in a single-pendulum setup. In addition, the mass m_1 was set to a constant of $1kg$ for simplicity, and the total mass m_p used in the single-pendulum tip-over stability analysis was equal to the sum

of m_1 and m_2.

4.1.2 Experimental Verification

To verify the crane's tip-over stability when it is equipped with the double-pendulum payload, the experimental setup shown in Figure 12 was used with a small modification. The suspension cable was modified so that it could hold an extra mass in the middle of the cable, thus creating a double-pendulum setup. This extra mass imitates the hook in an actual crane system. For this experiment, the mass is set to about $1kg$. The maximum possible payload data is then collected following the exact same procedure taken in the single-pendulum experiments. Given the initial swing angle, the payload at the end of the cable is increased incrementally until the crane starts bucking.

4.2 Static Stability Analysis

First, the static stability analysis of the mobile boom crane with the double-pendulum setup is performed. In this analysis, the crane is assumed to be stationary. Therefore, there is no pendulum swing dynamics induced to the system. This leads the double-pendulum static stability analysis to give nearly identical results to those of the single-pendulum case. Because of the extra hook mass in the double-pendulum setup, the location of the center of mass is now slightly higher than that of the single-pendulum case. However, the difference produces negligible changes in the resulting tip-over stability margin angle measurement, thus is not critical in the static case.

For the tip-over calculation, the crane parameters listed in Table 1 are used. Figure 44 and Figure 45 shows the maximum possible payload predicted by the static stability analysis and obtained by the experiment. The experimental data shows a good match with the prediction, verifying that the static stability analysis estimates the tip-over stability of the mobile boom crane accurately. Also, the results are found to be nearly identical to that of the single-pendulum case in Figure 14 and

Figure 15. This again is because there is no pendulum swing dynamics induced, thus both the single- and the double-pendulum contributes equally to the tip-over torque calculation.

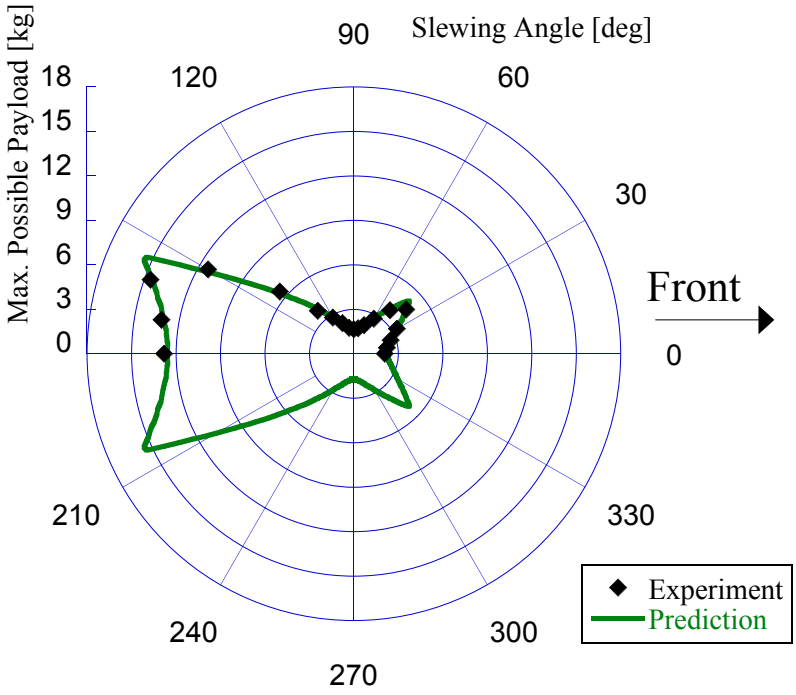

Figure 44: Experimental Data of Static Stability Analysis [DP] - [α=0°]

4.3 Pseudo-Dynamic Stability Analysis

To include the effect of the double-pendulum payload swings into the tip-over stability analysis, the pseudo-dynamic stability analysis discussed in the single-pendulum setup is extended for the double-pendulum case.

The double-pendulum payload is a complicated non-linear system whose motion is governed by a set of coupled ordinary differential equations. In the case of the accelerating suspension point moved in a straight line, the payload swing angles φ_1 and φ_2, as shown in Figure 43, can be expressed by the linearized equations of motion as:

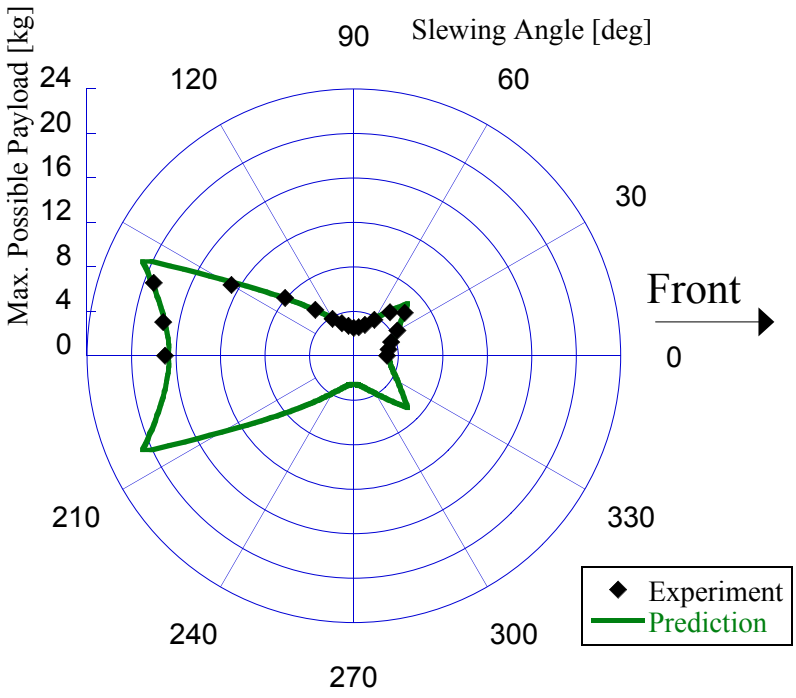

Figure 45: Experimental Data of Static Stability Analysis [DP] - [α=30°]

$$\ddot{\varphi}_1(t) = -\frac{g}{l_1}\varphi_1(t) + \frac{g}{l_1}\frac{m_2}{m_1}\varphi_2(t) - \frac{1}{l_1}M = -A\varphi_1(t) + B_1\varphi_2(t) - CM \tag{4.1}$$

$$\ddot{\varphi}_2(t) = \frac{g}{l_1}\varphi_1(t) - \left(\frac{g}{l_2} + \frac{g}{l_1}\frac{m_2}{m_1} + \frac{g}{l_2}\frac{m_2}{m_1}\right)\varphi_2(t) + \frac{1}{l_1}M = A\varphi_1(t) - B_2\varphi_2(t) + CM \tag{4.2}$$

where M is the magnitude of the acceleration input. When these equations are solved to obtain the time response, they predict a complex behavior. An example of such responses is shown in Figure 46. The figure shows the time response of the payloads m_1 and m_2 by plotting the swing angles φ_1 and φ_2, indicated by the dashed and solid lines respectively. This case was produced by giving the base a bang-coast-bang acceleration command of $1m/s^2$ with a $2.5sec$ coasting time. The responses show two frequency modes, and have very complex dynamics. Their dynamics are subjected to the magnitude and the timings of the input impulses, and the double-pendulum cable and mass settings. The masses do not swing in phase together, so they have distinct

influences on the tip-over stability, and thus add more complexity to the analysis.

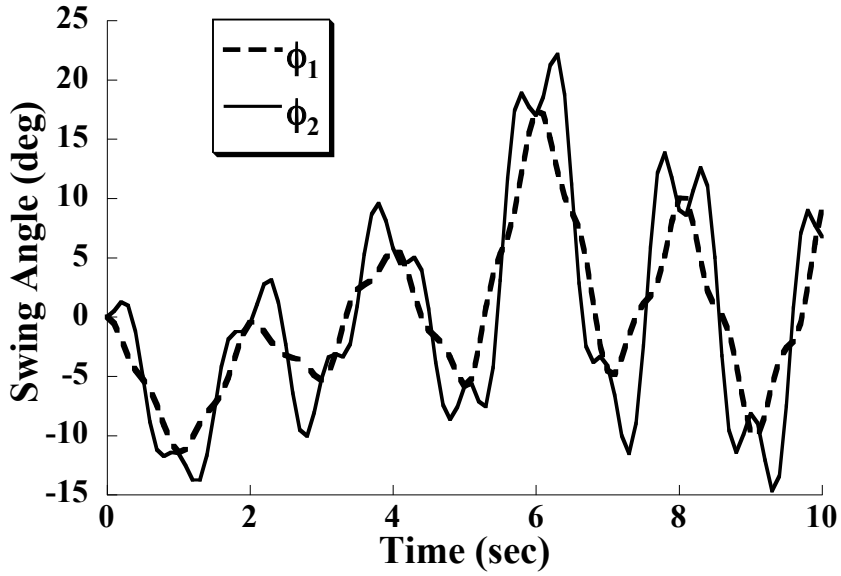

Figure 46: Example of Double-Pendulum Payload Response

When the double-pendulum system is moved in a very simple motion, the theoretical maximum swing angles $\varphi_{1,max}$ and $\varphi_{2,max}$ can be computed. For example, using (4.1) and (4.2), the time response of the swing angles for an acceleration impulse input are governed by:

$$\begin{aligned}\varphi_1(t) = &\frac{-CM}{-\omega_1^2+\omega_2^2}cos(\omega_1 t) + \frac{CM}{-\omega_1^2+\omega_2^2}cos(\omega_2 t) + \frac{(B_1-B_2)CM}{\omega_1^2\omega_2^2} + \\ &+ \left(\frac{-(B_1-B_2)CM}{\omega_1^2\omega_2^2} - \frac{(B_1-B_2)CM}{(\omega_2^2-\omega_1^2)\omega_2^2}\right)cos(\omega_1 t) + \\ &+ \frac{(B_1-B_2)CM}{(\omega_2^2-\omega_1^2)\omega_2^2}cos(\omega_2 t)\end{aligned} \tag{4.3}$$

$$\varphi_2(t) = \frac{CM}{-\omega_1^2+\omega_2^2}cos(\omega_1 t) + \frac{-CM}{-\omega_1^2+\omega_2^2}cos(\omega_2 t) \tag{4.4}$$

where ω_1 and ω_2 are the two modes of the natural frequencies.

Given the expression in the time domain, the theoretical maximum swing angles occur when all sine and cosine terms add up constructively. The maximum swing angles $\varphi_{1,max}$ and $\varphi_{2,max}$ are then given by:

$$|\varphi_{1,max}| = \frac{2CM}{-\omega_1^2 + \omega_2^2} + \frac{2(B_1 - B_2)CM}{\omega_1^2\omega_2^2} + \frac{2(B_1 - B_2)CM}{(\omega_2^2 - \omega_1^2)\omega_2^2} \tag{4.5}$$

$$|\varphi_{2,max}| = \frac{2CM}{-\omega_1^2 + \omega_2^2} \tag{4.6}$$

which may be applicable to the pseudo-dynamic stability analysis discussed in the previous chapter. However, since the double-pendulum payload exhibits a complex non-linear dynamics, it is highly difficult and computationally expensive to calculate the maximum swing angle magnitudes when the mobile boom crane undergoes complicated motions or is supplied with complicated inputs. In addition, because the double-pendulum induces a chaotic motion, it has sensitive dependence on the initial condition, which further complicates the dynamics.

To simplify the analysis and yet produce a conservative tip-over prediction, the maximum swing angle calculated for the single-pendulum case is directly applied to the double-pendulum pseudo-dynamic stability analysis. This is justified by assuming that the worst case swing occurs when both cable segments l_1 and l_2 are swung outward to form the same angle with the vertical direction ($\varphi_2 = \theta_2 = 0°$). Figure 47 illustrates this assumption.

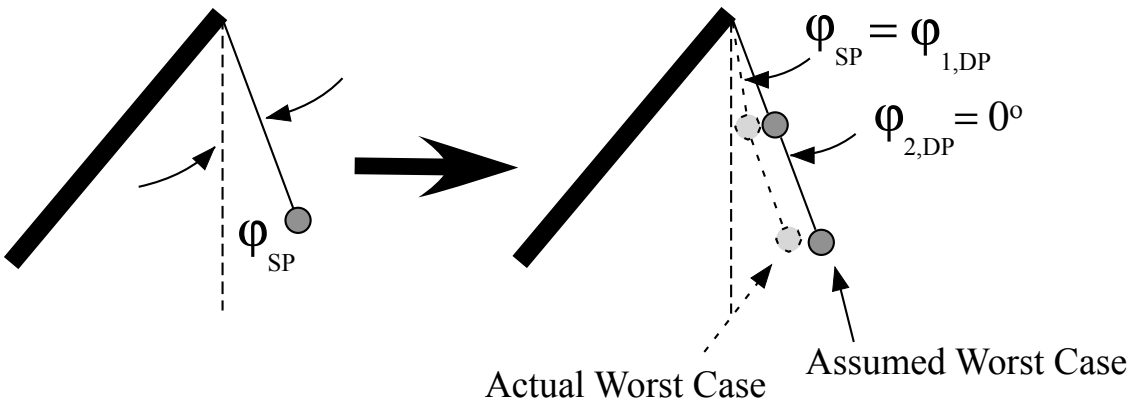

Figure 47: The Worst Case Payload Swing in the Double-Pendulum Analysis

In summary, in addition to the assumptions made in the pseudo-dynamic stability

analysis in Chapter 3, following factors were omitted to extend the analysis to the double-pendulum payload case.

- Payload swing dynamics of m_1 and m_2, and their influences to each other
- Dependency of the double-pendulum payload to the initial condition

4.3.1 Straight Base Motion

To predict the tip-over stability of the mobile boom crane moving in a straight line, the inertia force and the payload swing factors are added to the prediction model. In this analysis the mobile boom crane is equipped with the double-pendulum payload, and is moved using the same motion described in Section 3.2, using the same system parameters that were listed in Table 1.

As mentioned previously, the maximum swing angle calculated in (3.15), which is for the single-pendulum case, is used to calculate the worst double-pendulum payload swing. Setting the acceleration magnitude to $1m/s^2$ and the total payload suspension length to $1m$, the bang-coast-bang input causes a maximum swing angle φ_1 of $0.41rad$ (23.4°). Furthermore, the longitudinal payload swing φ is also added to a lateral payload swing θ to compensate for the fact that the pseudo-dynamic stability analysis does not take the centripetal force caused by the longitudinal swing into account. This idea was previously discussed in Section 3.1. In addition, the inertia forces acting on the boom and on the cart during the acceleration/deceleration of the driving is added to the prediction model.

After including the effect of the inertia forces and the double-pendulum payload swing into consideration, the prediction model is then used to study the tip-over stability characteristics of the mobile boom crane undergoing straightline base motion. Figure 48 shows the maximum possible payload predicted by the pseudo-dynamic method. The dash line indicates the static case of $0m/s^2$, and the solid line indicates the straightline base motion with the acceleration magnitude of $1.0m/s^2$. Similar

to the single-pendulum case, the maximum payload values decrease when the crane is in motion, due to the inertia forces and the payload swing that creates extra contribution to the tip-over torque. The reduction in the tip-over stability can be observed throughout the range of β, except for $\beta = 160°$-$200°$. Again, at the rear of the cart the prediction over-estimation can be observed. This result reveals that the overall tip-over characteristics of the mobile boom crane does not change significantly whether it is equipped with a single- or double-pendulum payload.

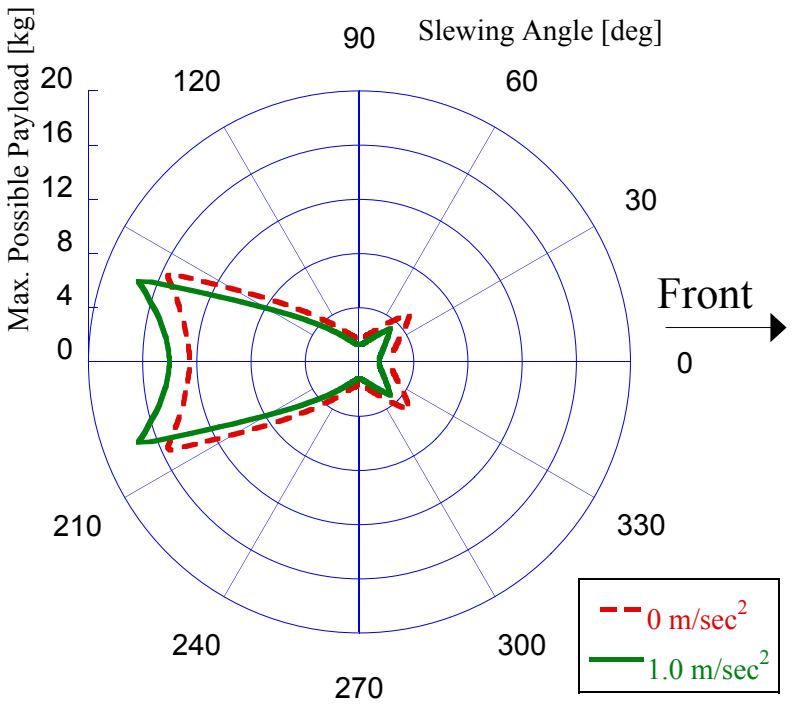

Figure 48: Maximum Possible Payload of Pseudo-Dynamic Stability Analysis for Straight Base Motion [DP]

Experiments were performed to verify the pseudo-dynamic stability analysis for the double-pendulum setup in the straightline base motion case. Figure 49 shows the experimental results when the acceleration magnitude was set to $1.0m/s^2$, and the boom slew and luff angles were set to 0° and 30° respectively. The figure shows a good match between the experimental data and the prediction. The prediction line closely estimated the maximum payload values for $\beta = 0°$-$150°$. The last data point at

$\beta = 180°$, however, does not lie on the prediction line. Similar to the single-pendulum case, the pseudo-dynamic stability analysis returns over-estimated prediction when the boom points toward the back of the cart. However, again, because this error occurs where the boom is very stable, this does not compromise the usefulness of the method in the tip-over prediction. The results verify that the pseudo-dynamic stability analysis can be applied to the double-pendulum case.

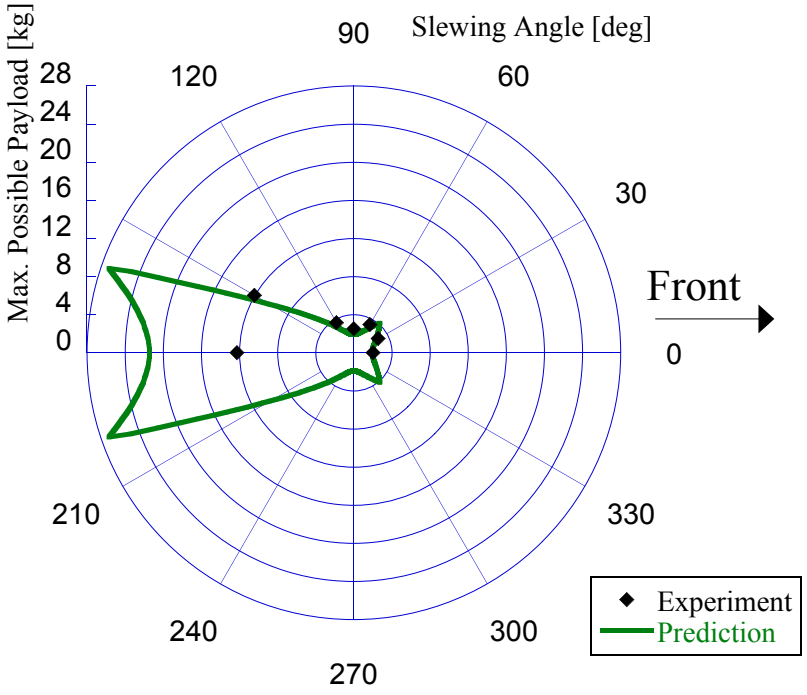

Figure 49: Experimental Data of Pseudo-Dynamic Stability Analysis for Straight Base Motion [DP] - [a=1.0m/s^2, α=30°]

4.3.2 Circular Path Motion

The circular path motion of the mobile boom crane with the double-pendulum setup is analyzed using a similar approach. As discussed in Section 3.3, the mobile boom crane is driven in a circular path at a constant cart velocity, v, in this analysis. As shown in Figure 31 and in Figure 32, the motion induces the centripetal forces on the cart's center of mass and on the payloads. The same magnitude of the centripetal force acting on the boom and the cart is applied to the double-pendulum case, using

the equation in (3.17).

Each payload in the double-pendulum is also subjected to the individual centripetal force acting on them, which results in a steady-state swing angle deflection. However, because the pseudo-dynamic stability analysis for the double-pendulum setup utilizes the maximum swing angle calculation from the single-pendulum case, this factor is omitted from the consideration. Instead, the maximum swing angle calculation in (3.20) is used to compute the maximum swing angle $\varphi_{1,ss}$ for the double-pendulum setup.

Figure 50 shows the maximum payload prediction by the analysis when the crane is moved at cart velocities of: $1.0m/s$, $2.0m/s$, and $3.0m/s$. The general shape of the prediction line, again, is very similar to that of the single-pendulum case. The effect of mobile boom crane driving in a counter-clockwise circle is also clearly shown in the plot. The motion causes the prediction line to elongate along the path direction because in this direction the effect of the centripetal force is minimized. Thus it leads to a greater tip-over stability. At the higher cart velocities, this effect is more clearly observed. Even with the double-pendulum payload setup, the effect of the cart driving through the motion is captured by the pseudo-dynamic stability analysis.

Figure 51 shows experimental data compared with the predicted value calculated by the pseudo-dynamic stability analysis. In this case, the cart drives at the constant speed of $1.0m/s$ counter-clockwise and the boom is at a luffing angle of $45°$. The experimental data shows a close match with the prediction. The experimental data toward the back of the cart cannot be obtained because the payload values are too large and exceed the maximum weight that the experimental apparatus can support. However, the collected data still proves that the pseudo-dynamic stability analysis correctly predict the tip-over of the mobile boom crane with the double-pendulum payload in the circular path motion.

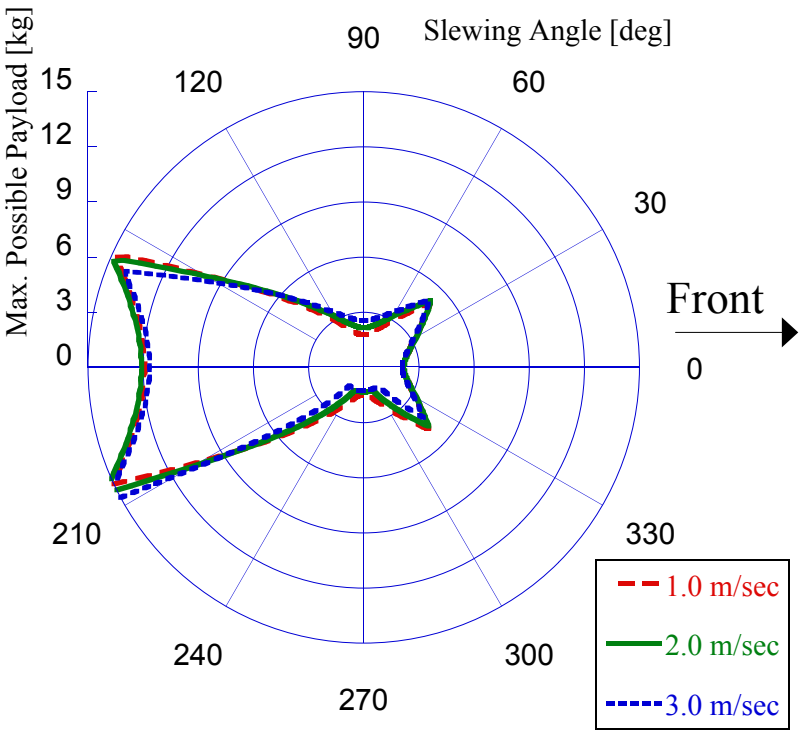

Figure 50: Maximum Possible Payload of Pseudo-Dynamic Stability Analysis for Circular Path Motion [DP]

4.3.3 Boom Slewing Motion

The slewing motion of the single-pendulum setup discussed in Section 3.4 was extended to the double-pendulum case. As seen in Figure 36 and Figure 37, the rotating boom induces the centripetal force acting on the boom's center of mass. Similar to the circular path motion case above, the centripetal force calculated in the single-pendulum case can be used directly to the double-pendulum case since the boom itself is unchanged in its structure. The payload swing angle $\varphi_{1,ss}$ is computed using the relationship in (3.26). Like the circular path motion case, the effect of the centripetal force acting on each individual payload is ignored in the pseudo-dynamic stability analysis.

Figure 52 shows the pseudo-dynamic stability analysis results for the mobile boom crane slewing the boom. Two different angular accelerations $\dot{\omega}$ of $0.5m/s^2$ and

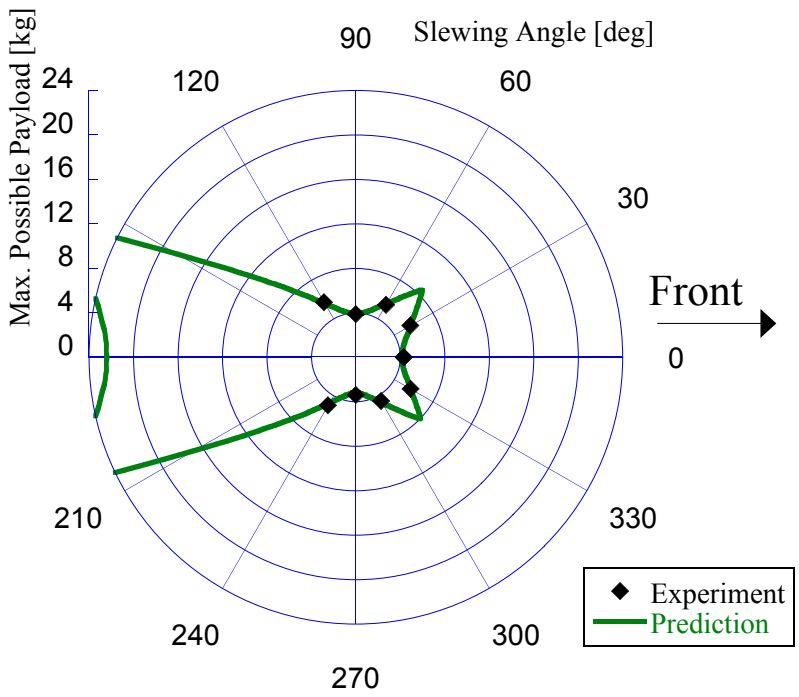

Figure 51: Experimental Data of Pseudo-Dynamic Stability Analysis for Circular Path Motion [DP] - [v=1.0m/s, α=45°]

$0.75m/s^2$ were used to accelerate the boom up to constant slewing speeds of $0.73rad/s$ and $1.09rad/s$. The predicted results again show a similar tip-over behavior as compared to the single-pendulum case. The figure shows that the maximum payload value increases as the luffing angle increases. Also, slewing the boom at the higher rate decreases the tip-over stability. Switching the payload to the double-pendulum setup does not alter the general behavior of the tip-over stability of the mobile boom crane in the slewing motion, similar to the other motion cases. Therefore, the analysis performed in the single-pendulum case can be applied to the double-pendulum case with high confidence.

Figure 53 shows the pseudo-dynamic prediction and the experimental data for the boom slewing motion with $\dot{\omega}$=$0.5m/s^2$. Like the single-pendulum case, the data shows close correspondence with the prediction line. The slight difference, as mentioned previously, is most likely due to the inertia force acting on the boom, which is an

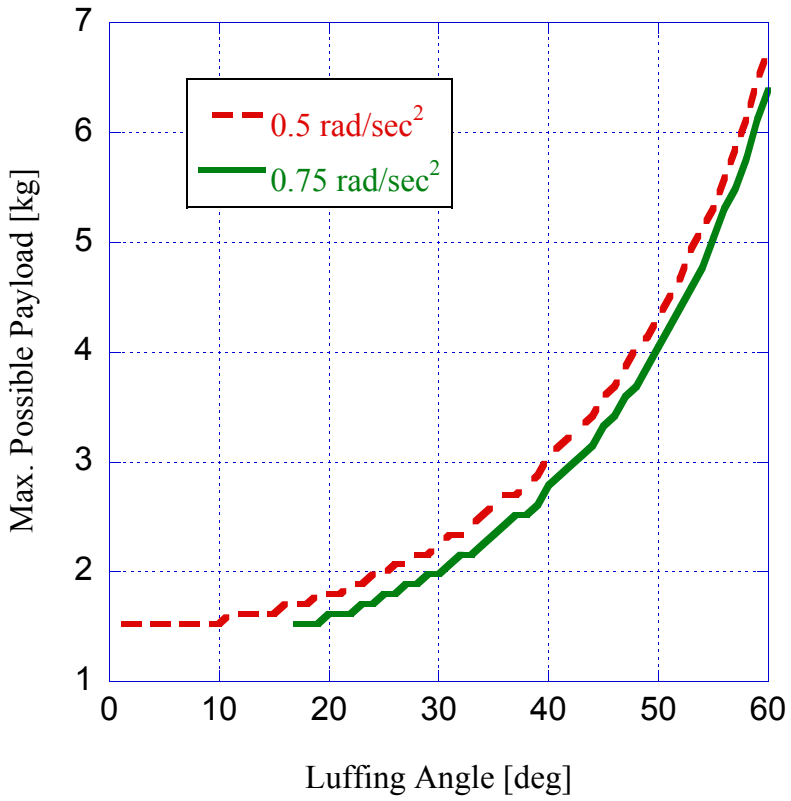

Figure 52: Maximum Possible Payload of Pseudo-Dynamic Stability Analysis for Boom Slewing Motion [DP]

effect that cannot be accurately realized by the experimental setup. This result increases the applicability of the pseudo-dynamic stability analysis method to the double-pendulum payload case.

4.3.4 Boom Luffing Motion

Similar to the other motion cases, the luffing motion for the single-pendulum setup discussed in Section 3.5 was extended to the double-pendulum case. The description of the motion is again exactly the same as the single-pendulum pseudo-dynamic stability analysis as illustrated in Figure 40. As discussed previously, there is assumed to be no inertia forces acting on the boom and the payload during the motion. This can be realized by maintaining a low rate of luffing speed and acceleration. The maximum payload swing φ_{max} for the luffing motion, shown in (3.29), is used in the analysis.

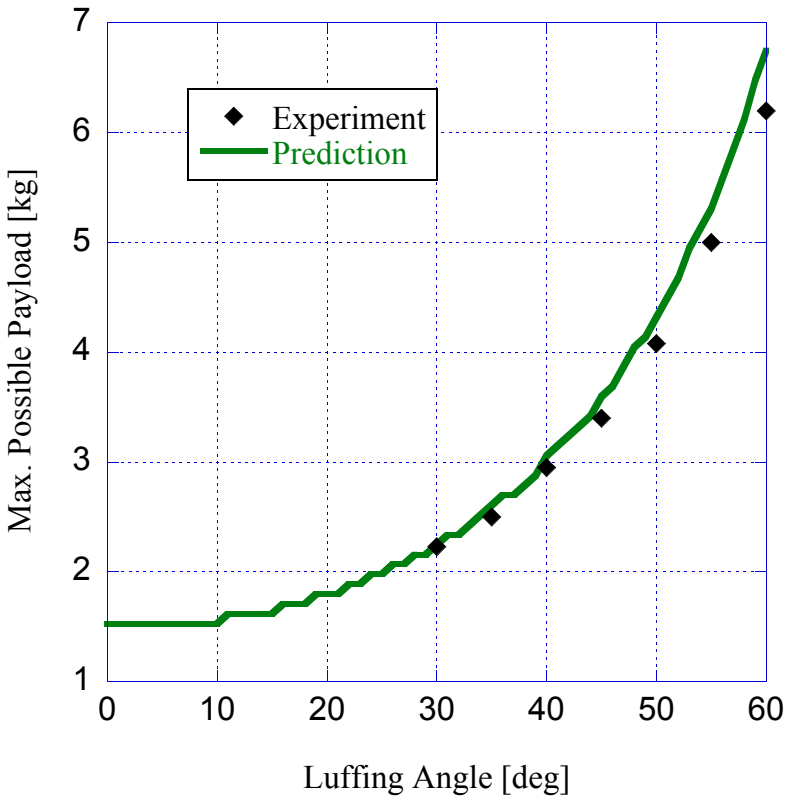

Figure 53: Experimental Data of Pseudo-Dynamic Stability Analysis for Boom Slewing Motion [DP] - [$\dot{\omega}$=$0.5 rad/s^2$]

This angle is again included into the prediction model as a constant deflection.

Figure 54 shows the pseudo-dynamic prediction when the boom is luffed downward at $\ddot{\alpha}$=$-0.05 rad/s^2$, $-0.25 rad/s^2$, and $-0.5 rad/s^2$ using a the bang-coast-bang command with the same maximum luffing velocity. Similar to the single-pendulum case, the tip-over stability line for each case is identical. This again is because they share the same maximum luffing speed, so they have the same φ_{max} calculated from (3.30) and thus the resulting tip-over torque contribution. Further evaluation of the tip-over stability during luffing motion is performed in Section 5.2.5 with the full dynamic simulation model.

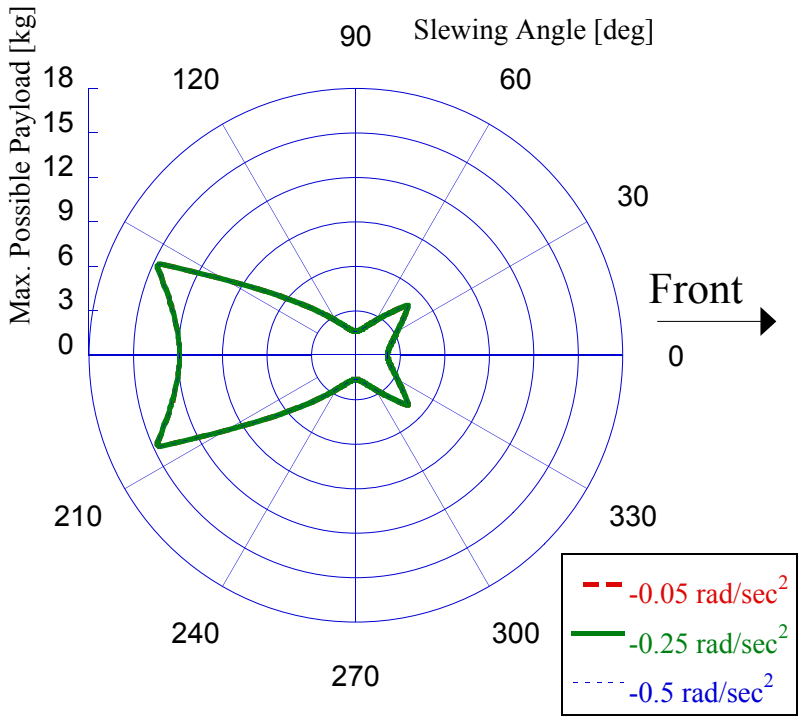

Figure 54: Maximum Possible Payload of Pseudo-Dynamic Stability Analysis for Boom Luffing Motion [DP]

4.4 Summary

In this chapter, the tip-over stability of a mobile boom crane with a double-pendulum payload setup was studied. A extra payload mass was added to the tip-over prediction model. In the static stability analysis, the stability of the crane was found to be nearly identical to the single-pendulum case when the payload and the cable length are adjusted for a fair comparison.

In the pseudo-dynamic stability analysis, the method developed for the single-pendulum case was applied to the double-pendulum case. The same crane motions were investigated for the mobile boom crane with the identical crane parameters from the previous cases. As a result, the same inertia and centripetal force were included in the tip-over calculation. Due to its complex dynamic nature, the double-pendulum payload swing was simplified by directly applying the maximum swing angle calculated in the single-pendulum case in Chapter 3. This is based on the

assumption that the worst case swing occurs when both cable segments are swung outward to form the same angle with the vertical direction. The tip-over stability predictions were generated by the pseudo-dynamic method for different levels of the input magnitude. Tip-over characteristics similar to the single-pendulum case were observed in the double-pendulum case. Experiments verified that the pseudo-dynamic stability analysis can be extended to the double-pendulum payload setup. Further verification will be performed with the full dynamic multi-body simulation model in the full dynamic stability analysis in Chapter 5.

CHAPTER V

FULL DYNAMIC STABILITY ANALYSIS

In the previous chapters, a pseudo-dynamic stability analysis method was introduced. The method utilized simplified pendulum dynamics and inertia effects in order to rapidly approximate the tip-over stability. Experiments were also conducted with making various assumptions and simplifications in the experimental apparatus. The results are, therefore, subject to those simplifying assumptions. Some mobile boom crane dynamics critical to the tip-over stability may or may not have been neglected. To conduct a more in-depth analysis and test the simple pseudo-dynamic method, this chapter presents a stability analysis that incorporates the full dynamic effects. The results in this chapter supports and supplements the results obtained with pseudo-dynamic stability analysis.

5.1 Dynamic Multi-Body Simulation Model of a Mobile Boom Crane

A double-pendulum crane can exhibit a rich and complex dynamic behavior that can impact the tip-over stability of the mobile crane's platform. Thus, the full dynamic effects of payload swings, as well as all other inertial and dynamic forces that can contribute to the tip-over, will be considered in this chapter. To fully investigate the stability analysis of the double-pendulum mobile boom crane, a dynamic multi-body simulation model of the crane was developed. Figure 55 shows the top view of a schematic of the multi-body model of the mobile boom crane.

The origin of the coordinate system **A** is located on the ground. The cart's position in the Newtonian coordinate system **N** is defined by a vector $[xy]$ that describes the location of the origin of **A** and a rotation about a vertical axis (angle ψ). The boom

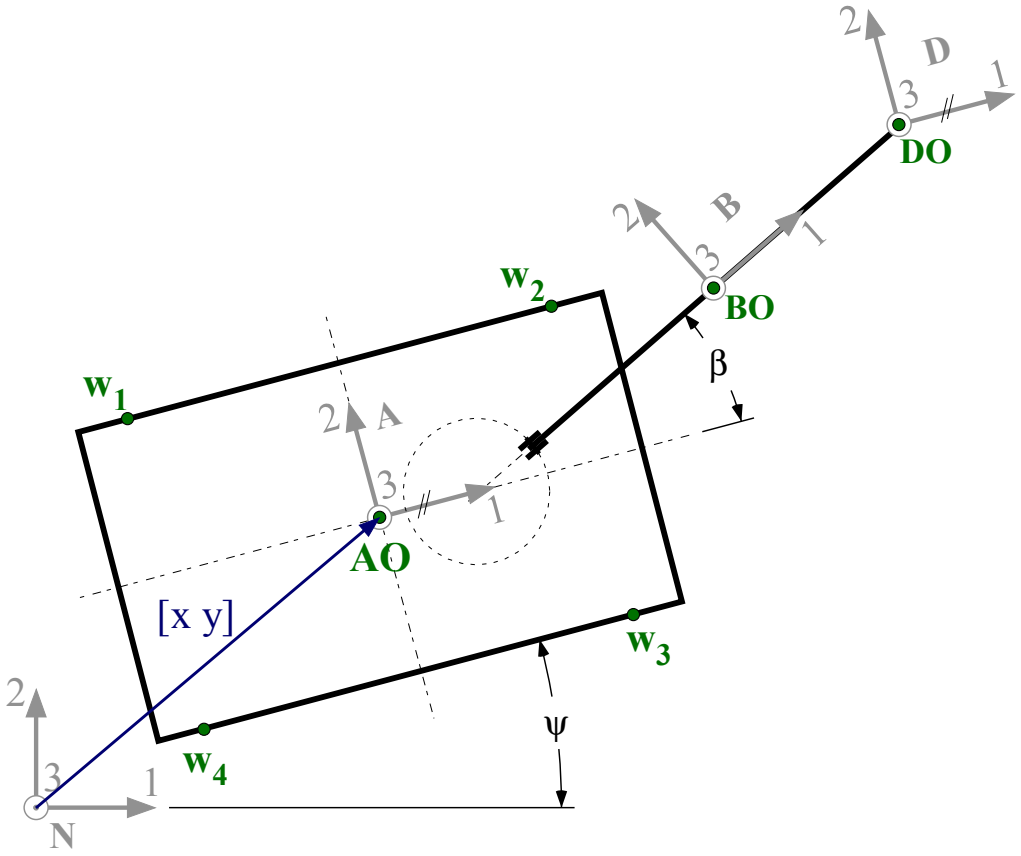

Figure 55: Model of the Multi-Body Simulation (Top View)

rotates relative to the cart (angle β). The coordinate system **D**, that contains the payload, is always aligned with **A**. Thus, it is possible to describe the payload swing angles relative to the cart.

Figure 56 shows a side view of the model. The cart can pitch along its lateral axis, described by angle q_1. It can also move up and down because the tires and suspension are modeled with spring/damper elements. Therefore, the vector from point AO to point CC (indicated as a dotted line in Figure 56) has a variable length, but is always aligned with coordinate system **C**, specifically the unit vector C_3. The cart motion is constrained by wheel-ground contacts, that act through the spring-damper subsystems that model the tires and suspension. To better match the behavior with that of a real system, these forces are limited to compressive forces only so that the

springs do not pull the wheels back to the ground. The payload swing angles are measured relative to the coordinate system **D**. The basic dimensions and masses of the model used in the simulation are taken from the experimental crane apparatus utilized in the static and pseudo-stability analysis experiments, which were given in Table 1.

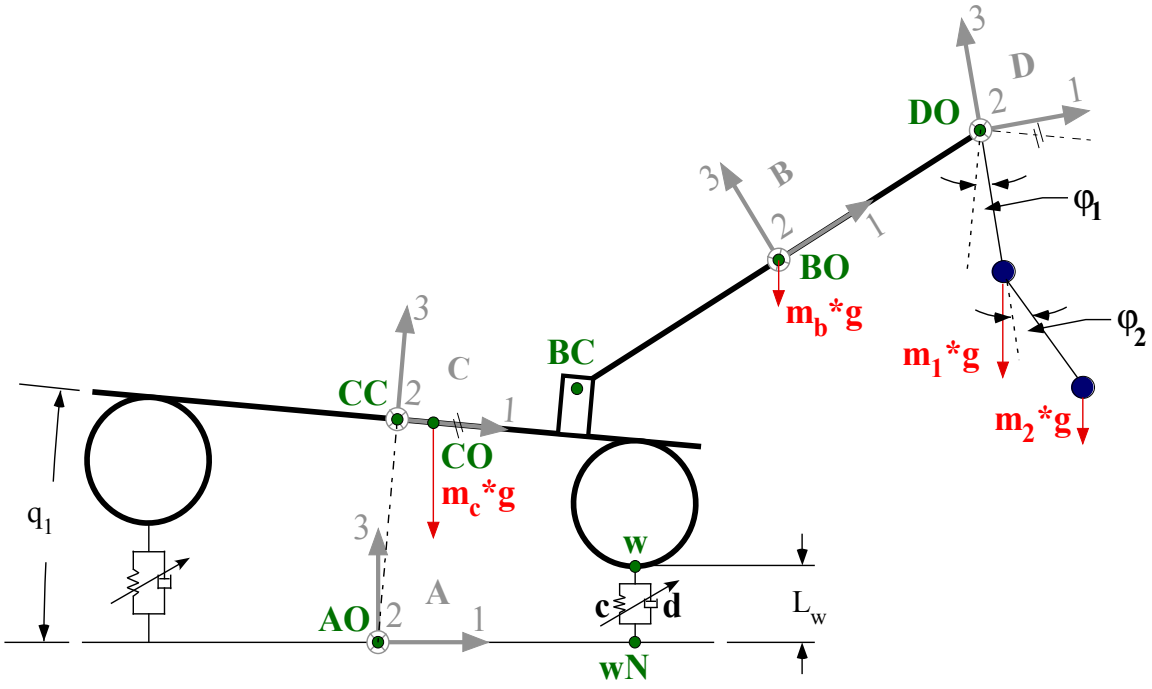

Figure 56: Model of the Multi-Body Simulation (Side View)

Figure 57 shows the simulation model from the back view. The location of the center of the cart CC is defined by a vector that is collinear with the upward pointing axis of the coordinate system **C**. The cart rotates relative to the **A** frame about the longitudinal axis of the cart, described by angle q_2.

As shown in Figure 56 and Figure 57, the full dynamic simulation model developed is equipped with a double-pendulum payload. The model, however, can be used to simulate the full dynamics of the mobile boom crane with a single-payload simply by assuming very small values for l_2 and m_2. When the simulation model is used to obtain the tip-over stability results for a single-pendulum, the second set length and

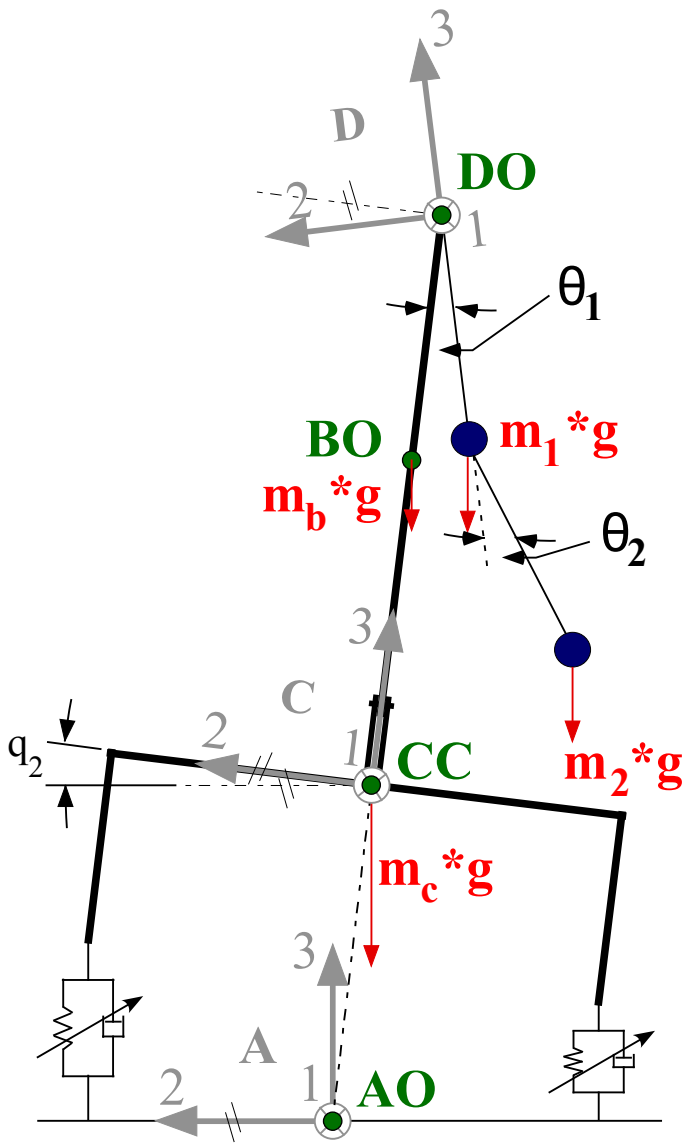

Figure 57: Model of the Multi-Body Simulation (Back View)

mass is set to 1 percent of that of the first (l_2=0.01l_1, m_2=0.01m_1).

The equations of motion for the system were generated using Kane's method. A software package called AUTOLEV is used to aid the generation of the equations of motion and the simulation code in MATLAB. The AUTOLEV source code can be found in the appendix.

5.2 Full Dynamic Stability Analysis

By simulating the response of the full dynamic model, a further verification on the pseudo-dynamic stability analysis with the tip-over prediction model can be performed. The maximum possible payload results from the prediction model and the pseudo-dynamic stability analysis are compared to those obtained from the full dynamic simulation. The simulation results are obtained by continuously increasing the payload mass until tip-over is observed.

5.2.1 Static Stability Analysis

Recall that with the static stability analysis the results from the single-pendulum and double-pendulum cases were nearly identical. This is also found to be true by running the full dynamic simulation without any motion. Figure 58 shows the maximum possible payload result for the static case when the boom is at luffing angle $\alpha = 0°$. The predicted values are plotted in a solid line, and the simulated results are plotted in a circle for a whole slewing angle β. The prediction and the simulation shows a very close match in their results.

The simulations were tested for different luffing angles. In Figure 59 and Figure 60, the maximum possible payload results for the prediction and the simulation results are plotted for the luffing angle α of 30° and 45° respectively. In both plots, the results shows a high degree of correlation, which further validates the accuracy of the prediction model used in the static stability analysis. In addition, the close match between the experimental data and the simulation in Figure 58 and Figure 59 also increases the confidence.

5.2.2 Straight Base Motion

The results from the full dynamic stability analysis are compared against the results obtained by the pseudo-dynamic stability analysis for each mobile boom crane setup and motion studied in the previous chapters. Because the crane is in motion, the

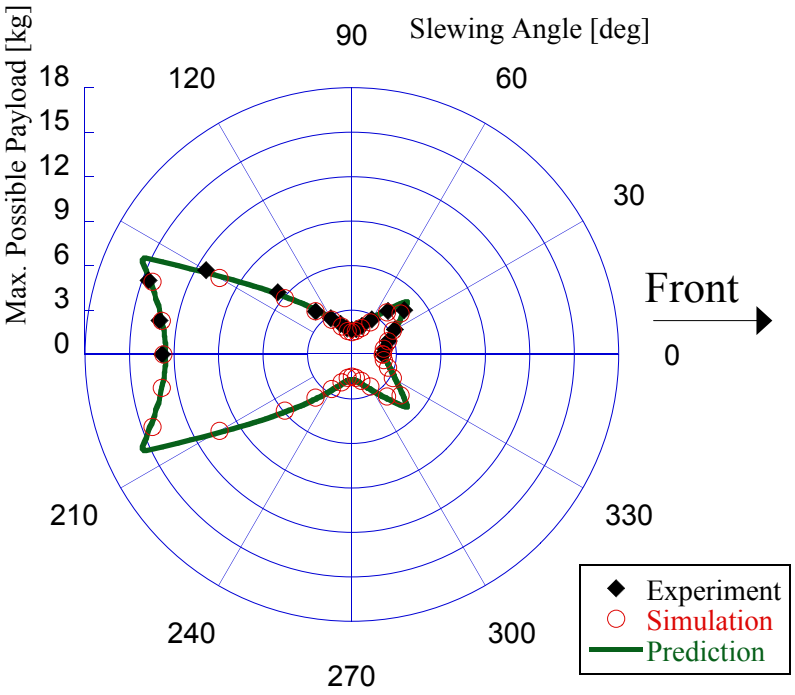

Figure 58: Maximum Possible Payload of Full Dynamic Stability Analysis for Static Case - [α=0°]

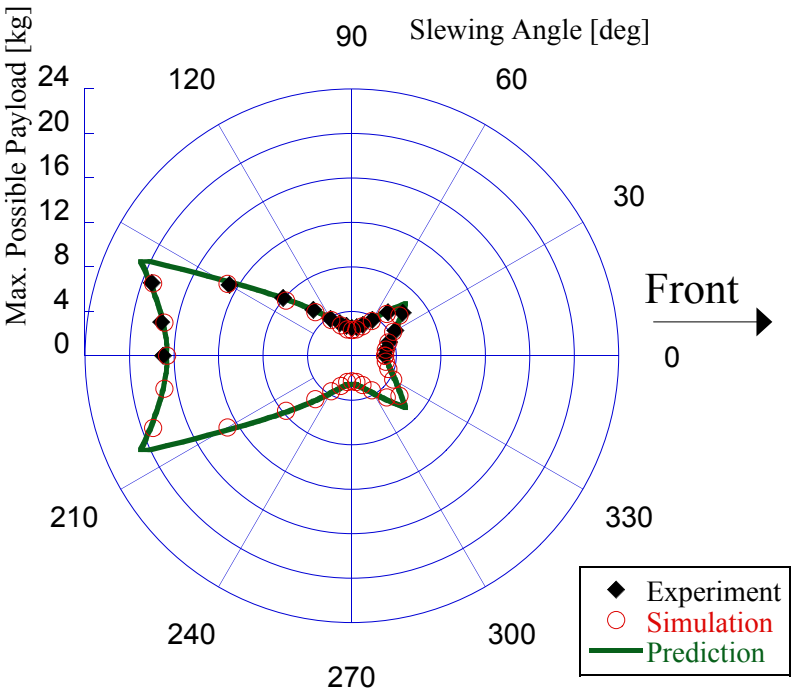

Figure 59: Maximum Possible Payload of Full Dynamic Stability Analysis for Static Case - [α=30°]

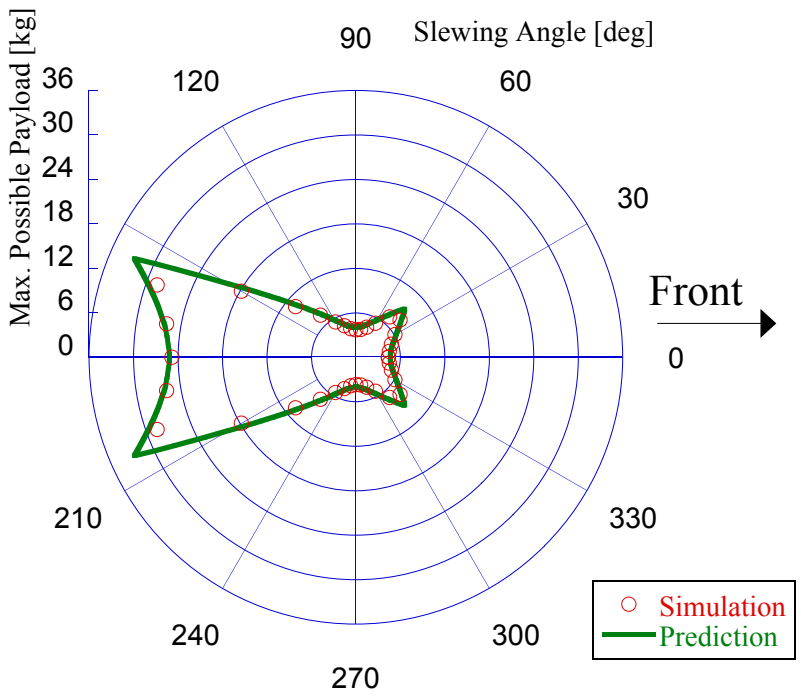

Figure 60: Maximum Possible Payload of Full Dynamic Stability Analysis for Static Case - [α=45°]

payload mass exhibits a different dynamic behavior in the single- and the double-pendulum cases. This leads to different tip-over stability results. For the straightline base motion with a bang-coast-bang acceleration command, the maximum possible payload mass for different values of acceleration magnitude and luffing angle for the single- and the double-pendulum cases are investigated.

Figure 61 shows the maximum payload results for the single-pendulum straightline base motion when the acceleration command has a magnitude of $1m/s^2$ at the luffing angle of 0°. The solid line represents the pseudo-dynamic prediction and the circles represent the simulated results. The results show a good match, except at the rear of the cart. As stated in the previous chapters, the pseudo-dynamic stability analysis tends to over-estimate the tip-over stability of the crane in this region.

Also as mentioned before, this error tends to grow as the luffing angle α increases in the pseudo-dynamic stability analysis. To study the effect of increasing α in the

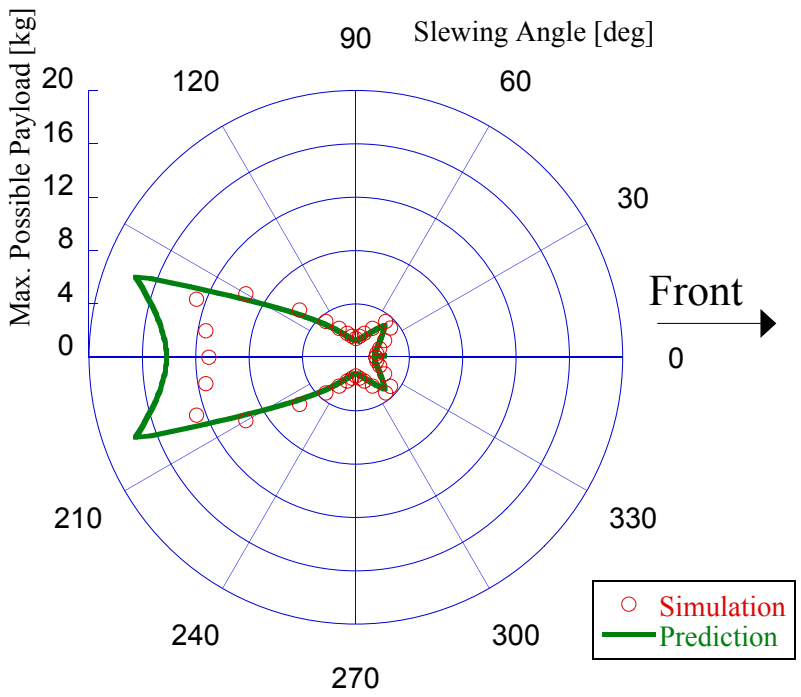

Figure 61: Maximum Possible Payload of Full Dynamic Stability Analysis for Single-Pendulum Straight Base Motion - [a=1m/s^2, α=0°]

pseudo-dynamic stability analysis, the same simulation shown in Figure 61 is performed with different luffing angles. Figure 62 and Figure 63 show the maximum possible payload results for $\alpha = 30°$ and 45° respectively. Again, in the $\beta = 160°$-200° region, the prediction line over-estimates the maximum possible payload values. The over-estimation becomes much larger than the $\alpha = 0°$ case in Figure 61, as expected. The results, however, match very well in all other β angles. This means that pseudo-dynamic stability analysis still returns an accurate prediction when the boom is pointing toward the front and to the sides. The plots also show a good agreement between the experimental data and the simulation results.

Moving the base at a faster acceleration rate also degrades the tip-over stability prediction of the pseudo-dynamic stability analysis. This is because higher acceleration produces larger payload swing, which increases the error in the tip-over torque estimation, as stated in Section 3.1. In Figure 64, the simulation result of straightline

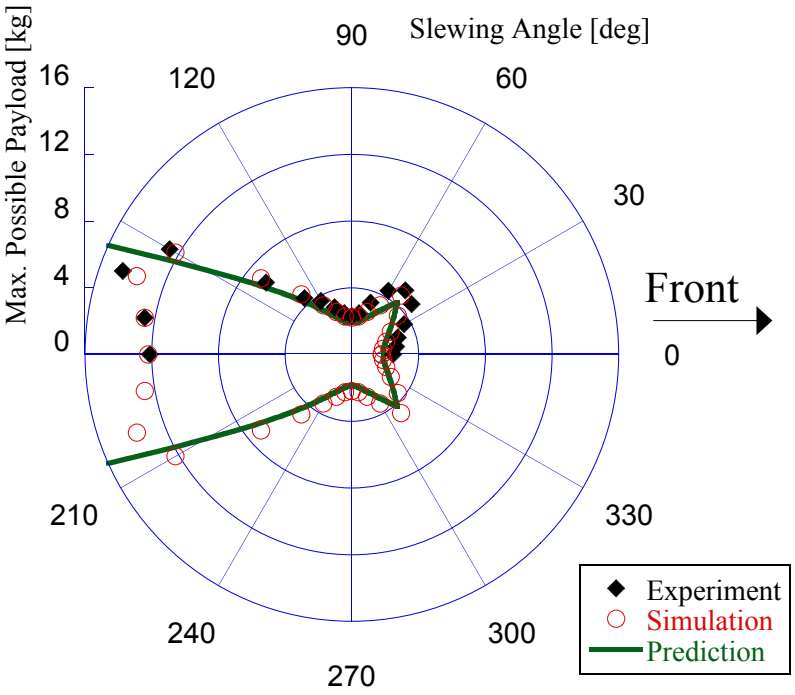

Figure 62: Maximum Possible Payload of Full Dynamic Stability Analysis for Single-Pendulum Straight Base Motion - [a=1m/s^2, α=30°]

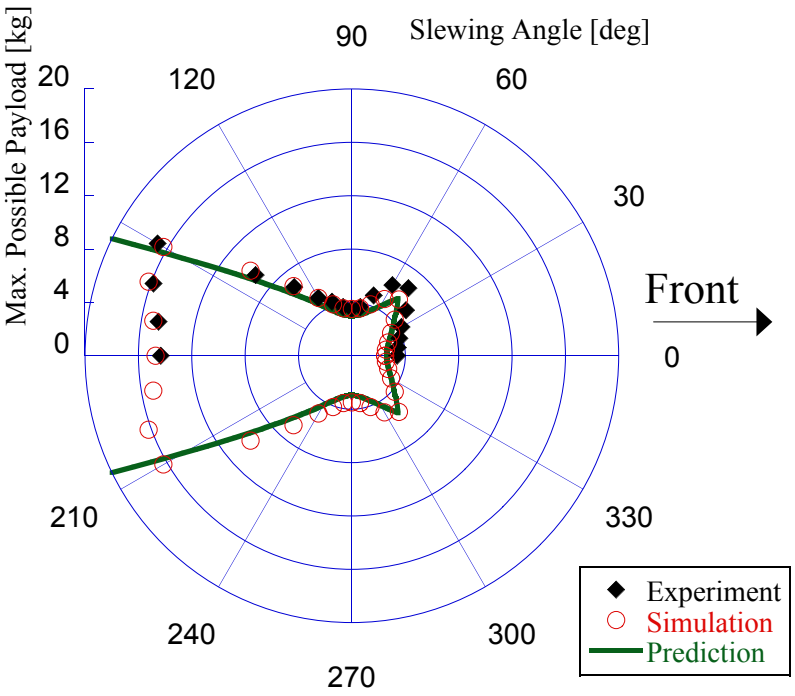

Figure 63: Maximum Possible Payload of Full Dynamic Stability Analysis for Single-Pendulum Straight Base Motion - [a=1m/s^2, α=45°]

base motion with an acceleration of $2m/s^2$ is shown. The plot again shows a similar shape as before. Compared to Figure 63, the accuracy of the prediction is slightly compromised. The pseudo-dynamic stability analysis prediction now over-estimates throughout the entire range of β.

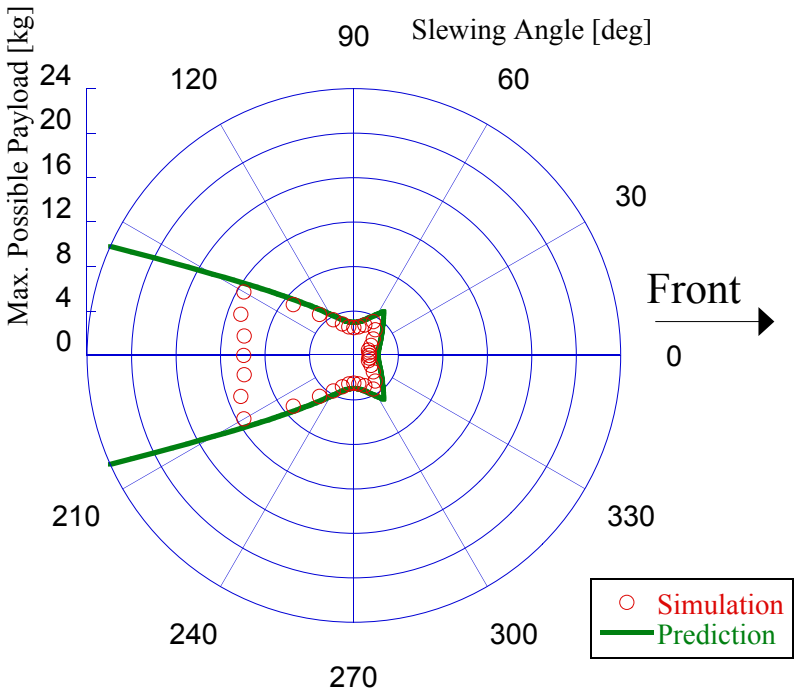

Figure 64: Maximum Possible Payload of Full Dynamic Stability Analysis for Single-Pendulum Straight Base Motion - [a=$2m/s^2$, α=45°]

The full dynamic stability analysis was also performed for the double-pendulum case. Figure 65 shows the maximum payload simulation results of the mobile boom crane with the double-pendulum setup when the acceleration command has a magnitude of $1m/s^2$ at the luffing angle of 0°. Figure 66 shows the results of the maximum payload mass when the boom is luffed up to $\alpha = 30°$. In both plots, similar characteristics as in the single-pendulum case are present. The predictions are found to be closely matched in most places, except near the back of the cart. The over-estimation grows larger as the luffing angle increases. The accuracy further decreases as the luffing angle and the acceleration magnitude increases. Figure 67 shows the result when the acceleration command is increased to a magnitude of $1.5m/s^2$ and the luffing

angle is raised to 45°.

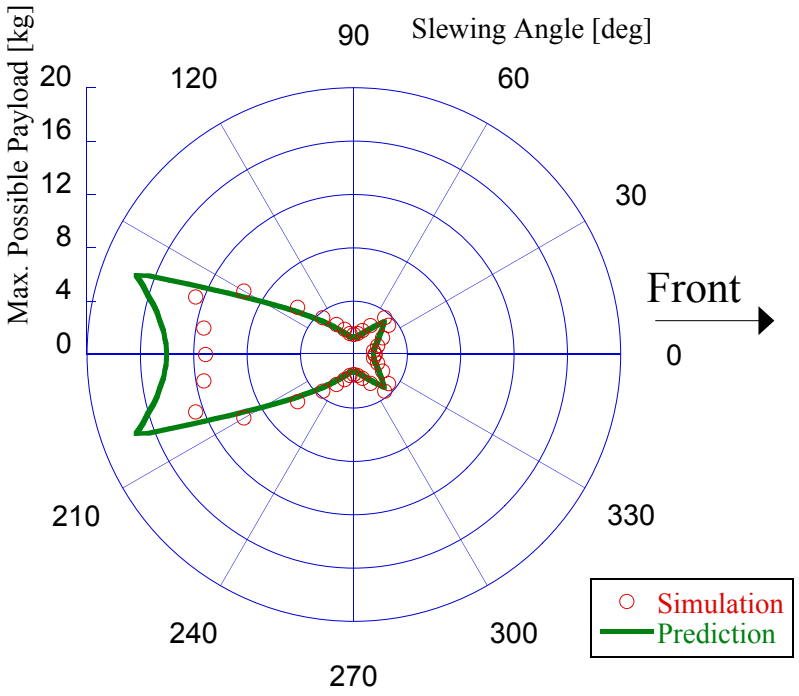

Figure 65: Maximum Possible Payload of Full Dynamic Stability Analysis for Double-Pendulum Straight Base Motion - [a=1m/s^2, α=0°]

As seen, the full dynamic stability analysis reveals that the pseudo-dynamic stability analysis in both the single- and the double-pendulum cases tends to over-estimate the tip-over stability near the back of the cart, in the range β = 160°-200°. The accuracy of the prediction is also reduced as the acceleration magnitude and the luffing angle increases. The majority of the error, however, occurs in the region where the cart is very stable. Since the pseudo-dynamic stability analysis still returns a good prediction in the region where the cart is less stable, thus much critical to be accurate, the method is useful for the tip-over stability prediction of the mobile boom crane.

5.2.3 Circular Path Motion

The full dynamic stability analysis was performed for the circular path motion at different cart velocities. To define the cart's steering motion, a state-space representation of the front axle steering model is utilized:

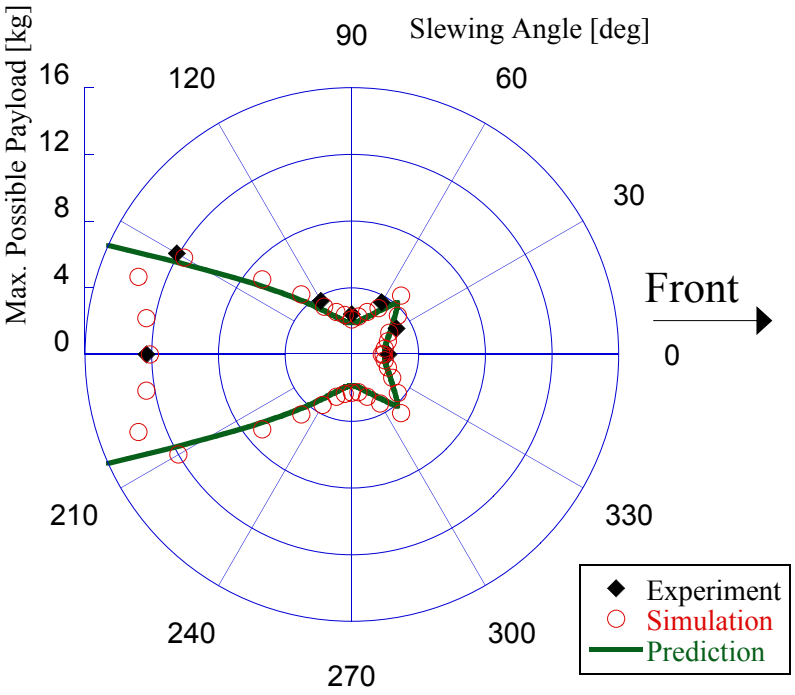

Figure 66: Maximum Possible Payload of Full Dynamic Stability Analysis for Double-Pendulum Straight Base Motion - [a=1m/s^2, α=30°]

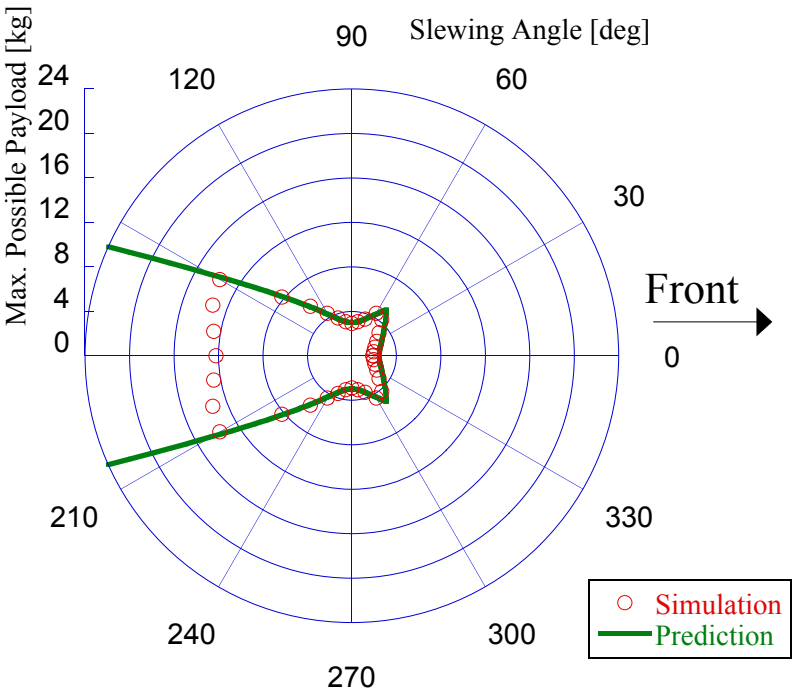

Figure 67: Maximum Possible Payload of Full Dynamic Stability Analysis for Double-Pendulum Straight Base Motion - [a=1.5m/s^2, α=45°]

$$\frac{d}{dt}\begin{pmatrix} x \\ y \\ \psi \\ \gamma \end{pmatrix} = \begin{pmatrix} \cos(\psi+\gamma) \\ \sin(\psi+\gamma) \\ \frac{1}{l_c}\sin\gamma \\ 0 \end{pmatrix} v + \begin{pmatrix} 0 \\ 0 \\ 0 \\ 1 \end{pmatrix} \dot{\gamma} \tag{5.1}$$

where v is the cart's linear speed at the front axle, γ is the steering angle, x and y describe the front-axle center position, ψ defines the base orientation, and l_c is the wheel separation in the longitudinal direction. By specifying the linear velocity of the base and the steering angle rate, it is possible to simulate cornering motion of the mobile boom crane. For consistency, the steering rate in these simulations is set to $0.23 rad/s$ and is timed so that it produces the radius of curvature about $3.0m$.

Figure 68 shows the maximum possible payload values obtained from the full dynamic simulation, represented by the circles, and the prediction using pseudo-dynamic stability analysis, represented by the solid line. In this case, the crane is equipped with a single-pendulum payload and the base is set to run at a constant velocity of v=$1m/s$ with a boom luffing angle of $\alpha = 0°$. The prediction line shows a high congruence with the simulation data, except at the back of the cart near $\beta = 160°$-$200°$. Unlike the straightline base motion case, the pseudo-dynamic stability analysis underestimates the tip-over stability of the system in the circular path motion. However, the errors are relatively small. Also, because it slightly under-estimates the stability where the crane is most stable, the errors are beneficial in terms of producing a conservative prediction.

The simulation was performed for different velocity settings. Figure 69 and Figure 70 show the simulation results for the cart velocity of $2m/s$ and $3m/s$ respectively. In both plots, characteristics similar to the v=$1m/s$ case are observable. The prediction, however, starts to over-estimate the payload mass as the cart velocity increases. This can be seen in Figure 70 near the front of the cart. One interesting behavior to

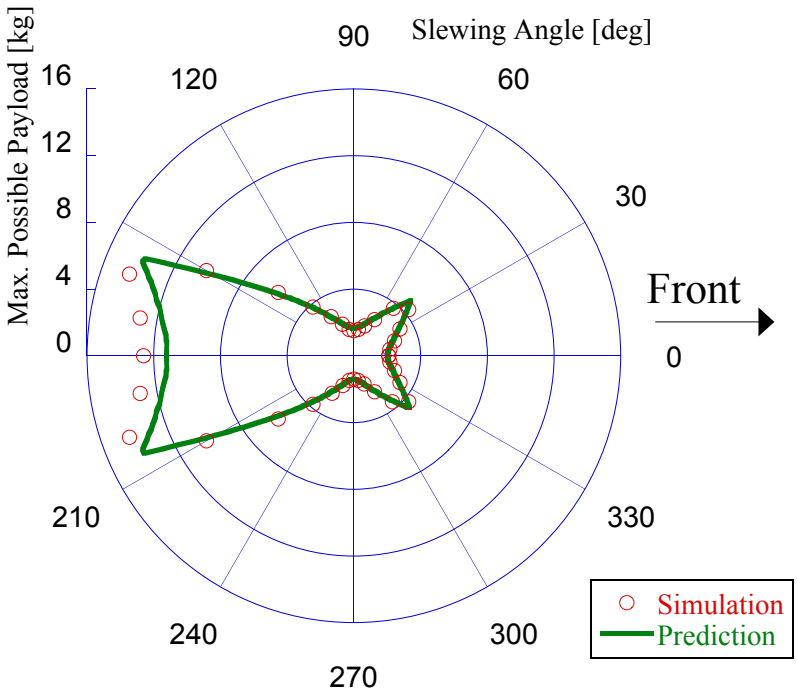

Figure 68: Maximum Possible Payload of Full Dynamic Stability Analysis for Single-Pendulum Circular Path Motion - [v=1m/s, α=0°]

note is that the prediction line has a diagonal stretch in its shape as the velocity magnitude increases. This is more obvious in Figure 70. This behavior is due to the cart undergoing a circular path motion in the counter-clockwise direction. The cart is found to be more tip-over stable when the boom is pointed along the path because this minimizes the curvature radius to the boom mass, and thus minimizes the effect of the centripetal force, which degrades the tip-over stability. If the cart is moving in the clock-wise direction, then the stretch would occur in the other diagonal direction.

Simulation results for non-zero luffing angles were also obtained. Figure 71 shows the experimental and simulation results when v=1m/s and $\alpha = 45°$. As mentioned before, the pseudo-dynamic stability analysis tends to lose prediction accuracy as α increases by under-estimating the tip-over stability during the circular path motion. This is still observed in the figure; the prediction line is scaled down at the rear of the cart, just like the $\alpha = 0°$ case. However, since the pseudo-dynamic method over-estimates the maximum possible payload values when α is increased, luffing the boom

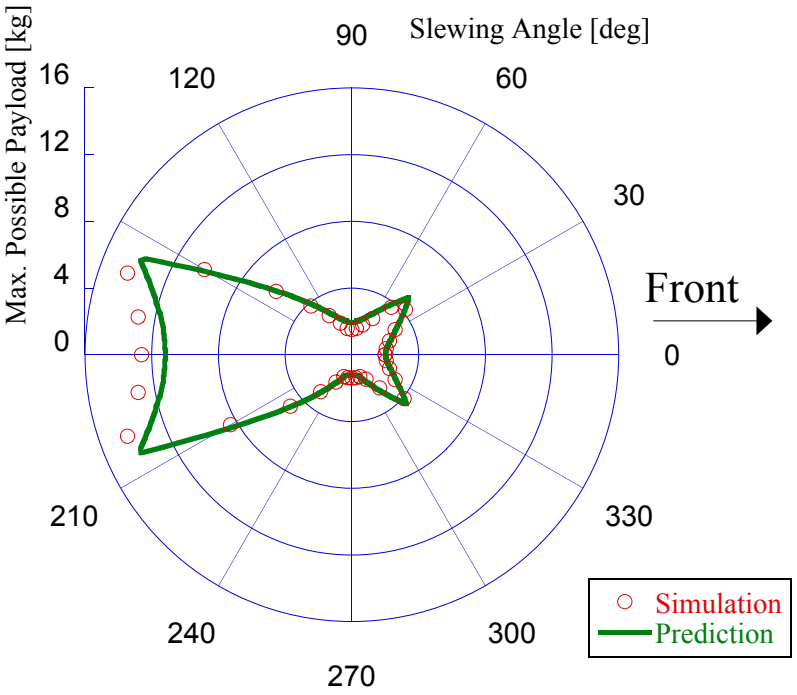

Figure 69: Maximum Possible Payload of Full Dynamic Stability Analysis for Single-Pendulum Circular Path Motion - [v=2m/s, α=0°]

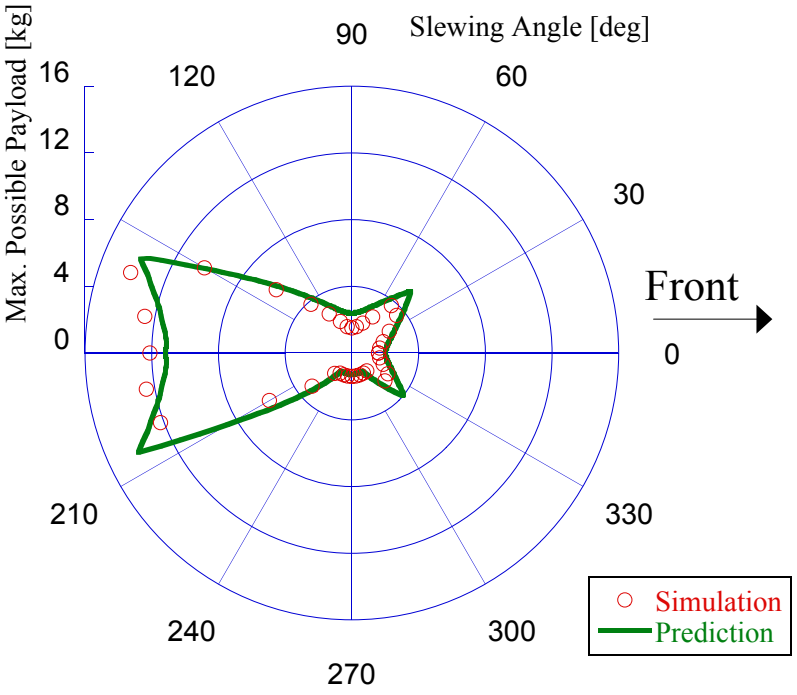

Figure 70: Maximum Possible Payload of Full Dynamic Stability Analysis for Single-Pendulum Circular Path Motion - [v=3m/s, α=0°]

up partially cancels the effect and produces a slightly better matching plot in Figure 71 than in the $\alpha = 0°$ case in Figure 68. The experimental data and the simulation also matched closely to each other.

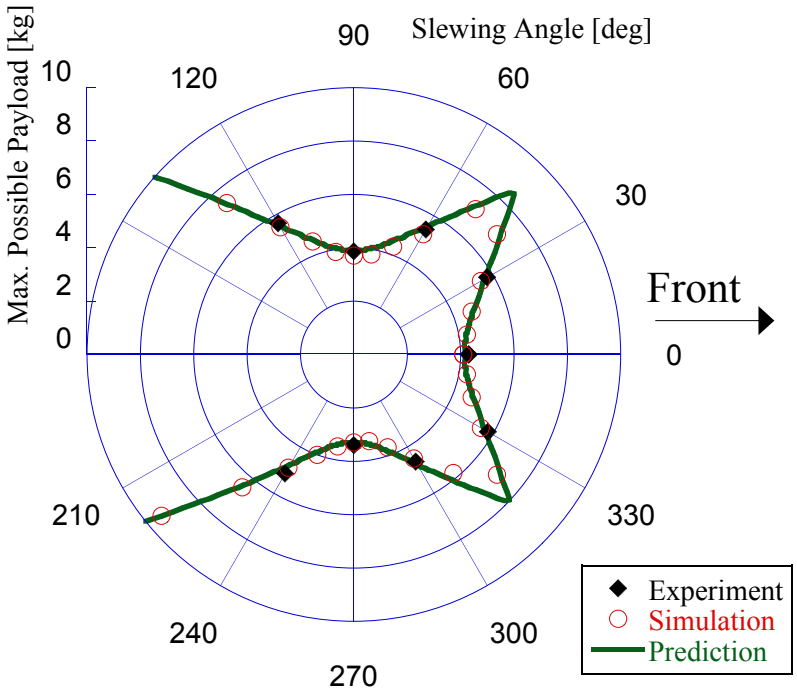

Figure 71: Maximum Possible Payload of Full Dynamic Stability Analysis for Single-Pendulum Circular Path Motion - [v=1m/s, α=45°]

Similar simulations were performed for the double-pendulum payload. Figure 72, Figure 73, and Figure 74 shows the maximum payload results for the mobile boom crane with the double-pendulum setup moving in the circular path with cart speeds of $1m/s$, $2m/s$, and $3m/s$ respectively. In the double-pendulum cases, similar tip-over stability behavior as for the single-pendulum case can be observed. The plots show a general agreement between the prediction and the simulation results, and indicate there is a slight under-estimation near the back of the cart. One key thing to note is that the diagonal stretch in the prediction line shape becomes more apparent in the double-pendulum case. The double-pendulum case also degrades the accuracy of the pseudo-dynamic prediction at the higher cart velocity, as seen in Figure 74. These are due to the rich and complex payload swinging dynamics that are neglected in the

pseudo-dynamic method. These effects occur to the greatest extend near the back of the cart. But they also manifest themselves in the critical area around $\beta = 90°$ and 270°.

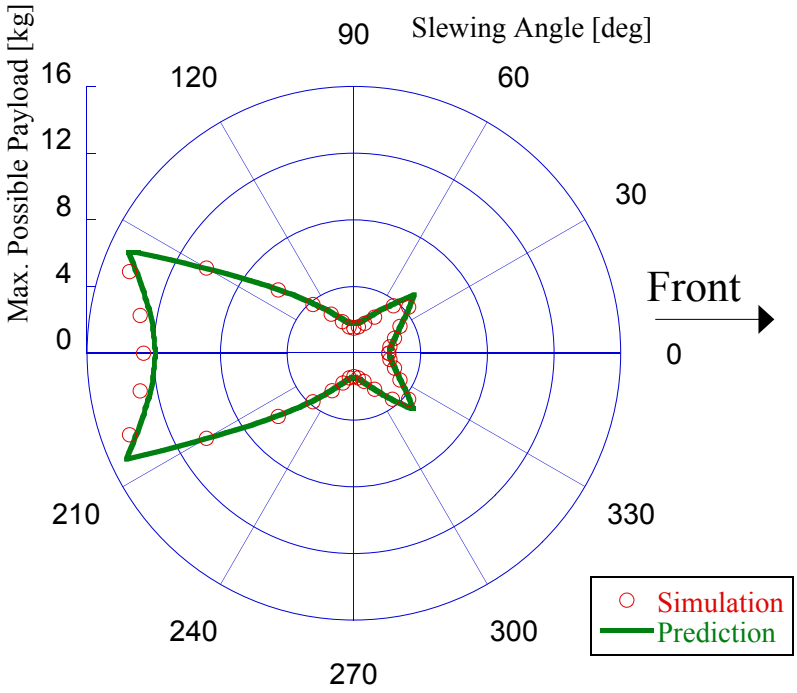

Figure 72: Maximum Possible Payload of Full Dynamic Stability Analysis for Double-Pendulum Circular Path Motion - [v=1m/s, α=0°]

At the higher luffing angles, the under-estimation of the pseudo-dynamic prediction is canceled by the over-estimation caused by the increased α. Figure 75 shows the double-pendulum case with $\alpha = 45°$. Similar to the single-pendulum case, the plot shows a high agreement between the prediction line, the simulation results and the experimental data.

The full dynamic stability analysis verified that the pseudo-dynamic stability analysis returns a good tip-over prediction for the circular path motion. The pseudo-dynamic method is found to under-estimate the maximum payload around $\beta = 160°$-200°, but this does not compromise the utility of the method in the tip-over stability analysis. Luffing the boom up, unlike other motion cases, is found to be helpful to

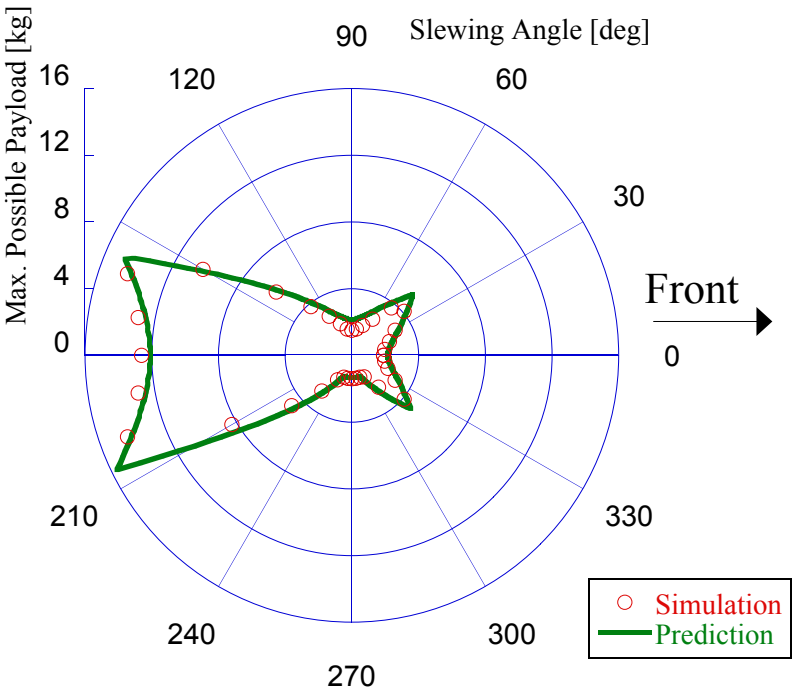

Figure 73: Maximum Possible Payload of Full Dynamic Stability Analysis for Double-Pendulum Circular Path Motion - [v=2m/s, α=0°]

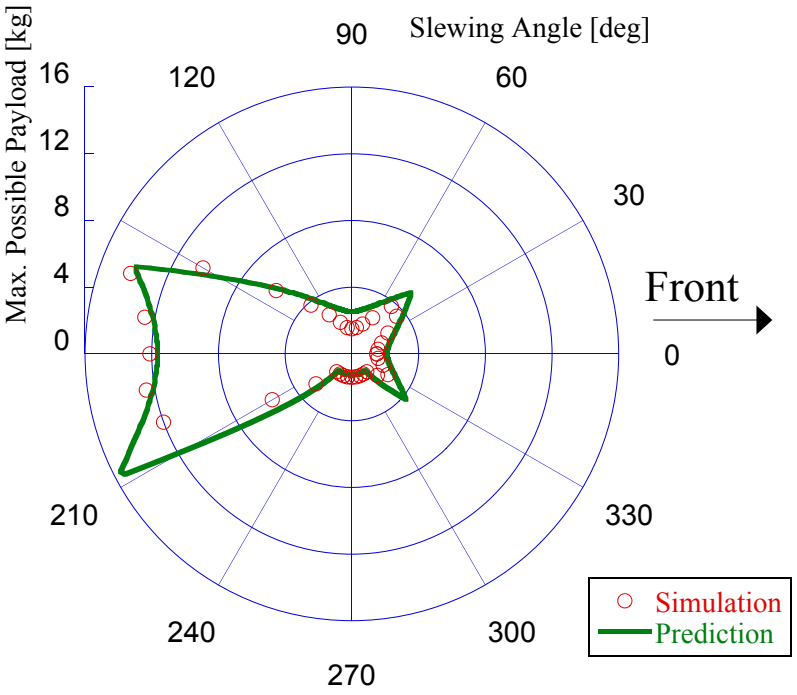

Figure 74: Maximum Possible Payload of Full Dynamic Stability Analysis for Double-Pendulum Circular Path Motion - [v=3m/s, α=0°]

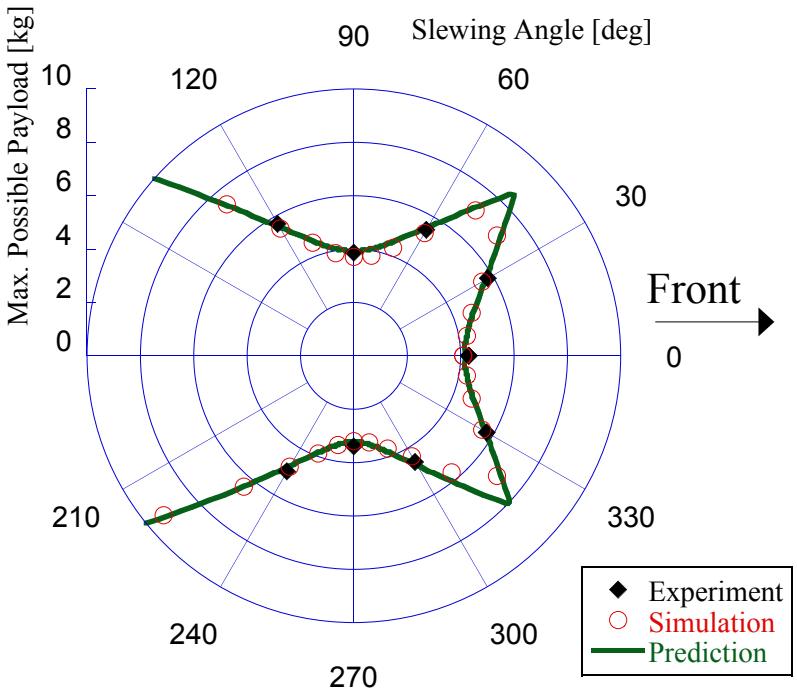

Figure 75: Maximum Possible Payload of Full Dynamic Stability Analysis for Double-Pendulum Circular Path Motion - [v=1m/s, α=45°]

the pseudo-dynamic stability analysis in the circular path motion. Also, the fact that the prediction line stretches its shape verifies that the method correctly incorporates the effect of the centripetal/inertial force. The method was verified to be applicable for both the single- and the double-pendulum setup. However, the pseudo-dynamic method starts to break down in the critical area near $\beta = 90°$ when the circular path velocity becomes large.

5.2.4 Boom Slewing Motion

The boom slewing motion was also simulated with the full dynamic stability analysis. Simulation results for different constant slewing rates were obtained for both the single- and the double-pendulum cases. The results were then compared with the pseudo-dynamic stability analysis prediction for a range of luffing angles to verify its accuracy.

Different values of slewing acceleration $\dot{\omega}$ were used to accelerate the boom to

different slewing rotational speeds. Figure 76 shows the maximum possible payload mass versus the luffing angle for the single-pendulum case when the boom slews at the constant rate of $\omega = 0.73 rad/s$ after being accelerated at $\dot{\omega}$=$0.5 rad/s^2$. The solid line indicates the predicted values, and the diamonds and the circles represent the experimental data and the simulation results respectively. As shown in the figure, the pseudo-dynamic method predicts the values fairy closely. As the luffing angle increases, the error between the prediction and the experiment/simulation also gets larger. However, the error is kept small even at high luffing angles. Also, because the error can be minimized by limiting the slewing speed and the luffing angle, this does not compromise the overall usefulness of the method.

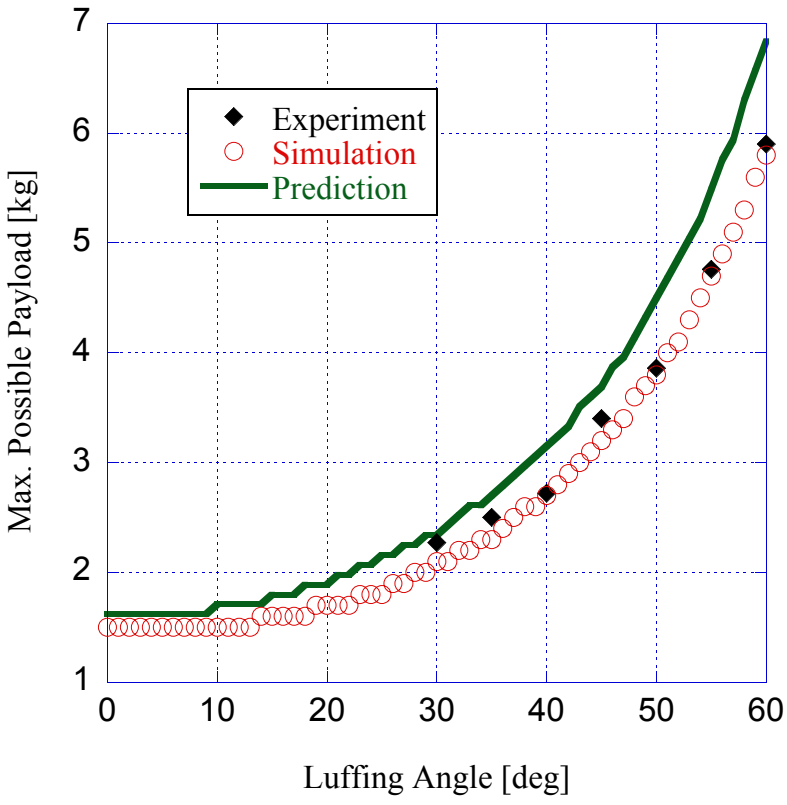

Figure 76: Maximum Possible Payload of Full Dynamic Stability Analysis for Single-Pendulum Boom Slewing Motion - [$\dot{\omega}$=$0.5 rad/s^2$]

Figure 77 shows the simulation results for slewing the boom at $\omega = 1.09 rad/s$ after being accelerated at $\dot{\omega}$=$0.75 rad/s^2$. It is clear that there is a large error between the

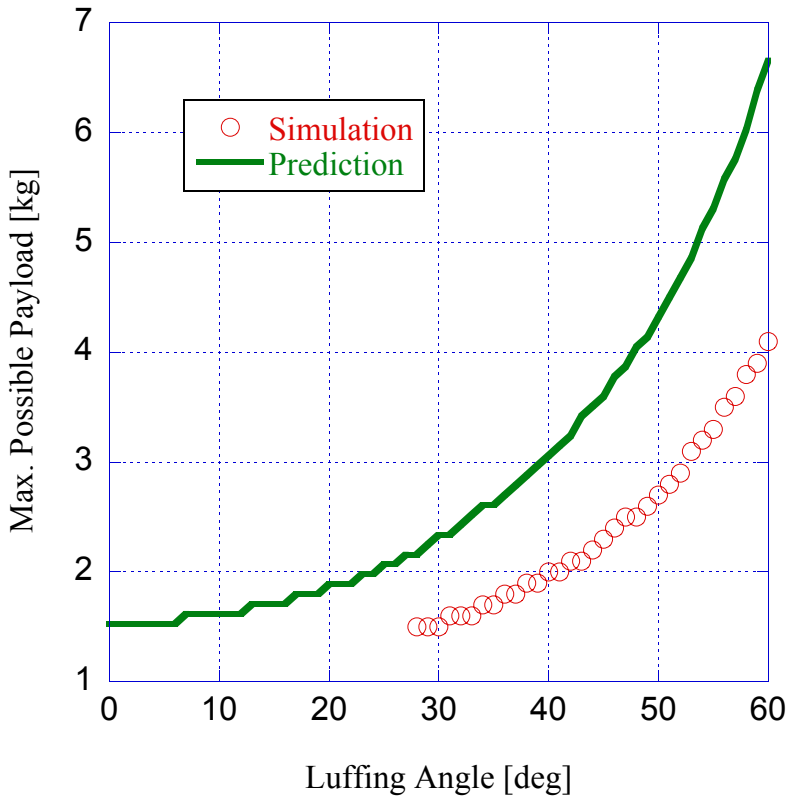

Figure 77: Maximum Possible Payload of Full Dynamic Stability Analysis for Single-Pendulum Boom Slewing Motion - [$\dot{\omega}$=0.75rad/s^2]

prediction and the simulation results. For $\alpha < 28°$, the method could not even predict the immediate tip-over of the mobile boom crane. This is due to the limitation of the pseudo-dynamic stability analysis discussed in Section 3.1. The method generates errors in the prediction as the magnitude of the input command increases because it causes a larger payload swing. Thus, for the boom slewing motion, it is critical that the slewing speed is kept low to produce a correct tip-over stability prediction.

For the double-pendulum case, the results show similar characteristics to the single-pendulum case. Figure 78 and Figure 79 show the maximum payload results for the double-pendulum case when slewing at $\omega = 0.73rad/s$ and $\omega = 1.09rad/s$ respectively. The pseudo-dynamic prediction returns a close estimation of the payload values to both the experimental data and simulation results when $\omega = 0.73rad/s$. At $\omega = 1.09rad/s$, the prediction over-estimates and results in a substantial error. In

addition, the full dynamic stability analysis suggests that the double-pendulum case is less stable compared to the single-pendulum case when the boom is slewing. As shown in Figure 79, the mobile boom crane tips over when $\alpha < 30°$, whereas in Figure 77 the boom crane can remain stable for α slightly less than 28°.

The full dynamic stability analysis shows that the pseudo-dynamic stability analysis can provide accurate tip-over prediction for a low slewing rate with both single- and double-pendulum payloads setup. However, the error may arise when either the luffing angle or the slewing rate is high. The under-estimation due to the increased α does not pose a significant problem. The error due to the increased speed, on the other hand, can be problematic since the pseudo-dynamic method no longer can provide highly accurate information. By maintaining a slow slewing speed, the method

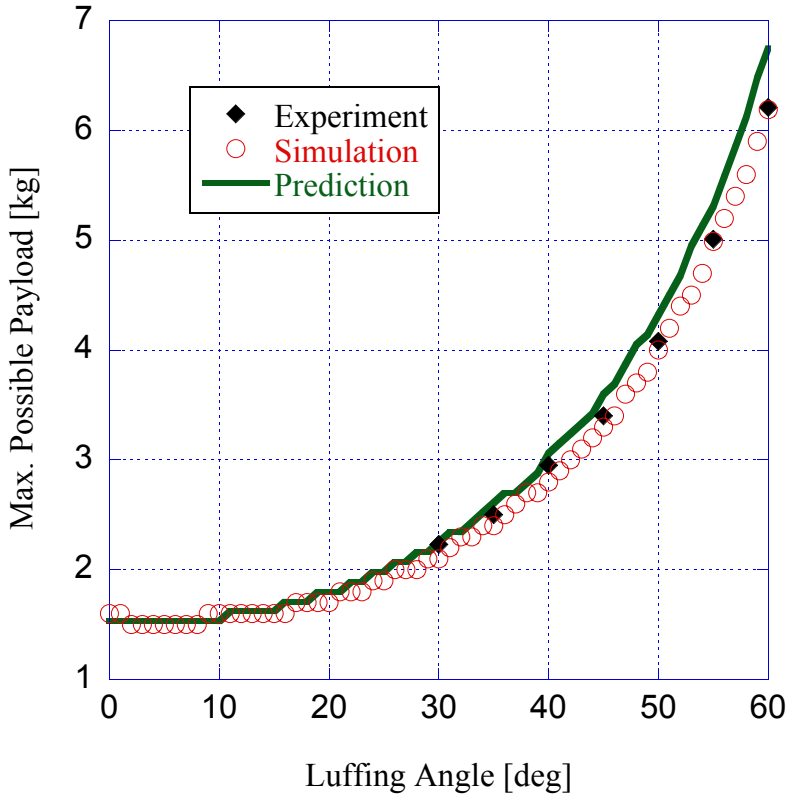

Figure 78: Maximum Possible Payload of Full Dynamic Stability Analysis for Double-Pendulum Boom Slewing Motion - [$\dot{\omega}$=0.5rad/s^2]

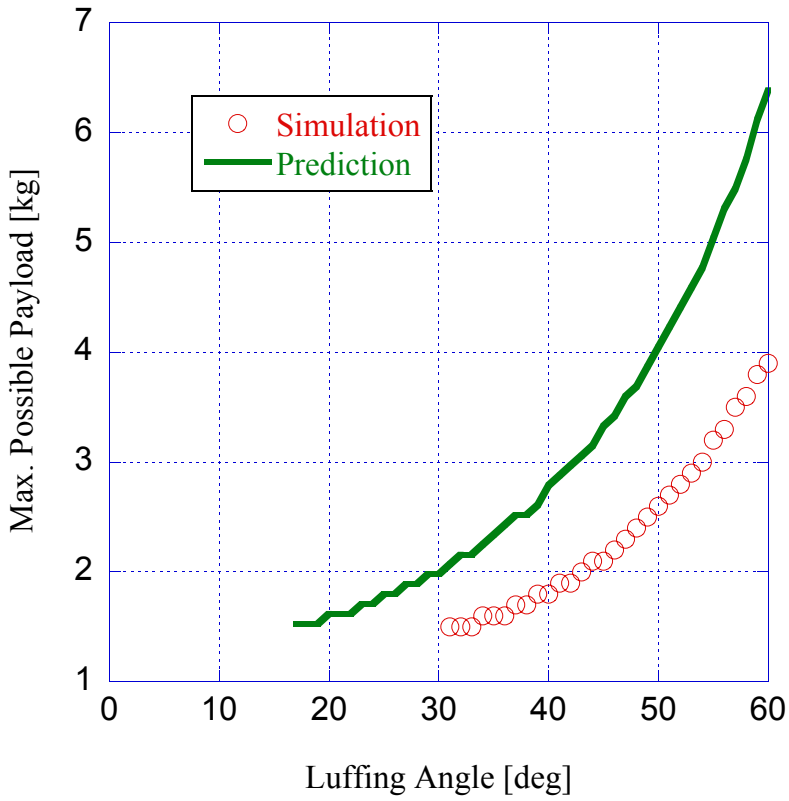

Figure 79: Maximum Possible Payload of Full Dynamic Stability Analysis for Double-Pendulum Boom Slewing Motion - [$\dot{\omega}$=0.75rad/s^2]

can be a useful tool to predict the tip-over of the mobile boom crane. Also, the single-pendulum case was found to be less stable than the double-pendulum case for constant boom slewing motion.

5.2.5 Boom Luffing Motion

Boom luffing motion was simulated, and the maximum possible payload values were obtained from the full dynamic stability analysis. The boom was initially set at $\alpha = 90°$ and then was luffed downward until $\alpha = 0°$ at a constant rate $\dot{\alpha}$. Different values of $\ddot{\alpha}$ were used to accelerate the luffing to the different constant speeds. The simulation results were obtained for a whole range of the slewing angle β at the different $\dot{\alpha}$ values, for both the single- and the double-pendulum payloads setup.

Figure 80 shows the maximum possible payload results obtained from the full dynamic simulation model and the predicted values from the pseudo-dynamic stability analysis when $\ddot{\alpha}$=$-0.05 rad/s^2$. Overall, the simulated results agree with the prediction very closely. However, near the back of the cart the pseudo-dynamic method slightly under-estimates the values. This, again, is due to the simplifications and assumptions made in the pseudo-dynamic analysis. The error, however, is small and the under-estimation helps to keep a conservative estimation.

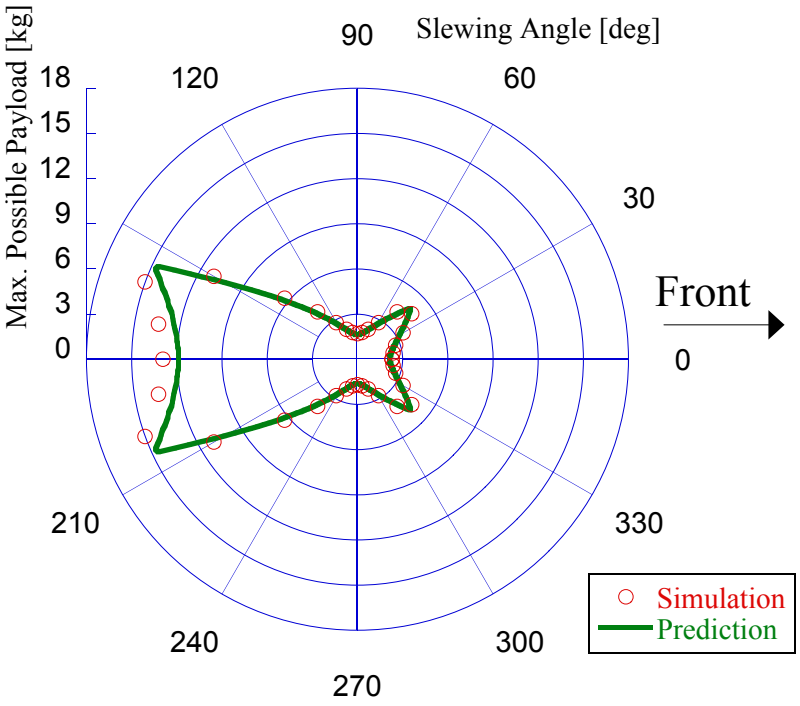

Figure 80: Maximum Possible Payload of Full Dynamic Stability Analysis for Single-Pendulum Boom Luffing Motion - [$\ddot{\alpha}$=$-0.05 rad/s^2$]

The simulation was also tested for different $\dot{\alpha}$ values. Figure 81 and Figure 82 show the simulation results for $\ddot{\alpha}$=$-0.25 rad/s^2$ and $\ddot{\alpha}$=$-0.5 rad/s^2$ respectively. In both plots, the simulation results and the pseudo-dynamic estimation match well. The prediction, as expected from the observations of the other motion cases, tends to over-estimate the values with increased $\dot{\alpha}$. This is especially vivid near the back and the front of the cart. To minimize the error due to the excessive payload swing that

compromises the pseudo-dynamic stability analysis, the magnitude of $\dot{\alpha}$ needs to be kept low.

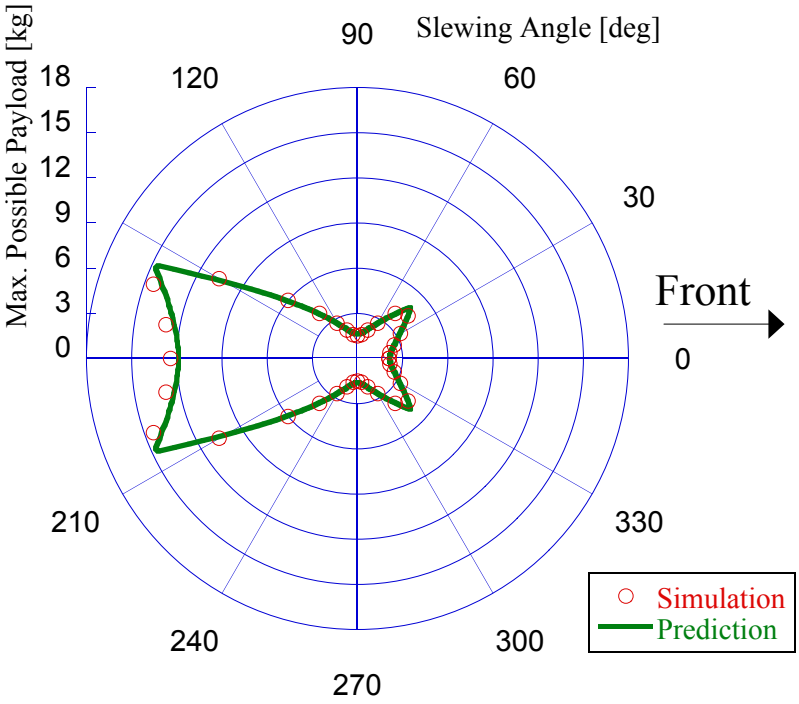

Figure 81: Maximum Possible Payload of Full Dynamic Stability Analysis for Single-Pendulum Boom Luffing Motion - [$\ddot{\alpha}$=$-0.25 rad/s^2$]

In Section 3.5, the pseudo-dynamic stability analysis returned an extremely close tip-over prediction for all $\ddot{\alpha}$ cases. The simulation results, however, show that the crane loses its tip-over stability when the boom is luffed down at higher $\ddot{\alpha}$ rates. The pseudo-dynamic method fails to capture on this behavior because of the assumption made in (3.28). To simplify the computation, the equation assumed a constant luffing rate $\dot{\alpha}$. As a result, the final φ_{max} estimation in (3.30) does not consider the swing contribution from $\ddot{\alpha}$. Therefore, the pseudo-dynamic stability analysis is unable to accurately predict the tip-over stability reduction due to the luffing acceleration magnitude.

In the double-pendulum case, the tip-over stability plots again presents similar trends as with the single-pendulum case. Figure 83, Figure 84, and Figure 85

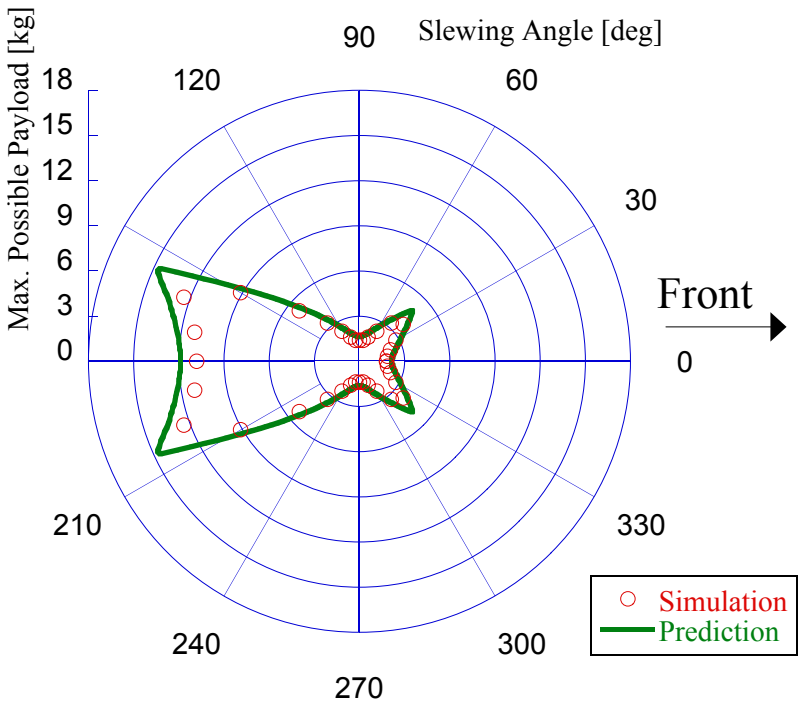

Figure 82: Maximum Possible Payload of Full Dynamic Stability Analysis for Single-Pendulum Boom Luffing Motion - [$\ddot{\alpha}$=$-0.5 rad/s^2$]

show the simulation results with the double-pendulum setup for $\ddot{\alpha}$=$-0.05 rad/s^2$, $\ddot{\alpha}$=$-0.25 rad/s^2$, and $\ddot{\alpha}$=$-0.5 rad/s^2$ respectively. In all cases, the simulation data and the predicted values matches well except for the back of the cart. The pseudo-dynamic prediction line under-estimates the payload values when the boom luffs downward at a slower rate. The prediction line tends to over-estimate as the luffing speed increases.

By performing the full dynamic stability analysis, it has been shown that the pseudo-dynamic stability analysis can provide good tip-over prediction for luffing motion of the mobile boom crane for both single- and double-pendulum payloads. There is a slight prediction error observed at the back of the cart. The analysis provides a conservative prediction for slower luffing rates. The accuracy of the prediction was found to be degraded as the luffing speed increases. To have a reliable prediction, again, it is important to limit the luffing speed to a relatively low rate.

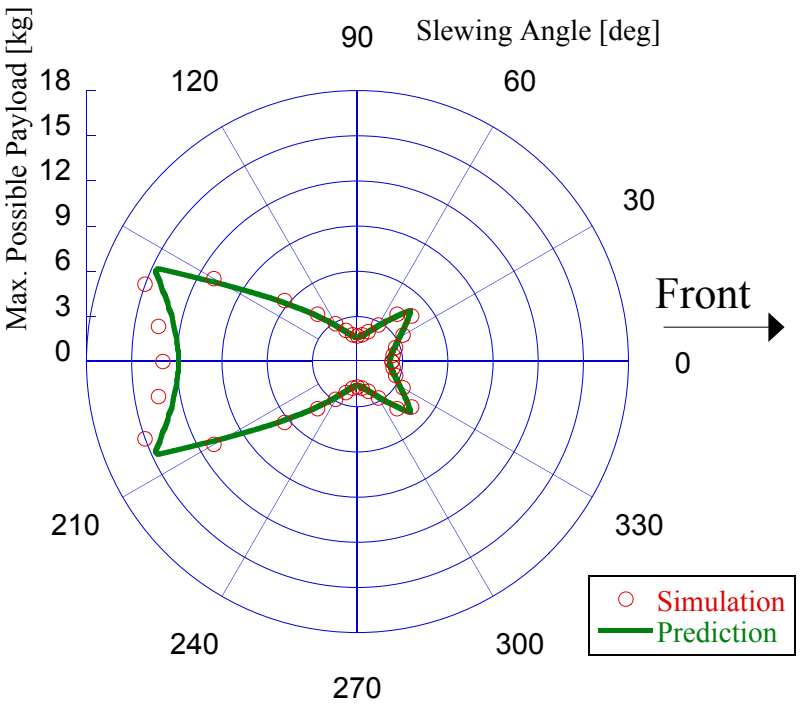

Figure 83: Maximum Possible Payload of Full Dynamic Stability Analysis for Double-Pendulum Boom Luffing Motion - [$\ddot{\alpha}$=$-0.05 rad/s^2$]

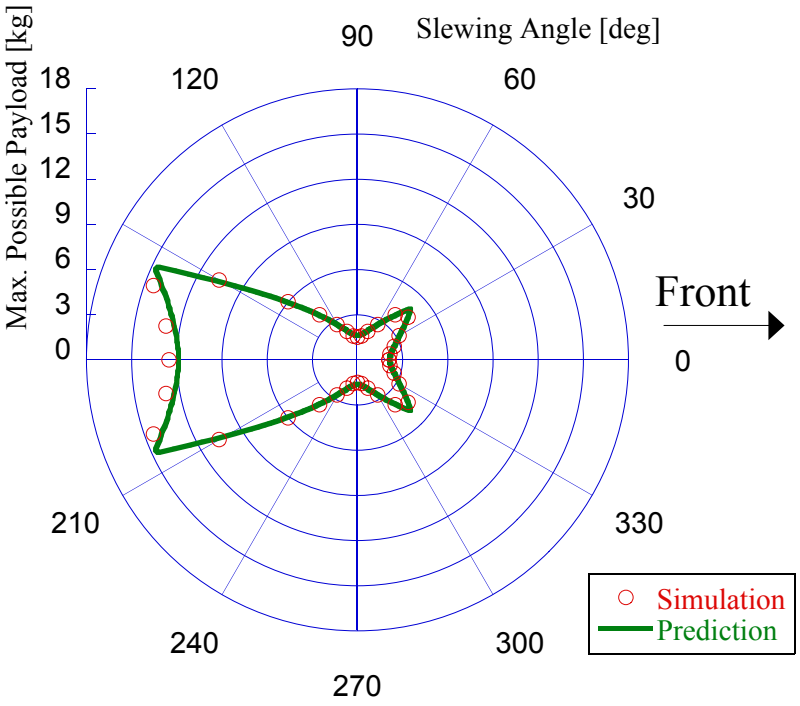

Figure 84: Maximum Possible Payload of Full Dynamic Stability Analysis for Double-Pendulum Boom Luffing Motion - [$\ddot{\alpha}$=$-0.25 rad/s^2$]

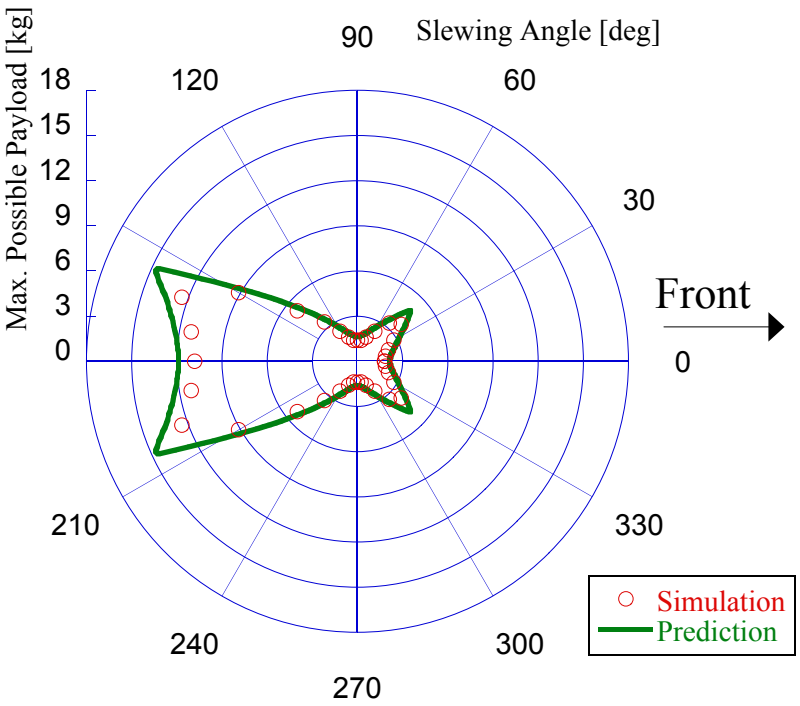

Figure 85: Maximum Possible Payload of Full Dynamic Stability Analysis for Double-Pendulum Boom Luffing Motion - [$\ddot{\alpha}$=$-0.5 rad/s^2$]

5.3 Summary

In this chapter, a full dynamic stability analysis was performed to verify the tip-over prediction computed by the simple prediction model and the pseudo-dynamic stability analysis. A dynamic multi-body simulation model was developed. The model was used to simulate mobile boom crane and the payload dynamics during common crane motions. The tip-over stability of the simulation model was observed by determining the maximum possible payload values.

In the static case, the prediction and the simulation show high agreement, proving that the static stability analysis accurately predicts tip-over when the crane is not in motion. In the dynamic case, the pseudo-dynamic prediction generally agrees with the simulation results. The pseudo-dynamic stability analysis, however, tends to produce prediction errors toward the back of the cart (β = 160°-200°). The error also tends to increase as the magnitude of the input and the luffing angle α

increases. This is an expected behavior that results from the simplifications made in the pseudo-dynamic stability analysis. The pseudo-dynamic stability analysis, however, successfully incorporates most of the dynamic effects into its prediction and accurately reflects them in the tip-over stability calculation. In addition, the errors can be limited by controlling the maximum values of the inputs and luffing angles. The errors at the rear of the cart can also be ignored because they occur at the boom configuration where the system is most stable. It is more critical to return a conservative and accurate tip-over prediction at the configurations that are less stable. The pseudo-dynamic stability analysis accurately predicts tip-overs in those situations. As a result of the full dynamic simulations, and the experimental results in the previous chapters, the simple prediction model and the pseudo-dynamic stability analysis have been proven to be useful tools for predicting tip-over stability.

CHAPTER VI

CONCLUSIONS AND FUTURE WORK

6.1 Conclusions

Preventing tip-over accidents of heavy machines, such as cranes, has a significant benefit in terms of protecting the lives of operators and reducing the risks of damage costs. At the same time, high productivity must be maintained for the operation. One of the possible ways to realize this is to develop a monitoring system which can predict when the tip-over occurs and send a warning signal.

This thesis investigated the tip-over stability of mobile boom cranes because of their high productivity and susceptibility to tip-over. The thesis presented a method to calculate an index, the tip-over stability margin angle, which characterizes the tip-over stability of the system's platform. Using the tip-over stability margin angle calculation and the simple prediction model of the mobile boom crane, an analysis of the tip-over stability of a stationary boom crane was performed as an initial step. The static stability analysis revealed the general characteristics of the mobile boom crane's tip-over stability.

Allowing boom cranes to move their base and boom while carrying a payload greatly enhances their workspace, and thus their productivity. However, these motions can result in large amounts of payload swing, and lead to a decrease in the tip-over stability of the crane. After studying the influence of the boom crane configuration on the tip-over stability in the static case, a pseudo-dynamic stability analysis was performed to investigate the tip-over stability of the cranes when they are in motion. The analysis provided insights into the mobile boom crane's tip-over stability

for simple and common crane motions. The pseudo-dynamic stability analysis incorporated the effects of driving and boom maneuvers without considering the entire complex dynamics in order to minimize the computational cost. The analysis and the experiments with the example setup showed that this approach provides a close estimation of the maximum possible payload that the mobile boom crane can carry without tip-over.

The tip-over stability analysis was extended to the double-pendulum payload to study the tip-over behavior of more complex cranes configurations. The extra mass of the hook was added to the simple prediction model. The hook mass in the suspension cable causes the payload to behave like a double-pendulum, which exhibits complex swing dynamics. To facilitate computation, the maximum swing angle calculated for the single-pendulum case was directly applied to the double-pendulum setup. This was justified by assuming that the worst case occurs when both cable segments are swung outward to form the same angle with the vertical direction. The calculated results and the experimental data verified that the pseudo-dynamic stability analysis successfully includes the double-pendulum payload into the tip-over stability calculation.

The dynamics of the payload swing and inertia forces during the driving and the boom maneuvers are very complex. The tip-over stability estimation during such maneuvers heavily dependent on the crane parameters and the input commands. In addition, since there were assumptions and simplifications made in the pseudo-dynamic stability analysis some critical factors that influence the tip-over stability may have been omitted. To obtain accurate crane tip-over stability data, a full dynamic simulation model of the mobile boom crane was developed and presented in Chapter 5. This model provided a very useful help to further understand the tip-over stability of the mobile boom crane. The simulation data verified that the pseudo-dynamic stability analysis is a useful tool to predict tip-overs.

6.2 Future Work

The results and insights gained in this thesis build a foundation for further work in the area of mobile boom crane tip-over stability analysis. There are many directions the future investigations can extend the analysis to.

First, the current pseudo-dynamic stability analysis presented in this thesis can be improved to return more accurate and robust predictions. As discussed, the pseudo-dynamic method tends to cause prediction errors near the back of the cart. Also, the method loses accuracy when the boom's luffing angle is increased, and when the payload swings widely due to a larger input magnitude. These limitations needs to be solved to further increase the utility and reliability of the pseudo-dynamic stability analysis.

Another way the future work can stem from this thesis is to analyze the tip-over stability of the boom crane when it carries a more complex payload. In this thesis, all payloads are treated as point masses. In a real application, however, the payload has a finite dimension and distributed mass. Depending on where the mass is hung from the cable, it can cause very complex payload dynamics [33]. In addition to the double-pendulum dynamics, these payloads can cause more complex behaviors [46, 47, 21]. In some cases, the payloads also can vary their mass during the operation. Examining these payload dynamics and analyzing their influence on the boom crane's tip-over stability is an important extension to study in this area.

The tip-over stability of cranes subjected to more complex driving and boom maneuvers also needs to be investigated. This thesis only considers the boom crane's the most basic motions and analyzes the payload swing caused by the simple maneuvers. To maximize their productivity, the cranes can initiate two or more of these motions simultaneously. Even more complicated motions can be realized to optimize the efficiency. The combined influences of the crane configuration and structure, and the complexity of the driving maneuver present unbounded possibilities for future topics.

Other types of machines, such as cherry-pickers and excavators, also present tip-over hazards. The prediction model developed in this thesis can be adapted to the other types of machines by replacing the boom crane with the corresponding structures. There has been research on modeling flexible arm structures and on their control strategies [5, 13, 17, 54, 34, 52]. Since replacing the crane alters the overall structure of the machine, they may present different tip-over stability characteristics. Additionally, the prediction model can be extended to include additional safety features such as stabilizing arms and counter weights. Implementing adjustable, training-wheel-like jacks can also help to prevent a mobile boom crane from tipping over. The effects and optimization of such safety equipment in improving the tip-over stability may be investigated in more detail.

Payload swing has a significant influence on boom crane's tip-over stability. Therefore, it is desirable to limit these effects. A possible solution to eliminate the payload oscillation is to use a command shaping technique called input shaping [44]. Input shaping has been successfully implemented on a variety of flexible systems. Several research groups have used input shaping on long reach manipulators to eliminate multiple modes of vibration and improve system tracking [44, 30, 31, 29, 7]. Input shaping has been implemented on many types of cranes, such as gantry or bridge cranes [14, 19, 48, 47] and a mobile tower crane [51]. Different types of input shaping, such as specified-deflection input shapers, are also designed [39, 43, 40, 41, 42].

To implement the input shaping controller on real mobile boom cranes, the actuator dynamics need to be closely investigated. Nonlinearities, such as the acceleration and velocity limits and saturation of the crane's actuators could degrade the performance of an input shaper. The influence of applying input shapers to limit maximum payload deflection and improve the crane's tip-over stability has been analyzed for simple driving maneuvers and shown to be effective for the single-pendulum case [38]. Future work could further develop input shaper design for mobile boom cranes, and

investigate its effects on tip-over stability for different payload settings and crane motions.

APPENDIX A

MATLAB SOURCE CODES

Source Code A.1: The Simple Tip-Over Prediction Model of the Mobile Boom Crane

```
function Results = SimpleModel(in_m_1, in_m_2, in_l_1, in_l_2, in_alpha_ini,
in_beta_ini, in_t_step, in_t_final, in_VorA, in_frame, in_vel0, in_t_offset,
in_Input_Type)

%%% Function: takes in the same simulation input from the Autolev full simulation
model.
%%% It returns the tip-over stability margin angle measure in degree.
%%% NOTE: The model predicts the tip-over tability of a MBC ONLY at that INSTANT
condition described by the parameters.
%%% NOTE: The model ignores 4 angle conditions [++, +-, -+, --] for phiOne and
thetaOne by looking only at the worst combination.

%%% New inputs NOT assigned in the Autolev Model: %%%%%%%%%%%%%%%%%%%%%%%%%
Type = in_Input_Type;
                % type of input command;
                % 0-static, 1-base acc., 2-cornering, 3-slewing, 4-luffing
                % 5-I.S. base acc., 6-I.S. cornering, 7-I.S. slewing,
                % 8-I.S. luffing
gamma = 0;      % in [deg], matter ONLY if Type = 2 or 6
SlopeFB = 0;    % in [deg], incline [+] and downhill [-]
SlopeS = 0;     % in [deg], incline sides; downhill to right [+] and to left [-]
% SlopeFB = SlopeFB*Deg2Rad;  % re-assign in [rad]
% SlopeS = SlopeS*Deg2Rad;    % re-assign in [rad]
%%%%%%%%%%%%%%%%%%%%%%%%%%%%%%%%%%%%%%%%%%%%%%%%%%%%%%%%%%%%%%%%%%%%%%%%%%%%

%%% NOTES!! %%%
% The global origin for all position vector is the origin of "Shadow" frame
( = Newtonian Frame origin).
% To mimic Single-Pendulum, use m=m1+m2 and l=l1+l2, and set m2,l2<<m1,l1.
%%%%%%%%%%%%%%%
```

```
31
32
33
34 % Initial Set-up:
35 Results = zeros(1,2);
36 I = eye(3,3);
37
38 % Conversion:
39 Rad2Deg = 180/pi;
40 Deg2Rad = pi/180;
41
42 % Re-assign inputs to the global variables defined in the Full-Dynamic Simulation.
43 m_1 = in_m_1;
44 m_2 = in_m_2;
45 l_1 = in_l_1;
46 l_2 = in_l_2;
47 alpha_ini = in_alpha_ini;
48 beta_ini = in_beta_ini;
49 t_step = in_t_step;
50 t_final = in_t_final;
51 VorA = in_VorA;
52 frame = in_frame;
53 vel0 = in_vel0;
54 t_offset = in_t_offset;
55
56 % Simulation Crane Parameters:
57 %------------------------+------------------+-------------+------------
58 % Quantity               | Value            | Units       | Description
59 %------------------------|------------------|-------------|-----------
60 bcom                     =  0.8;              % m           Constant
61 bl                       =  1.7;              % m           Constant
62 cl                       =  1.1;              % m           Constant
63 cw                       =  0.70;             % m           Constant
64 d1                       =  0.3;              % m           Constant
65 d2                       =  0.28;             % m           Constant
66 damp                     =  1000;             % N*sec/m     Constant
67 g                        =  9.81;             % m/sec^2     Constant
68 h                        =  0.14;             % UNITS       Constant
69 l1                       =  l_1;              % m           Constant
70 l2                       =  l_2;              % m           Constant
71 m1                       =  m_1;              % kg          Constant
```

```
m2                          =  m_2;              % kg          Constant
mB                          =  8.0;              % kg          Constant
mC                          =  24.9;             % kg          Constant
r                           =  0.14;             % m           Constant
stiff                       =  250000;           % N/m         Constant
xcom                        =  0.12;             % m           Constant
ycom                        =  0;                % m           Constant
gammapp                     =  0.0;              % UNITS       Constant
vpp                         =  0.0;              % UNITS       Constant

gamma                       =  gamma;            % UNITS       Initial Value
phiOne                      =  0.0;              % UNITS       Initial Value
phiTwo                      =  0.0;              % UNITS       Initial Value
psi                         =  0.0;              % UNITS       Initial Value
q1                          =  0.0;              % UNITS       Initial Value
q2                          =  0.0;              % UNITS       Initial Value
q3                          =  0.0;              % UNITS       Initial Value
%%%%% Luffing and Slewing Angles:
q4                          =  alpha_ini;        % UNITS       Initial Value
q5                          =  beta_ini;         % UNITS       Initial Value
%%%%%
thetaOne                    =  0.0;              % UNITS       Initial Value
thetaTwo                    =  0.0;              % UNITS       Initial Value
u1                          =  0.0;              % UNITS       Initial Value
u2                          =  0.0;              % UNITS       Initial Value
u3                          =  0.0;              % UNITS       Initial Value
u4                          =  0.0;              % UNITS       Initial Value
u5                          =  0.0;              % UNITS       Initial Value
v                           =  vel0;             % UNITS       Initial Value
x                           =  0.0;              % UNITS       Initial Value
xfront                      =  cl/2;             % UNITS       Initial Value
xtip                        =  0.0;              % UNITS       Initial Value
y                           =  0.0;              % UNITS       Initial Value
yfront                      =  0.0;              % UNITS       Initial Value
ytip                        =  0.0;              % UNITS       Initial Value
phiOnep                     =  0.0;              % UNITS       Initial Value
phiTwop                     =  0.0;              % UNITS       Initial Value
thetaOnep                   =  0.0;              % UNITS       Initial Value
thetaTwop                   =  0.0;              % UNITS       Initial Value
xp                          =  0.0;              % UNITS       Initial Value
yp                          =  0.0;              % UNITS       Initial Value
```

```
113
114 TINITIAL                  =  0.0;                % sec          Initial Time
115 TFINAL                    =  (t_final+t_offset);% sec          Final Time
116 INTEGSTP                  =  t_step;             % sec          Integration Step
117 PRINTINT                  =  1;                  % Pos. Int.   Print-Integer
118 ABSERR                    =  1.0E-08;            %              Absolute Error
119 RELERR                    =  1.0E-07 ;           %              Relative Error
120 %------------------------+------------------+-------------+-----------------
121
122
123
124 % Swing Angles due to Input Type:
125 % **using Single-Pendulum Swing Estimation Method.
126         % 0-static, 1-base acc., 2-cornering, 3-slewing, 4-luffing
127         % 5-I.S. base acc., 6-I.S. cornering, 7-I.S. slewing, 8-I.S. luffing
128 if Type == 0
129     phiOne = 0;
130     thetaOne = 0;
131     phiTwo = 0;
132     thetaTwo = 0;
133 elseif Type == 1
134     if q5>(pi/2) && q5<(3*pi/2)
135         phiOne = -1* (4*VorA/g*cos(SlopeFB*Deg2Rad))*Rad2Deg;
136     else
137         phiOne = (4*VorA/g*cos(SlopeFB*Deg2Rad))*Rad2Deg;
138     end
139     thetaOne = phiOne;
140     phiTwo = 0;
141     thetaTwo = 0;
142 elseif Type == 2
143     [phiOne, thetaOne] = SP_CorneringAngle(SlopeFB, SlopeS, q4, q5, cl, cw, r, xcom,
144 ycom, d1, d2, h, bcom, bl, l1, mC, mB, m1, VorA, v, t_step);
145     phiTwo = 0;
146     thetaTwo = 0;
147 elseif Type == 3
148     [phiOne, thetaOne] = SP_SlewingAngle(SlopeFB, SlopeS, q4, q5, cl, cw, r, xcom,
149 ycom, d1, d2, h, bcom, bl, l1, mC, mB, m1, VorA, v, t_step);
150     phiTwo = 0;
151     thetaTwo = 0;
152 elseif Type == 4
153     [phiOne, thetaOne]  = SP_LuffingAngle(SlopeFB, SlopeS, q4, q5, cl, cw, r, xcom,
```

```
ycom, d1, d2, h, bcom, bl, l1, mC, mB, m1, VorA, v, t_step);
    phiTwo = 0;
    thetaTwo = 0;
elseif Type == 5
    phiOne = atan(VorA*cos(SlopeFB*Deg2Rad)/g)*Rad2Deg;
    thetaOne = phiOne;
    phiTwo = 0;
    thetaTwo = 0;
elseif Type == 6
    [phiOne, thetaOne] = SP_CorneringAngle(SlopeFB, SlopeS, q4, q5, cl, cw, r, xcom,
ycom, d1, d2, h, bcom, bl, l1, mC, mB, m1, VorA, v, t_step);
    phiTwo = 0;
    thetaTwo = 0;
elseif Type == 7
    [phiOne, thetaOne] = SP_SlewingAngle(SlopeFB, SlopeS, q4, q5, cl, cw, r, xcom,
ycom, d1, d2, h, bcom, bl, l1, mC, mB, m1, VorA, v, t_step);
    phiTwo = 0;
    thetaTwo = 0;
elseif Type == 8
    [phiOne, thetaOne]  = 0.5*SP_LuffingAngle(SlopeFB, SlopeS, q4, q5, cl, cw, r,
xcom, ycom, d1, d2, h, bcom, bl, l1, mC, mB, m1, VorA, v, t_step);
    phiTwo = 0;
    thetaTwo = 0;
end



% Elementary Coordinate Frames:
Newton_0_TiltFB = rotation(2,SlopeFB);
TiltFB_0_Shadow = rotation(1,SlopeS);
Shadow_0_Slewing = rotation(3,q5);
Slewing_0_Boom = rotation(2,-q4);
Boom_0_Fix = rotation(2,q4) * rotation(3,-q5);
Fix_0_CableOne = rotation(2,-phiOne) * rotation(1,thetaOne);
CableOne_0_CableTwo = rotation(2,-phiTwo) * rotation(1,thetaTwo);

% Transformation Matrices to Newtonian Frame:
Newton_0_Shadow = Newton_0_TiltFB * TiltFB_0_Shadow;
Newton_0_Slewing = Newton_0_Shadow * Shadow_0_Slewing;
Newton_0_Boom = Newton_0_Slewing * Slewing_0_Boom;
Newton_0_CableOne = Newton_0_Boom * Boom_0_Fix * Fix_0_CableOne;
```

```
Newton_O_CableTwo = Newton_O_CableOne * CableOne_O_CableTwo;

% Position Vectors:
Shadow_P_Origin_to_w1 = [-cl/2; cw/2; 0];
Shadow_P_Origin_to_w2 = [cl/2; cw/2; 0];
Shadow_P_Origin_to_w3 = [cl/2; -cw/2; 0];
Shadow_P_Origin_to_w4 = [-cl/2; -cw/2; 0];
Shadow_P_Origin_to_CC = [0; 0; 2*r];
Shadow_P_CC_to_CartO = [xcom; ycom; 0];
Shadow_P_CC_to_SlewingO = [d1; 0; 0];
Slewing_P_SlewingO_to_CB = [d2; 0; h];
Boom_P_CB_to_BoomO = [bcom; 0; 0];
Boom_P_CB_to_CableOneO = [bl; 0; 0];
CableOne_P_CableOneO_mOne = [0; 0; -l1];
CableOne_P_CableOneO_CableTwoO = CableOne_P_CableOneO_mOne;
CableTwo_P_CableTwoO_mTwo = [0; 0; -l2];

% Position Vectors in Newtonian Frame:
Newton_P_Origin_to_CartO = Newton_O_Shadow * (Shadow_P_Origin_to_CC +
Shadow_P_CC_to_CartO);
Newton_P_Origin_to_BoomO = Newton_O_Shadow * (Shadow_P_Origin_to_CC +
Shadow_P_CC_to_SlewingO) + Newton_O_Slewing * Slewing_P_SlewingO_to_CB +
Newton_O_Boom * Boom_P_CB_to_BoomO;
Newton_P_Origin_to_mOne = Newton_O_Shadow * (Shadow_P_Origin_to_CC +
Shadow_P_CC_to_SlewingO) + Newton_O_Slewing * Slewing_P_SlewingO_to_CB +
Newton_O_Boom * Boom_P_CB_to_CableOneO + Newton_O_CableOne *
CableOne_P_CableOneO_mOne;
Newton_P_Origin_to_mTwo = Newton_P_Origin_to_mOne + Newton_O_CableTwo *
CableTwo_P_CableTwoO_mTwo;
Newton_P_Origin_to_w1 = Newton_O_Shadow * Shadow_P_Origin_to_w1;
Newton_P_Origin_to_w2 = Newton_O_Shadow * Shadow_P_Origin_to_w2;
Newton_P_Origin_to_w3 = Newton_O_Shadow * Shadow_P_Origin_to_w3;
Newton_P_Origin_to_w4 = Newton_O_Shadow * Shadow_P_Origin_to_w4;

% Center Of Mass Calculation:
Mass_Tot = mC+mB+m1+m2;
Newton_P_Origin_to_COM = (Newton_P_Origin_to_CartO * mC + Newton_P_Origin_to_BoomO
* mB + Newton_P_Origin_to_mOne * m1 + Newton_P_Origin_to_mTwo * m2) / Mass_Tot;

% Dynamic and Inertial Effects:
        % 0-static, 1-base acc., 2-cornering, 3-slewing, 4-luffing
```

```
        % 5-I.S. base acc., 6-I.S. cornering, 7-I.S. slewing, 8-I.S. luffing
if Type == 0
    Newton_W_inertia_at_COM = [0; 0; 0; 0; 0; 0];
elseif Type == 1
    Newton_W_inertia_at_COM = -1*VorA*[1; 0; 0; 0; 0; 0];
elseif Type == 2
    Newton_W_inertia_at_COM = DP_Cornering_InertiaForce(SlopeFB, SlopeS, q4, q5, cl,
cw, r, xcom, ycom, d1, d2, h, bcom, bl, l1, mC, mB, m1, VorA, v, phiOne, thetaOne,
l2, m2, t_step);
elseif Type == 3
    Newton_W_inertia_at_COM = DP_Slewing_InertiaForce(SlopeFB, SlopeS, q4, q5, cl,
cw, r, xcom, ycom, d1, d2, h, bcom, bl, l1, mC, mB, m1, VorA, v, phiOne, thetaOne,
l2, m2, t_step);
elseif Type == 4
    Newton_W_inertia_at_COM = [0; 0; 0; 0; 0; 0];
elseif Type == 5
    Newton_W_inertia_at_COM = -1*VorA*[1; 0; 0; 0; 0; 0];
elseif Type == 6
    Newton_W_inertia_at_COM = DP_Cornering_InertiaForce(SlopeFB, SlopeS, q4, q5, cl,
cw, r, xcom, ycom, d1, d2, h, bcom, bl, l1, mC, mB, m1, VorA, v, phiOne, thetaOne,
l2, m2, t_step);
elseif Type == 7
    Newton_W_inertia_at_COM = DP_Slewing_InertiaForce(SlopeFB, SlopeS, q4, q5, cl,
cw, r, xcom, ycom, d1, d2, h, bcom, bl, l1, mC, mB, m1, VorA, v, phiOne, thetaOne,
l2, m2, t_step);
elseif Type == 8
    Newton_W_inertia_at_COM = [0; 0; 0; 0; 0; 0];
end

% Total Wrench Applied at COM:
Newton_W_gravity_at_COM = Mass_Tot * g * [0; 0; -1; 0; 0; 0];
Newton_W_total_at_COM = Newton_W_inertia_at_COM + Newton_W_gravity_at_COM;
Newton_F_total_at_COM = Newton_W_total_at_COM(1:3,1);
Newton_T_total_at_COM = Newton_W_total_at_COM(4:6,1);

% Tip-over Prediction Method - Edge Preparation Setup:
Shadow_Edge1 = Shadow_P_Origin_to_w2 - Shadow_P_Origin_to_w1;
Shadow_Edge2 = Shadow_P_Origin_to_w3 - Shadow_P_Origin_to_w2;
Shadow_Edge3 = Shadow_P_Origin_to_w4 - Shadow_P_Origin_to_w3;
Shadow_Edge4 = Shadow_P_Origin_to_w1 - Shadow_P_Origin_to_w4;
Newton_Edge1 = Newton_O_Shadow * Shadow_Edge1;
```

```
Newton_Edge2 = Newton_O_Shadow * Shadow_Edge2;
Newton_Edge3 = Newton_O_Shadow * Shadow_Edge3;
Newton_Edge4 = Newton_O_Shadow * Shadow_Edge4;
Newton_Edge1_norm = Newton_Edge1 / norm(Newton_Edge1);
Newton_Edge2_norm = Newton_Edge2 / norm(Newton_Edge2);
Newton_Edge3_norm = Newton_Edge3 / norm(Newton_Edge3);
Newton_Edge4_norm = Newton_Edge4 / norm(Newton_Edge4);
Newton_I1 = (I-Newton_Edge1_norm*Newton_Edge1_norm')*
(Newton_P_Origin_to_w2-Newton_P_Origin_to_COM);
Newton_I2 = (I-Newton_Edge2_norm*Newton_Edge2_norm')*
(Newton_P_Origin_to_w3-Newton_P_Origin_to_COM);
Newton_I3 = (I-Newton_Edge3_norm*Newton_Edge3_norm')*
(Newton_P_Origin_to_w4-Newton_P_Origin_to_COM);
Newton_I4 = (I-Newton_Edge4_norm*Newton_Edge4_norm')*
(Newton_P_Origin_to_w1-Newton_P_Origin_to_COM);

% Tip-over Prediction Method - Net Force and Torque Preparation Setup:
f1 = (I-Newton_Edge1_norm*Newton_Edge1_norm')*Newton_F_total_at_COM;
f2 = (I-Newton_Edge2_norm*Newton_Edge2_norm')*Newton_F_total_at_COM;
f3 = (I-Newton_Edge3_norm*Newton_Edge3_norm')*Newton_F_total_at_COM;
f4 = (I-Newton_Edge4_norm*Newton_Edge4_norm')*Newton_F_total_at_COM;
n1 = (Newton_Edge1_norm*Newton_Edge1_norm')*Newton_T_total_at_COM;
n2 = (Newton_Edge2_norm*Newton_Edge2_norm')*Newton_T_total_at_COM;
n3 = (Newton_Edge3_norm*Newton_Edge3_norm')*Newton_T_total_at_COM;
n4 = (Newton_Edge4_norm*Newton_Edge4_norm')*Newton_T_total_at_COM;
f_n1 = cross((Newton_I1/norm(Newton_I1)),n1)/norm(Newton_I1);
f_n2 = cross((Newton_I2/norm(Newton_I2)),n2)/norm(Newton_I2);
f_n3 = cross((Newton_I3/norm(Newton_I3)),n3)/norm(Newton_I3);
f_n4 = cross((Newton_I4/norm(Newton_I4)),n4)/norm(Newton_I4);
f1_star = f1+f_n1;
f2_star = f2+f_n2;
f3_star = f3+f_n3;
f4_star = f4+f_n4;

% Check for a Tip-over Angle:
sign1 = -1*sign(dot(cross((Newton_I1/norm(Newton_I1)),
(f1_star/norm(f1_star))),Newton_Edge1_norm));
angle1 = sign1*acos(dot((f1_star/norm(f1_star)),(Newton_I1/norm(Newton_I1))));
sign2 = -1*sign(dot(cross((Newton_I2/norm(Newton_I2)),
(f2_star/norm(f2_star))),Newton_Edge2_norm));
angle2 = sign2*acos(dot((f2_star/norm(f2_star)),(Newton_I2/norm(Newton_I2))));
```

```
318 sign3 = -1*sign(dot(cross((Newton_I3/norm(Newton_I3)),
319 (f3_star/norm(f3_star))),Newton_Edge3_norm));
320 angle3 = sign3*acos(dot((f3_star/norm(f3_star)),(Newton_I3/norm(Newton_I3))));
321 sign4 = -1*sign(dot(cross((Newton_I4/norm(Newton_I4)),
322 (f4_star/norm(f4_star))),Newton_Edge4_norm));
323 angle4 = sign4*acos(dot((f4_star/norm(f4_star)),(Newton_I4/norm(Newton_I4))));
324 angle = [angle1, angle2, angle3, angle4];
325
326 % Calculate the Tip-Over Stability Margin
327 angle_cr = min(angle);
328 if angle_cr <=0
329     Results = 0;    % Tips Over and No Margin
330 else
331     Results = angle_cr*Rad2Deg;
332 end
```

APPENDIX B

AUTOLEV SOURCE CODES

Source Code B.1: Simulation of a Mobile Boom Crane

```
% mobileboom.al
% Generates equations of motion for MATLAB simulations of a Mobile Boom Crane
% Created by Andreas Rauch based on an existing model developed by Joshua
% Vaughan and Jon Danielson

% Default settings
Autoz off                                % switching off intermediate variables

% Newtonians, bodies, frames, points, particles
Newtonian N                              % Newtonian reference system
Bodies C, B, D                           % bodies with mass and inertia for cart,
                                         % boom, cable
Frames Bbeta, Dalpha, Dbeta, Dphi        % intermediate frames for boom/payload
Frames A, E                              % intermediate frames for cart
Points BC, CC, FA                        % point for boom attachment, cart center
                                         % and front axle center point
Points w1, w2, w3, w4                    % wheel contact points
Points w1N, w2N, w3N, w4N                % wheel contact points on ground
Particle payload                         % payload as a point mass

% Variables, constants
Motionvariables' u1', u2', u3'           % motion variables for cart tipping/sag
Motionvariables' phi'', theta''           % motion variables for payload swing
Variables x'', y'', q1', q2', q3'        % variables for cart motion, tipping/sag
Variables u4', u5', q4', q5'             % variables for boom motion
Variables Lw1', Lw2', Lw3', Lw4'         % variables for wheel deflection
Variables psi'', gamma''                 % variables for cart rotation/steering
Variables v'', xfront'', yfront''        % cart velocity and front axle motion
Variables F1, F2, F3, F4                 % variables for wheel normal forces
Variables xtip', ytip', xtipacc, ytipacc % variables for boom tip motion
Constants la, la2, bc, r, h, g, lb       % constants for crane properties, gravity
Constants l, lc, damp, stiff             % constants for crane properties
```

```
33 Constants mb, mp, mc, lcom, bcom, lbcom      % constants for crane properties
34 Specified specx'', specy'', specgamma'       % variables to specify cart motion
35 Specified specv'                             % variables to specify cart motion
36 Specified specalpha'', specbeta''            % variables to specify boom motion
37
38 % Masses, inertias
39 Mass C = mc, B = mb, payload = mp, D = 0            % mass of cart, boom, payload,
40                                                    % cable
41 Inertia C, mc/12*bc^2, mc/12*lc^2, mc/12*(lc^2+bc^2)% inertia of cart
42 Inertia B, 0, IB = mb/12*lb^2, IB                   % inertia of boom
43 Inertia D, 0,0,0                                   % inertia of cable
44
45 % Auxiliary variables
46 q1' = u1                                      % forward/backward pitch angle / angular
47                                               % velocity
48 q2' = u2                                      % lateral tilt angle / angular velocity
49 q3' = u3                                      % cart sag / vertical velocity
50 q4' = u4                                      % luff angle / angular velocity
51 q5' = u5                                      % slew angle / angular velocity
52 u4' = specalpha''                             % specifying luff acceleration
53 u5' = specbeta''                              % specifying slew acceleration
54 v' = specv'                                   % linear acceleration of front axle
55 gamma' = specgamma'                           % angular velocity of steering
56 xfront' = v*cos(psi+gamma)                    % equation of motion for x coordinate of
57                                               % front axle center
58 yfront' = v*sin(psi+gamma)                    % equation of motion for y coordinate of
59                                               % front axle center
60 xfront'' = Dt(xfront')                        % acceleration of front axle center point
61                                               % in x-direction
62 yfront'' = Dt(yfront')                        % acceleration of front axle center point
63                                               % in-y direction
64 psi' = v/lc*sin(gamma)                        % equation of motion for angular velocity
65                                               % of cart about vertical axis
66 psi'' = Dt(psi')                             % angular acceleration of the cart about
67                                               % vertical axis
68
69 % Position vectors
70 P_NO_FA> = xfront*N1> +yfront*N2>             % position of front axle center point
71                                               % in N
72 P_AO_FA> = lc/2*A1>                           % position of front axle in relation to
73                                               % AO
```

```
P_AO_CC> = (2*r+q3)*C3>                          % from AO to cart center
P_CC_CO> = lcom*C1>+bcom*C2>                     % from cart center to cart center of mass
P_CC_w1> = -lc/2*C1> + bc/2*C2> - 2*r*C3>        % from cart center to wheel contact
                                                % point 1
P_CC_w2> = lc/2*C1> + bc/2*C2> - 2*r*C3>         % from cart center to wheel contact
                                                % point 2
P_CC_w3> = lc/2*C1> - bc/2*C2> - 2*r*C3>         % from cart center to wheel contact
                                                % point 3
P_CC_w4> = -lc/2*C1> - bc/2*C2> - 2*r*C3>        % from cart center to wheel contact
                                                % point 4
P_CC_BbetaO> = la*C1>                           % from cart center to tower rotation
                                                % center
P_BbetaO_BC> = la2*Bbeta1> + h*Bbeta3>          % from rotation center to boom attachment
                                                % point
P_BC_DO> = lb*B1>                               % from boom attachment point to boom end
P_BC_BO> = lbcom*B1>                            % from boom attachment point to boom
                                                % center of mass
P_DO_payload> = -l*D3>                          % from boom end to payload
P_NO_w1N> = xfront*N1>+yfront*N2>-lc*A1>+bc/2*A2>    % position of wheel 1 contact
                                                    % point on ground in N
P_NO_w2N> = xfront*N1>+yfront*N2>+bc/2*A2>           % position of wheel 2 contact
                                                    % point on ground in N
P_NO_w3N> = xfront*N1>+yfront*N2>-bc/2*A2>           % position of wheel 3 contact
                                                    % point on ground in N
P_NO_w4N> = xfront*N1>+yfront*N2>-lc*A1>-bc/2*A2>    % position of wheel 4 contact
                                                    % point on ground in N

% Angular velocities
W_A_N> = psi'*N3>                               % of intermediate frame A in N
W_E_N> = W_A_N> + u1*C2>                        % of intermediate frame E in N
W_C_N> = W_E_N> + u2*E1>                        % of cart in N
W_B_N> = W_C_N> + u5*Bbeta3> - u4*B2>           % of boom in N
W_D_N> = W_B_N>-phi'*Dphi2> + theta'*D1>        % of cable in N

% Rotation matrices
Simprot(N, A, 3, psi)                           % rotation of cart
Simprot(A, E, 2, q1)                            % forward/backward pitching of cart
Simprot(E, C, 1, q2)                            % lateral tilting of cart
Simprot(C,Bbeta,3,q5)                           % rotation of boom
Simprot(Bbeta,B,2,-q4)                          % luffing of boom
Simprot(B,Dalpha,2,q4)                          % intermediate frame in order to get
```

```
                                        % swing angles in a vertical reference
                                        % frame, not perpendicular to boom
Simprot(Dalpha,Dbeta,3,-q5)             % intermediate frame in order to get
                                        % swing angles in a reference frame
                                        % with the same direction as the cart
Simprot(Dbeta,Dphi,2,-phi)              % payload swing to the front/back
Simprot(Dphi,D,1,theta)                 % lateral payload swing

% Velocities
V_AO_N> = Dt(P_NO_AO>, N)               % velocity of AO in N
V_CO_N> = Dt(P_NO_CO>, N)               % velocity of cart center of mass in N
V_CC_N> = Dt(P_NO_CC>, N)               % velocity of cart center in N
V_DO_N> = Dt(P_NO_DO>,N)                % velocity of boom tip in N
V_payload_N> = Dt(P_NO_payload>,N)      % velocity of payload in N
V_BC_C> = 0>                            % velocity of boom attachment relative
                                        % to cart
V2pts(N, C, CO, BC)                     % velocity of BC in N
V2pts(N, B, BC, BO)                     % velocity of boom center in cart
V2pts(N, C, CO, w1)                     % velocity of wheel 1 contact point in N
V2pts(N, C, CO, w2)                     % velocity of wheel 2 contact point in N
V2pts(N, C, CO, w3)                     % velocity of wheel 3 contact point in N
V2pts(N, C, CO, w4)                     % velocity of wheel 4 contact point in N
V2pts(N, A, AO, w1N)                    % velocity of wheel 1 contact point on
                                        % ground in N
V2pts(N, A, AO, w2N)                    % velocity of wheel 2 contact point on
                                        % ground in N
V2pts(N, A, AO, w3N)                    % velocity of wheel 3 contact point on
                                        % ground in N
V2pts(N, A, AO, w4N)                    % velocity of wheel 4 contact point on
                                        % ground in N

% Accelerations
A_CO_N> = Dt(V_CO_N>, N)                % acceleration of cart center of mass
                                        % in N
A_CC_N> = Dt(V_CC_N>, N)                % acceleration of cart center in N
A2pts(N,B,BC,BO)                        % acceleration of boom center in N
A2pts(N,B,BO,DO)                        % acceleration of boom tip in N
A_payload_N> = Dt(V_payload_N>, N)      % acceleration of payload in N

% Angular accelerations
ALF_A_N> = Dt(W_A_N>, N)                % of intermediate frame A in N
```

```
156 ALF_E_N> = Dt(W_E_N>, N)                    % of intermediate frame E in N
157 ALF_C_N> = Dt(W_C_N>, N)                    % of cart in N
158 ALF_B_N> = Dt(W_B_N>, N)                    % of boom in N
159 ALF_D_N> =  Dt(W_D_N>, N)                  % of cable in N
160
161 % Forces
162 Gravity(-g*N3>)                            % gravity force
163 Lw1 = Dot(P_NO_w1>, N3>)                   % wheel 1 deflection
164 Lw2 = Dot(P_NO_w2>, N3>)                   % wheel 2 deflection
165 Lw3 = Dot(P_NO_w3>, N3>)                   % wheel 3 deflection
166 Lw4 = Dot(P_NO_w4>, N3>)                   % wheel 4 deflection
167 Lw1' = Dot(V_w1_N>, N3>)                   % wheel 1 deflection rate
168 Lw2' = Dot(V_w2_N>, N3>)                   % wheel 2 deflection rate
169 Lw3' = Dot(V_w3_N>, N3>)                   % wheel 3 deflection rate
170 Lw4' = Dot(V_w4_N>, N3>)                   % wheel 4 deflection rate
171 F1 = -stiff*Lw1-damp*Lw1'                 % normal force at wheel 1 (has to be
172                                            % changed in MATLAB to be compressive
173                                            % only)
174 F2 = -stiff*Lw2-damp*Lw2'                 % normal force at wheel 2 (has to be
175                                            % changed in MATLAB to be compressive
176                                            % only)
177 F3 = -stiff*Lw3-damp*Lw3'                 % normal force at wheel 3 (has to be
178                                            % changed in MATLAB to be compressive
179                                            % only)
180 F4 = -stiff*Lw4-damp*Lw4'                 % normal force at wheel 4 (has to be
181                                            % changed in MATLAB to be compressive
182                                            % only)
183 Force(w1N/w1, F1*N3>)                      % normal force at wheel 1
184 Force(w2N/w2, F2*N3>)                      % normal force at wheel 2
185 Force(w3N/w3, F3*N3>)                      % normal force at wheel 3
186 Force(w4N/w4, F4*N3>)                      % normal force at wheel 4
187
188 % Equations of motion
189 Zero = Fr() + FrStar()
190 Kane()
191
192 % Motion of cart and boom tip
193 x'' = Dot(A_CC_N>, N1>)                    % cart center motion in N1>/x-direction
194 y'' = Dot(A_CC_N>, N2>)                    % cart center motion in N2>/y-direction
195 xtip' = Dot(V_DO_N>, N1>)                  % boom tip motion in N1>/x-direction
196 ytip' = Dot(V_DO_N>, N2>)                  % boom tip motion in N2>/y-direction
```

```
197 xtipacc = Dot(A_DO_N>, N1>)                  % boom tip motion in N1>/x-direction
198 ytipacc = Dot(A_DO_N>, N2>)                  % boom tip motion in N2>/y-direction
199
200 %Generate MATLAB code for simulation
201 UnitSystem kg, meter, sec
202 Input la= 0.3 m, la2 = 0.28 m, bc = 0.70 m, r = 0.14 m, mc = 24.9 kg
203 Input tFinal = 20, mp = 2 kg, lc = 1.1 m, l = 1 m, stiff = 250000 N/m, lcom = 0.12 m
204 Input g = 9.81 m/sec^2, mb = 8.0 kg, lb = 1.7 m, h = 0.14, damp = 1000 N*sec/m
205 Input bcom = 0 m, lbcom = 0.8 m
206 Output T sec, xfront m, xfront' m/sec, xfront'' m/sec^2, x m, x' m/sec, x'' m/sec^2,
207 xtip m, xtip' m/sec, xtipacc m/sec^2, yfront m, yfront' m/sec, yfront'' m/sec^2, y m,
208 y' m/sec, y'' m/sec^2, ytip m, ytip' m/sec, ytipacc m/sec^2, phi degree,
209 theta degree, F1 N, F2 N, F3 N, F4 N, q1 deg, q2 deg, q3 m, Lw1 m, Lw2 m, Lw3 m,
210 Lw4 m, q4 deg, u4 deg/sec, u4' deg/sec^2, q5 deg, u5 deg/sec, u5' deg/sec^2
211 CODE Dynamics() mobileboom.m
```

REFERENCES

[1] Abdel-Rahman, E. and Nayfeh, A., "Pendulation reduction in boom cranes using cable length manipulation," *Nonlinear Dynamics*, vol. 27, no. 3, pp. 255–269, 2002.

[2] Abdel-Rahman, E., Nayfeh, A., and Masoud, Z., "Dynamics and control of cranes: A review," *Journal of Vibration and Control*, vol. 9, no. 7, pp. 863–908, 2003.

[3] Abo-Shanab, R. and Sepehri, N., "Tip-over responses of hydraulic mobile cranes," *Transactions of the Canadian Society for Mechanical Engineering*, vol. 30, pp. 391–412, 2006.

[4] Acarman, T. and Ozguner, U., "Rollover prevention for heavy trucks using frequency shaped sliding mode control," *Vehicle System Dynamics*, vol. 44, pp. 737–762, 2006.

[5] Arash Kiyoumarsi, M. A. and Mirzaeian-Dehkordi, B., "The mathematical modeling of a double-pendulum system as a physical model of flexible arm robot," May 30-June 1 2007.

[6] Arnold, E., Sawodny, O., Hilderbrandt, A., and Schneider, K., "Anti-sway system for boom cranes based on an optimal control approach," in *American Control Conference*, vol. 4, (Denver, CO), pp. 3166–71, 2003.

[7] Banerjee, A. K. and Singhose, W. E., "Command shaping in tracking control of a two-link flexible robot," *Journal of Guidance, Control, and Dynamics*, vol. 21, pp. 1012–1015, 1998.

[8] Bertoluzzo, M., Buja, G., Cuogo, L., Sulligoi, G., and Zagatti, E., "Anti-roll control for by-wire lift truck," in *EUROCON*, (Belgrade, Serbia & Montenegro), 2005.

[9] Bouton, N., Lenain, R., Thuilot, B., and Fauroux, J.-C., "A rollover indicator based on the prediction of the load transfer in presence of sliding: application to an all terrain vehicle," in *IEEE International Conference on Robotics and Automation*, (Rome, Italy), 2007.

[10] CDC, "http://www.cdc.gov/elcosh/docs/d0800/d000804/1.jpg," Accessed: 11:15am, July 12, 2008.

[11] Daichi D. Fujioka, Andreas Rauch, W. S. and Jones, T., "Stability analysis of mobile boom cranes with double-pendulum payloads," in *American Control Conference*, (St. Louis, Missouri), 2009.

[12] Danielson, J., "Mobile boom cranes and advanced input shaping control," Master's thesis, Georgia Institute of Technology, 2008.

[13] Farshad Khorrami, S. J. and Tzes, A., "Experiments on rigid body-based controllers with input preshaping for a two-link flexible manupilator," *Transactions on Robotics and Automation*, vol. 10, pp. 55–65, 1994.

[14] Forest, C., Frakes, D., and Singhose, W., "Input-shaped control of gantry cranes: Simulation and curriculum development," in *Proceedings of the ASME Design Engineering Technical Conference*, vol. 6, (Sep 9-12 2001, Pittsburgh, PA, United States), pp. 1877–1884, 2001.

[15] Ghasempoor, A. and Sepehri, N., "A measure of machine stability for moving base manipulators," 1995.

[16] Guo, W., Liu, D., Yi, J., and Zhao, D., "Passivity-based-control for double-pendulum-type overhead cranes," in *IEEE Region 10 Annual International Conference*, (Chiang Mai, Thailand), pp. D546–D549, 2004.

[17] Hiroshi Ueno, Y. X. and Yoshida, T., "Modeling and control strategy of a 3-d flexible space robot," November 3-5 1991.

[18] Jesus Morales, Jorge L. Martinez, A. M. J. S. A. G.-C. and Pequeno-Boter, A., "Center of gravity estimation and control for a field mobile robot with a heavy manipulator," in *IEEE International COnference on Mechatronics*, (Malaga, Spain), 2009.

[19] Khalid, A., Huey, J., Singhose, W., Lawrence, J., and Frakes, D., "Human operator performance testing using an input-shaped bridge crane," *Journal of Dynamic Systems, Measurement and Control*, vol. 128, pp. 835–841, 2006.

[20] Kiliçaslan, S., Balkan, T., and Ider, S., "Tipping loads of mobile cranes with flexible booms," *Journal of Sound and Vibration*, vol. 223, no. 4, pp. 645–657, 1999.

[21] Kim, D. and Singhose, W., "Human operator learning on double-pendulum bridge cranes," in *Proceedings of the ASME International Mechanical Engineering Congress and Exposition*, vol. 9, (Seattle, WA, United States), pp. 1959–1965, 2007.

[22] Kim, D. and Singhose, W., "Performance studies of human operators driving double-pendulum bridge cranes," in *Control Engineering Practice*, 2010.

[23] Kogan, J., *Lifting and conveying machinery*. Ames, Iowa, USA: Iowa State University Press, 1985.

[24] Lawrence, J. W., *Crane Oscillation Control: Nonlinear Elemenets and Educational Improvements*. PhD thesis, 2006.

[25] Lee, Y. and Yi, S.-J., "Rollover prevention for sport utility vehicle using fuzzy logic controller," in *ICMIT 2005: Control Systems and Robotics, Proc. of SPIE*, vol. 6042, 2005.

[26] Lewis, D., Parker, G., Driessen, B., and Robinett, R., "Command shaping control of an operator-in-the-loop boom crane," in *American Control Conference*, vol. 5, (Philadelphia, Pennsylvania), pp. 2643–7, 1998.

[27] Lim, T. H., Kim, Y. S., Choi, J. H., Lee, H. S., and Yang, S. Y., "Development of tipping-over rate computation system for hydraulic excavator having crane function," in *Proceedings: KORUS 2004, 8th Korea-Russia International Symposium on Science and Technology*, pp. 76–79, 2005.

[28] Liu, D., Guo, W., and Yi, J., *GA-Based Composite Sliding Mode Fuzzy Control for Double-Pendulum-Type Overhead Crane*, pp. 792–801. Berlin: Springer-Verlag, 2005.

[29] Love, L., Magee, D., and Book, W., "A comparison of joint control algorithms for teleoperated pick and place tasks using a flexible manipulator," in *Proceedings of IEEE International Conference on Systems, Man and Cybernetics*, vol. 2, (San Antonio, TX, USA), pp. 1257–62, 1994.

[30] Magee, D. P. and Book, W. J., "Eliminating multiple modes of vibration in a flexible manipulator," in *Proceedings of IEEE International Conference on Robotics and Automation*, vol. 2, (Atlanta, GA, USA), pp. 474–479, 1993.

[31] Magee, D. and Book, W., "Implementing modified command filtering to eliminate multiple modes of vibration," in *Proceedings of American Control Conference - ACC '93*, vol. 3, (San Francisco, CA, USA), pp. 2700–4, 1993.

[32] Malcher, D., Eskandarian, A., and Delaigue, P., "Dynamics models for vehicle roll motion in prerollover manoeuvres," *Proceedings of the Institution of Mechanical Engineers, Part K: Journal of Multi-body Dynamics*, vol. 221, pp. 291–301, 2007.

[33] Manning, R., *Improving the Control of Two-Mode Flexible Systems with Input Shaping*. PhD thesis, 2008.

[34] Manning, R. and Singhose, W., "Frequency variations and control of two-ink robot arms with varying payloads," in *International Symposium on Flexible Automation*, (Atlanta, GA), 2008.

[35] Papadopoulos, E. and Rey, D., "A new measure of tipover stability margin for mobile manipulators," in *International Conference on Robotics and Automation*, (Minneapolis, Minnesota), pp. 3111–3116, 1996.

[36] P+H, C. S. P., "http://www.crane-spare-parts.com/images/p+h-crane-spare-parts.jpg," Accessed: 10:30am, July 12, 2008.

[37] Qiang Huang, S. S. and Tanie, K., "Motion planning for a mobile manipulator considering stability and task constraints," in *IEEE International COnference on Robotics and Automation*, (Leuven, Beigium), pp. 2192–2198, 1998.

[38] Rauch, A., *Stability Analysis of Mobile Boom Cranes*. PhD thesis, 2008.

[39] Robertson, M. J. and Singhose, W. E., "Deflection vector diagrams for a mass under pd control," in *Proceedings of the American Control Conference*, vol. 4, (Denver, CO, United States), pp. 2815–2820, 2003.

[40] Robertson, M. J. and Singhose, W. E., "Closed-form deflection-limiting commands," in *Proceedings of the American Control Conference*, vol. 3, (Portland, OR, United States), pp. 2104–2109, 2005.

[41] Robertson, M. J. and Singhose, W. E., "Robust analytic deflection-limiting commands," in *Proceedings of the American Control Conference*, vol. 2006, (Minneapolis, MN, United States), pp. 363–368, 2006.

[42] Robertson, M. J. and Singhose, W. E., "Specified-deflection command shapers for second-order position input systems," *Journal of Dynamic Systems, Measurement and Control*, vol. 129, pp. 856–859, 2007.

[43] Robertson, M. J., *Command generation for tethered satellite systems*. PhD thesis, Georgia Institue of Technology, 2005.

[44] Singer, N. and Seering, W., "Preshaping command inputs to reduce system vibration," *Journal of Dynamic Systems, Measurement and Control, Transactions ASME*, vol. 112, pp. 76–82, 1990.

[45] Singhose, W. and Kim, D., "Manipulation with tower cranes exhibiting double-pendulum oscillations," in *IEEE Int. Conf. on Robotics and Automation*, (Rome, Italy), 2007.

[46] Singhose, W. and Kim, D., "Manipulation with tower cranes exhibiting double-pendulum oscillations," in *Proceedings of the IEEE International Conference on Robotics and Automation*, (Rome, Italy), pp. 4550–4555, 2007.

[47] Singhose, W., Kim, D., and Kenison, M., "Input shaping control of double-pendulum bridge crane oscillations," *Journal of Dynamic Systems, Measurement, and Control*, vol. 130, 2008.

[48] Sorensen, K. L., Singhose, W., and Dickerson, S., "A controller enabling precise positioning and sway reduction in bridge and gantry cranes," *Control Engineering Practice*, vol. 15, pp. 825–837, 2007.

[49] Towarek, Z., "Dynamic stability of a crane standing on soil during the rotation of the boom," *International Journal of Mechanical Sciences*, vol. 40, no. 6, pp. 557–574, 1998.

[50] Tullacalder, "http://www.tullacalder.com.au/images/gallery/crane.jpg," Accessed: 12:15pm, February 26, 2008.

[51] Vaughan, J., Singhose, W., Debenest, P., Fukushima, E., and Hirose, S., "Initial experiments on the control of a mobile tower crane," in *Proceedings of the ASME International Mechanical Engineering Congress and Exposition*, (Seattle, WA, United States), pp. 1861–1866, 2007.

[52] Wang, X. and Su, X., "Modeling and sliding mode control of the upper arm of a shotcrete robot with hydraulic actuator," in *International Conference on Integration Technnology*, (Shezhen, China), pp. 714–718, 2007.

[53] Xiuping Mu, Q. W. and Sepehri, N., "On tip-over situation of mobile platforms via impact effects," in *IEEE Conference on Control Applications*, (Tronto, Canada), pp. 1546–1551, 2005.

[54] Zuo, K. and Wang, D., "Closed loop shaped-input control of a class of manipulators with a single flexible link," in *International Conference on Robotics and Automation*, (Nice, France), pp. 782–787, 1992.